creative commons
COMMONS DEED

저작자표시-비영리-변경금지 2.0 대한민국

이용자는 아래의 조건을 따르는 경우에 한하여 자유롭게

- 이 저작물을 복제, 배포, 전송, 전시, 공연 및 방송할 수 있습니다.

다음과 같은 조건을 따라야 합니다:

저작자표시. 귀하는 원저작자를 표시하여야 합니다.

비영리. 귀하는 이 저작물을 영리 목적으로 이용할 수 없습니다.

변경금지. 귀하는 이 저작물을 개작, 변형 또는 가공할 수 없습니다.

- 귀하는, 이 저작물의 재이용이나 배포의 경우, 이 저작물에 적용된 이용허락조건을 명확하게 나타내어야 합니다.
- 저작권자로부터 별도의 허가를 받으면 이러한 조건들은 적용되지 않습니다.

저작권법에 따른 이용자의 권리는 위의 내용에 의하여 영향을 받지 않습니다.

이것은 이용허락규약(Legal Code)을 이해하기 쉽게 요약한 것입니다.

Disclaimer

dCollection

약학박사 학위논문

Role of macrophage-derived heme oxygenase-1 in tumor microenvironment

종양 미세환경에서 대식세포 헴 산화 효소의 역할

2019년 2월

서울대학교 대학원

협동과정 종양생물학 전공

김 승 현

Role of macrophage-derived heme oxygenase-1 in tumor microenvironment

종양 미세환경에서 대식세포 헴 산화 효소의 역할

지도교수 서 영 준

이 논문을 약학박사 학위논문으로 제출함

2018년 10월

서울대학교 대학원

협동과정 종양생물학 전공

김 승 현

김승현의 약학박사 학위논문을 인준함

2019년 1월

위 원 장 _____ (인)

부위원장 _____ (인)

위 원 _____ (인)

위 원 _____ (인)

위 원 _____ (인)

Role of macrophage-derived heme oxygenase-1 in tumor microenvironment

by

Seung Hyeon Kim

A Thesis Submitted to the Interdisciplinary Graduate Program
in Partial Fulfillment of the Requirements
for the Degree of Doctor of Philosophy
in Cancer Biology at the Seoul National University
Seoul, Korea

January 2019
Approved by thesis committee:

_____

_____

_____

_____

_____

Abstract

Role of macrophage-derived heme oxygenase-1 in tumor microenvironment

Seung Hyeon Kim

Under the supervision of Professor Young-Joon Surh

Cancer Biology

The Graduate School

Seoul National University

One of the most common treatment options for breast cancer is chemotherapy. After chemotherapy, however, unwanted host effects provoke tumor recurrence and aggressiveness of cancer cells which often arise as a consequence of disruption in the patient's immune system. Lymphocytes, such as $CD8^+$ cytotoxic T cells which have capability of suppressing cancer

progression, are depleted following chemotherapy. Tumor-associated macrophages (TAMs), an abundant set of tumor-infiltrating myeloid cells in tumor microenvironment, play an important role in immunosuppression which often occurs during conventional chemotherapy. Dying cancer cells generated during the chemotherapy can potentially hijack accumulated TAMs, provoking tumor recurrence. Therefore, reprogramming of TAMs to maximize the chemotherapeutic efficacy is considered a promising novel anticancer strategy. In this study, I investigated whether tumor cell debris generated as a consequence chemotherapy can reduce therapeutic efficacy by modulating the activity of tumor-infiltrating macrophages. In a 4T1 syngeneic murine breast cancer model, the expression of the M1 marker, CD86 in the TAMs and the infiltration of $CD8^+$ T cells was reduced following paclitaxel (PTX) treatment. PTX treatment also resulted in an enhancement of heme oxygenase-1 (HO-1) expression in tumor-infiltrating myeloid cells engulfing tumor cell debris. Consistent with the *in vivo* profile of TAMs, bone marrow-derived macrophages (BMDMs) phagocytosing breast tumor cell debris exhibited significant upregulation of HO-1 expression. HO-1 induction in BMDMs engulfing breast tumor cell debris inhibited M1 polarization and reprogramed macrophages to the M2 phenotype. In contrast, inhibition of HO-1 activity with zinc protoporphyin IX resulted in sustained M1 macrophage activity of BMDMs co-cultured

with breast cancer cell debris. Therapeutic efficacy of PTX to suppress the tumor growth was significantly enhanced in HO-1 knock out mice bearing 4T1 breast cancer. Consistent with that finding, pharmacologic inhibition of HO-1 activity augmented the therapeutic efficacy of PTX by stimulating $CD86^+$ M1 TAMs in a 4T1 breast cancer. Furthermore, blockade of HO-1 in breast tumor bearing mice promoted $CD8^+$ T cell infiltration and activity. Taken together, the above findings suggest that tumor cell debris-induced HO-1 overexpression in macrophages during chemotherapy dampens therapeutic efficacy by manipulating anti-tumor immunity.

Keywords

breast cancer, tumor-associated macrophages, chemotherapy, tumor cell debris, heme oxygenase-1

Student number: 2014-30674

TABLE OF CONTENTS

LIST OF FIGURES

Appendix

LIST OF ABBREVIATIONS

CD36	cluster of differentiation 36
CD86	cluster of differentiation 86
CD206	cluster of differentiation 206
CO	carbon monoxide
CORM-3	CO-releasing molecule
FACS	fluorescence activated cell sorting
FBS	fetal bovine serum
FITC	fluorescein isothiocyanate
Hb	Hemoglobin
HEPES	4-(2-hydroxyethyl) piperazine-1-ethanesulfonic acid
HO-1	heme oxygenase-1
HOCl	hypochlorous acid
IL	Interleukin
WT	Wild type
KO	Knockout
KCl	potassium chloride
$MgCl_2$	magnesium chloride

MPO	Myeloperoxidase
HO-1	heme oxygenase-1
PE	Phycoerythrin
PI	propidium iodide
PMSF	phenylmethylsulfonyl fluoride
PPAR-γ	peroxisome proliferator-activated receptor-gamma
RT-PCR	reverse transcription-polymerase chain reaction
PVDF	polyvinylidene difluoride
SDS	sodium dodecyl sulfate
siRNA	small interfering RNA
TauCl	taurine chloramine
TNF-α	tumor necrosis factor alpha
ZnPP IX	zinc protoporphyrin IX

1. Introduction

Breast cancer, one of the most commonly diagnosed malignancies in women worldwide, is often treated with chemotherapy (Tong, Wu, Cho, & To, 2018). After chemotherapy, however, unwanted host effects provoke tumor recurrence and increase cancer cell aggressiveness, often via disruption of the patient's immune system (Anampa, Makower, & Sparano, 2015; Du, Key, Osborne, Mahnken, & Goodwin, 2003; Li et al., 2008; Verma et al., 2016). The response to chemotherapy is affected by the tumor microenvironment (TME), which is the complex region in which cancer cells interact with the tumor stroma (Hirata & Sahai, 2017; Maman & Witz, 2018). Chemotherapy can alter the proportion and activity of lymphocytes, including $CD8^+$ cytotoxic T lymphocytes, which play major roles in reducing cancer progression (McCoy, Lake, van der Most, Dick, & Nowak, 2012; Onyema et al., 2015; Samanta et al., 2018; Verma et al., 2016). Accordingly, potentiating the functional activity of cytotoxic lymphocytes, including $CD8^+$ T cells, has become a central goal of many anti-tumor therapies (Coffelt & de Visser, 2015). One example of this is the combined use of chemotherapeutic agents plus immune-stimulators that target anti-tumor immunity (Galluzzi, Senovilla, Zitvogel, & Kroemer, 2012; Hirata & Sahai, 2017).

Tumor-associated macrophages (TAMs), which act as a bridge between innate and adaptive immunity, could potentially be targeted to complement chemotherapeutic efficacy (Mantovani, Marchesi, Malesci, Laghi, & Allavena, 2017). Increased infiltration of TAMs into tumors following chemotherapy has been correlated with a poor prognosis (DeNardo et al., 2011; Zhao et al., 2017). Notably, TAMs exhibit a dual relationship with cancer in response to environmental signals (Mantovani et al., 2017): those associated with poor clinical outcome display the M2 (alternatively activated) phenotype that promotes tumor progression through immunosuppression (Mantovani et al., 2017), whereas those induced by local signals display the M1 (classically activated) phenotype which possess cytotoxic and T-cell-mediated anti-tumor activities (Biswas & Mantovani, 2010; Lewis & Pollard, 2006; Mantovani et al., 2017). Recent studies have focused on the role of environmental factors and the modulation of these factors to skew TAMs toward M1 TAMs for enhancing the host anti-tumor response (Baer et al., 2016; Fridman, Zitvogel, Sautes-Fridman, & Kroemer, 2017; Kaneda et al., 2016; Pyonteck et al., 2013).

For decades, anti-cancer therapies have focused on destroying cancer cells to reduce tumor growth (Y. S. Chang, Jalgaonkar, Middleton, & Hai, 2017; Sulciner et al., 2017). When such therapies kill tumor cells, tumor cell debris (apoptotic cells, necrotic cells and cell fragments) can be generated in

surrounding area (Sulciner et al., 2017). Importantly, the tumor cell debris generated by chemotherapy can contribute to accelerating tumor growth (J. Chang et al., 2018; Sulciner et al., 2017). Macrophages critically remove dead cells (Gregory & Pound, 2011; Kumar, Calianese, & Birge, 2017; Roca et al., 2017), and their phagocytosis of apoptotic cancer cells has been suggested to promote tumor growth by modulating TAM activity (Brown, Recht, & Strober, 2017; Cunha et al., 2018; Ringleb et al., 2017; Voss et al., 2017). However, little is understood regarding the molecular mechanisms underlying the interaction between cytotoxic agent-generated tumor cell debris and TAMs.

Chemotherapy-induced oxidative stress is one mechanism through which cancer cells are killed (Gorrini, Harris, & Mak, 2013). However, cancer cells can bypass oxidative cell death by activating their anti-oxidant defense system (Gorrini et al., 2013; Na & Surh, 2014; Nitti et al., 2017). The overexpression of stress-responsive antioxidative enzyme, heme oxygenase-1 (HO-1), was reported to be associated with poor prognosis in breast cancer patients receiving chemotherapy (Hopper, Meinel, Steiger, & Otterbein, 2018; Muliaditan et al., 2018; Nitti et al., 2017). Conversely, HO-1 inactivation can promote the effectiveness of anti-cancer therapy to inhibit tumor growth (Alaoui-Jamali et al., 2009; Di Biase et al., 2016; Fang, Sawa, Akaike, Greish, & Maeda, 2004; Metz et al., 2010; Miyake et al., 2010;

Muliaditan et al., 2018). Recent studies suggest that the induction of HO-1 in TAMs plays an important role in cancer progression (Halin Bergstrom et al., 2016; Hughes et al., 2015; Muliaditan et al., 2018). However, the role of overexpressed HO-1 in TAMs during chemotherapy remains poorly understood. In this study, I demonstrate that breast tumor cell debris-induced HO-1 expression in TAMs can diminishes the efficacy of Paclitaxel (PTX), a representative anticancer drug frequently used for the treatment of breast cancer.

2. Materials and Methods

Materials

Dulbecco's modified Eagle's medium (DMEM), penicillin, streptomycin and fetal bovine serum (FBS) were obtained from Gibco-BRL (Grand Island, NY, USA). PTX, lipopolysaccharide (LPS), hemoglobin (Hb) and antibodies against actin were purchased from Sigma-Aldrich Co (St. Louis, MO, USA). Red blood cell lysis buffer was a product from Biolegend (San Diego, CA, USA). Anti-Nrf2 was purchased from Abcam (Cambridge, UK). Anti-HO-1 and zinc protoporphyrin IX (ZnPP) were supplied by Enzo Life Sciences, Inc (Farmingdale, NY, USA). Anti-rabbit and anti-mouse horseradish peroxidase-conjugated secondary antibodies were provided by Zymed Laboratories Inc (San Francisco, CA, USA). Polyvinylidene difluoride (PVDF) membranes were supplied from Gelman Laboratory (Ann, Arbor, MI, USA) and enhanced chemiluminescent (ECL) detection kit was obtained from Amersham Pharmacia Biotech (Buckinghamshire, UK).

Human study

This study was approved by the institutional review board (IRB) of Seoul National University Hospital (Seoul, South Korea), and all patients provided signed informed consent for collection of specimens. (IRB number: 1807-061-957)

Animal study

Balb/c mice (6~9 weeks old) were purchased from Orient Bio (Gyeonggi-Do, South Korea). HO-1 KO mice, in which the HO-1 gene was deleted by targeted gene knockout, were kindly provided by Dr. M.A. Perrella (Harvard Medical School, Boston, MA, USA). 4T1 murine mammary adenocarcinoma cells (1 $x10^5$) were subcutaneously implanted in the mammary glands of female Balb/c mice as previously described (Pulaski & Ostrand-Rosenberg, 2001). Tumors were grown for 10 days before mice were injected with chemotherapeutic agents. Tumor size was measured by caliper (width x length x height x 0.52 = mm^3). All the animals were maintained according to the relevant institutional animal care guidelines. Animal experimental procedures were approved by the institutional animal care and use committee at Seoul National University, South Korea. (IACUC number: SNU-170710-2)

Macrophage depletion study

Established 4T1 tumors were injected with clodronate liposomes (1 mg/mouse; FormuMax Scientific, Inc. Sunnyvale, CA, USA) every 4 day in combination with PTX (5 mg/kg) or ZnPP (40 mg/kg). Depletion of macrophages was confirmed by flow cytometry.

Cell culture

To generate primary BMDMs, I obtained bone marrow cells by flushing the long bones of mice (6~12 weeks old). Bone marrow cells were plated in DMEM supplemented with 10% FBS, 100 μg/ml streptomycin, 100 U/ml penicillin and 20 ng/ml M-CSF (Biolegend, San Diego, CA, USA) and cultured for 7 days to allow for macrophage differentiation. Human MDA-MB231 cells and murine 4T1 cells were purchased from the American Type Culture Collection (ATCC, Manassas, VA, USA) and cultured in DMEM supplemented with 10% FBS, 100 μg/ml streptomycin and 100 U/ml penicillin. Cells were maintained at 37℃ in a humidified atmosphere of 5% CO_2.

Bioinformatic analysis

Microarray data were extracted from the Gene Expression Omnibus database (GSE 43816; National Center for Biotechnology Information, Bethesda, MD, USA; https://www.ncbi.nlm.nih.gov/.geo/). Heatmaps were generated using the R software (Bioconductor, ComplexHeatmap package).

Macrophage polarization

To generate M1-polarized macrophages, BMDMs were incubated with LPS (100 ng/ml) for 24 h as previously described (Kaneda et al., 2016).

Generation of tumor cell debris

Tumor cell debris was generated by incubating breast cancer cells ($1x10^7$) in medium supplemented with PTX (1 mM) for 24 h. The presence of dead cells among the debris was confirmed by the annexin V/PI assay. 5-fluorouracil (5-FU)-generated tumor cell debris was acquired by culturing breast cancer cells ($1x10^7$) in medium supplemented with 5-FU (500 μM) for 48 h.

Isolation of single cells from mouse tumors

Tumors were collected from mice and dissociated into single cells as described previously (Pachynski, Scholz, Monnier, Butcher, & Zabel, 2015). Specifically, tumor implanted mice were euthanized and tumors were harvested. Tumors were then minced and mechanically disaggregated. And the disaggregated tumors were passed through a 40 μM filter using DMEM supplemented with 2% FBS to prepare a single cell suspension.

Flow cytometric analysis

Single-cell suspensions were washed with PBS containing 1% FBS and non-specific antibody binding was blocked with anti-mouse CD16/32 Fc receptor block antibody (Biolegend, San Diego, CA, USA). The cells were then stained by incubation on ice for 30 min with the following fluorescence-conjugated antibodies: anti-mouse CD45 APC, anti-mouse CD45.2 BV510, anti-mouse CD11b Alexa Fluor700, anti-mouse F4/80 PerCP/Cy5.5, anti-mouse F4/80 APC, anti-mouse Ly-6C PE/Cy7, anti-mouse Ly-6G APC/Cy7, anti-mouse CD3ε Alexa Fluor 700, anti-mouse CD8a PE/Cy7, anti-mouse CD4 PE, anti-mouse CD206 FITC and anti-mouse CD36 PE. The cells were washed with PBS and subjected to flow cytometry. Dead cells were excluded

by DAPI (Thermo Fisher Scientific, Waltham, MA, USA) staining.

For intracellular staining, cells were incubated with ionomycin (1 μg/ml) and phorbol myristate acetate (PMA, 100 ng/ml) for 4 h at 37℃ in a humidified atmosphere of 5% CO_2 in the presence of a protein transport inhibitor (Brefeldin A; Monensin, Thermo Fisher Scientific, Waltham, MA, USA). Cells were fixed and permeabilized with a fixation/permeabilization buffer set (Thermo Fisher Scientific, Waltham, MA, USA), and then stained with the following antibodies: anti-mouse IL-12p40 PE, anti-mouse TNF-α FITC, anti-mouse IFN-γ APC (all from Biolegend, San Diego, CA, USA) and anti-mouse Foxp3 FITC (Thermo Fisher Scientific, Waltham, MA, USA).

To examine the presence of EpCAM as an intracellular marker of breast tumor cell debris, cells were fixed with 2% formaldehyde in PBS for 30 min at room temperature, permeabilized with 0.1% Tween-20 in PBS for 15 min at room temperature, and stained with anti-mouse EpCAM FITC (Biolegend). To stain intracellular HO-1, I used a fixation/permeabilization buffer set (Thermo Fisher Scientific, Waltham, MA, USA), according to the manufacturer's instruction. Briefly, the cells were stained with anti-HO-1 in buffer, washed with PBS and analyzed by flow cytometry. I used FACS Calibur, LSR Fortessa X-20 and FACS Aria III (BD, Franklin Lakes, NJ, USA) machines for the above-listed analyses. All samples were analyzed

using the Flow jo software package (Tree Star, Ashland, OR, USA).

Cell sorting

Single-cell suspensions obtained from tumors were stained with DAPI, anti-CD45 APC and anti-CD11b Alexa Fluor700 and subjected to FACS using a FACS Aria III (BD, Franklin Lakes, NJ, USA). Live cells were identified as $CD45^+$ $CD11b^+$.

Immunofluorescence

Tumor specimens were fixed, paraffin-embedded and sectioned, and the sections were deparaffinized and rehydrated by serial washes with graded xylene and alcohol. For immunofluorescence staining, tissue sections were boiled in 10 mM sodium citrate (pH 6), subjected to serial washing, blocked with 5% FBS in PBST (PBS + 0.1 % Tween 20) and co-stained with HO-1 (Enzo, Farmingdale, NY, USA) or CD8 Alexa Fluor 594 (Biolegend, San Diego, CA, USA) or CD11b Alexa Fluor 488 (Biolegend, San Diego, CA, USA) or CD206 (Biolegend, San Diego, CA, USA) and DAPI (Thermo

Fisher Scientific, Waltham, MA, USA) overnight at 4°C. To analyze the phagocytosis of macrophages, isolated myeloid cells were incubated with F4/80 (Santa Cruz, Dallas, TX, USA). The resulting $CD11b^+$ $F4/80^+$ cells were dispensed to glass slides, permeabilized for 5 min at room temperature using 0.2% Triton X-100 in PBS and blocked with 3% bovine serum albumin (BSA) in PBS containing 0.1% Triton X-100 for 1 h at room temperature. Anti-mouse EpCAM Alexa Fluor 594 (Biolegend, San Diego, CA, USA) was used to stain tumor cell debris in macrophages. To assess the expression of HO-1 in macrophages, myeloid cells were incubated with F4/80 (Santa Cruz, Dallas, TX, USA), permeabilized, stained with HO-1 (Enzo, Farmingdale, NY, USA) and incubated with the appropriate secondary antibodies. Nuclei were counterstained with DAPI and immunofluorescence images were collected on a Zeiss LSM 710 confocal microscope (Zeiss, Germany).

Phagocytosis assay

PTX-induced tumor cell debris was stained with 1 µl of 1 mg/ml pHrodo-SE (Thermo Fisher Scientific, Waltham, MA, USA) for 30 min at room temperature. BMDMs were co-cultured with pHrodo-SE-labeled tumor cell debris. After incubation for 8 h, the phagocytic activity of BMDMs was

assessed by flow cytometry or confocal microscopy.

Quantitative PCR

Total RNA was isolated from cells and tumor tissues using the TRIzol™ reagent (Invitrogen, Carlsbad, CA, USA) according to the manufacturer's instructions and reverse transcribed using murine leukemia virus reverse transcriptase (Promega, Madison, WI, USA). qPCR analysis was performed using a 7300 Real-Time PCR System (Thermo Fisher Scientific, Waltham, MA, USA). Gene expression data are presented relative to an internal control. The following primers were utilized:

Gene symbol	Primer sequences
Hmox1	Forward: GATAGAGCGCAACAAGCAGAA Reverse: CAGTGAGGCCCATACCAGAAG
Cxcl9	Forward: GGAGTTCGAGGAACCCTAGTG Reverse: GGGATTTGTAGTGGATCGTGC
Cxcl10	Forward: CCAAGTGCTGCCGTCATTTTC Reverse: GGCTCGCAGGGATGATTTCAA
Il10	Forward: GCTCTTACTGACTGGCATGAG Reverse: CGCAGCTCTAGGAGCATGTG

Tnf	Forward: CCCTCACACTCAGATCATCTTCT Reverse: GCTACGACGTGGGCTACAG
Il12b	Forward: TGGTTTGCCATCGTTTTGCTG Reverse: ACAGGTGAGGTTCACTGTTTG
Actb	Forward: TGCTAGGAGCCAGAGCAGTA Reverse: AGTGTGACGTTGACATCCGT

Western blot analysis

Whole-cell lysates or tumor extracts were prepared by suspending the cells or tumor tissues in lysis buffer (Cell Signaling Technology, Danvers, MA, USA) containing protease inhibitors (Roche, Switzerland) on ice, followed by centrifugation for 15 min at 13,000 *g*. Protein concentrations were assessed by a BSA assay (Invitrogen, Carlsbad, CA, USA). Proteins were resolved by sodium dodecyl sulfate polyacrylamide gel electrophoresis (SDS-PAGE) and transferred to PVDF membranes (Gelman Laboratory, Ann, Arbor, MI, USA). The membranes were incubated with primary antibodies at 4℃ overnight, washed and incubated with horseradish peroxidase-conjugated secondary antibodies. The results were developed with ECL reagents (Amersham Pharmacia Biotech, Buckinghamshire, UK) according to the manufacturer's instructions and visualized using a LAS

4000 (Fujifilm Life Science, Tokyo, Japan).

Statistics

Data are presented as the mean ± SEM (standard error of the mean). For between-group differences in the mouse experiments, significance was determined using one-way ANOVA analysis with a Tukey's post hoc test. The Student's *t*-test was used to compare data from control and experimental conditions. The analyses were applied using SigmaPlot 12 (Systat Software, San Jose, CA, USA).

3. Results

Chemotherapy facilitates development an immunosuppressive TME in breast cancer

Chemotherapy acts as a double-edged sword in the regulation of cancer progression (Y. S. Chang et al., 2017; Karagiannis et al., 2017). Therapy-induced changes of the TME often abrogate treatment efficacy via unwanted host effects, such as modification of immune cell infiltration and increases in immunosuppressive factors (Engblom, Pfirschke, & Pittet, 2016; Maman & Witz, 2018). To investigate the impact of chemotherapy on host, I analyzed a published gene expression dataset obtained from breast cancer patients who received chemotherapeutic treatment (GSE 43816) (Gruosso et al., 2016). I found that the expression levels of immunosuppressive genes were upregulated, while those of genes associated with immune stimulation were downregulated after chemotherapy (Fig. 1A). To verify the chemotherapy-associated changes in immune cell subsets, I measured the proportion of immune cells in the breast cancer patient who received chemotherapy. Immunofluorescence staining revealed that the number of intratumoral $CD8^+$ T cells decreased (Fig. 1B), while that of infiltrated M2

TAMs (identified by positivity for CD11b and CD206) increased in tumor tissues after chemotherapy (Fig. 1C). Next, I examined the impact of cytotoxic therapy on anti-tumor immunity in the TME. For this purpose, I used a syngeneic murine breast cancer (4T1) model in which mice were treated with PTX (Fig. 1D), one of the most commonly used chemotherapeutic agents (Di Biase et al., 2016; Ruffell et al., 2014; Rugo et al., 2015). As expected, systemic administration of PTX inhibited the growth of 4T1 tumors (Fig. 1E, F). To determine whether PTX treatment altered the proportion of tumor-infiltrating immune cells, I analyzed infiltrating immune cells stained with fluorochrome-conjugated antibodies by flow cytometry (Cassetta et al., 2016). I examined the proportion of $CD8^+$ cytotoxic T lymphocytes, which play a decisive role in suppressing tumor growth, and found that the percentage of recruited $CD8^+$ T cells was significantly reduced in the PTX-treated group (Fig. 1G). To investigate whether PTX treatment alters the proportion of TAMs in a 4T1 breast cancer model, I measured infiltrating TAMs stained with fluorochrome-conjugated antibodies by flow cytometry. I found that administration of PTX markedly downregulated the surface expression of the M1 marker CD86 (Cunha et al., 2018) in infiltrated TAMs (Fig. 1H).

Phagocytosis of tumor cell debris regulates the polarization of

macrophages to a pro-tumor phenotype

Chemotherapy affects the polarization of TAMs toward immunosuppressive functions that suppress anti-tumor immunity (Dijkgraaf et al., 2013; Hughes et al., 2015; Mantovani & Allavena, 2015). To understand how PTX therapy alters the TAM phenotype, I considered the physiological events that characterize the TME after cytotoxic therapy. Given that macrophages function to clear cell debris in the TME (Roca et al., 2017), I examined whether phagocytosis of the tumor cell debris generated by chemotherapy could contribute to TAM polarization. The proportion of macrophages phagocytosing breast tumor cell debris (identified by positivity for the breast cancer cell marker, $EpCAM^+$) was increased after PTX treatment (Fig. 2A). I observed that tumor cell debris ($EpCAM^+$) was engulfed by macrophages ($F4/80^+$ cells) from 4T1 tumor-bearing mice injected with PTX (Fig. 2B). To further investigate the role of tumor cell debris in the polarization of macrophages, I co-cultured BMDMs with 4T1 or MDA-MB-231 breast cancer cells treated with PTX for 24 h. PTX-induced cell death was confirmed by annexin V/propidium iodide (PI) staining analysis. After co-culture, I examined markers of M1- and M2-polarized macrophages (Engblom et al., 2016; Genard, Lucas, & Michiels, 2017) and found that the mRNA levels of *Tnf* and *Il12b* were reduced in M1-polarized BMDMs co-

cultured with cancer cell debris (Fig. 2C-F). Consistent with these observations, the percentages of macrophages expressing TNF-α or IL-12p40 were decreased following co-culture with tumor cell debris (Fig. 2G, H). I further confirmed that the proportion of macrophages expressing TNF-α or IL-12p40 following co-culture with viable breast cancer cells was decreased (Fig. 2G, H). Proteins secreted from tumor cells have been shown to inhibit M1 polarization, thereby reducing the anti-tumor immune response (Ubil et al., 2018). To investigate whether such debris could affect the polarization of macrophages to the M2 phenotype, I examined the expression of the M2 marker, CD206 in macrophages co-cultured with tumor cell debris or viable breast cancer cells. The CD206 expression levels of macrophages were higher in macrophages treated with tumor cell debris compared to those co-cultured with viable breast cancer cells (Fig. 2I, J). BMDMs co-incubated with breast tumor cell debris also showed elevated mRNA levels of *Il10* which is an immunosuppressive M2 marker (Fig. 2K, L). Danger-associated molecular patterns (DAMPs) from dead cells contribute to promoting tumors by triggering immunosuppression (Hernandez, Huebener, & Schwabe, 2016). Macrophages co-cultured with tumor cell debris showed increased *Il10* mRNA levels compared to macrophages treated with DAMPs released from PTX-generated tumor cell debris (Fig. 2K, L). These results suggest that engulfment of tumor cell

debris induces an immunosuppression that could be an important aspect of the TME changes seen in the wake of anti-cancer therapy. To evaluate the expression of phosphatidylserine (PS) recognition receptor on the surface of M2 TAMs (Niu et al., 2017; H.-W. Wang & Joyce, 2010), I verified the expression of CD36 in BMDMs treated with tumor debris. The expression levels of CD36 were higher in macrophages exposed to breast cancer cell debris compared to those co-cultured with viable breast cancer cells (Fig. 2M, N).

Engulfment of tumor cell debris induces HO-1 expression in macrophages

Chemotherapy for tumor eradication in breast cancer patients has been reported to upregulate HO-1 expression, which is associated with the low survival rate (Gorrini et al., 2013; Muliaditan et al., 2018). Moreover, TAMs represent the major tumoral source of HO-1 in breast cancer (Muliaditan et al., 2018). To determine whether HO-1 expression of TAMs was enhanced after chemotherapy, the HO-1 expression of macrophages in human breast cancer samples was measured. HO-1 overexpression of infiltrated macrophages was evident following chemotherapy (Fig. 3A). Likewise,

Hmox1 mRNA expression levels of tumor-infiltrating myeloid cells were enhanced in the PTX-treated 4T1 breast cancer group relative to untreated 4T1 breast cancer group (Fig. 3B). Consistent with the mRNA levels, the protein expression of HO-1 in TAMs was also increased in PTX treated group compared to non-treated group (Fig. 3C). The elevated expression of HO-1 in TAMs derived from 4T1 tumor-bearing mice injected with PTX was confirmed by immunofluorescence staining (Fig. 3D). In another experiment, BMDMs co-cultured with tumor cell debris showed induction of HO-1 expression to a greater extent than did the untreated group (Fig. 3E, F). To further determine whether tumor cell debris is critical for the overexpression of HO-1 in macrophages following chemotherapy, the expression levels of HO-1 in macrophages co-cultured with viable breast cancer cells or PTX-generated tumor cell debris were compared. Macrophages co-incubated with breast cancer cell debris showed significantly higher levels of HO-1 than those co-cultured with viable breast cancer cells (Fig. 3G, H).

HO-1 overexpression triggered by phagocytosis of tumor cell debris regulates the polarization of macrophages

Given that HO-1 is an important factor for the polarization of macrophages, it could be a promising target in cancer immunotherapy (Mantovani et al., 2017; Naito, Takagi, & Higashimura, 2014; Vijayan, Wagener, & Immenschuh, 2018). To test whether the tumor cell debris-induced HO-1 overexpression of macrophages is essential for their polarization, I used HO-1-deficient BMDMs from HO-1 knockout (HO-1 KO) mice. First, I examined whether ablation of HO-1 could affect the activation of M1-polarized macrophages treated with tumor cell debris. The proportion of M1 macrophages (identified by the expression of TNF-α and IL-12p40) was significantly decreased in wild-type (WT) cells co-cultured with 4T1 tumor cell debris, whereas HO-1 KO macrophages were unaffected by this treatment (Fig. 4A, B). To further explore the role of HO-1 activity in macrophage polarization, I used ZnPP, which is a pharmacologic inhibitor of HO-1. I found that the ZnPP-mediated inhibition of HO-1 activity restored the mRNA levels of *Tnf* and *Il12b* in M1-polarized macrophages co-cultured with 4T1 tumor cell debris (Fig. 4C, D) or MDA-MB-231 tumor cell debris (Fig. 4E, F). Then, I examined whether inhibition of HO-1 activity could affect M2 polarization. The expression of CD206 in HO-1-deficient macrophages treated with tumor cell debris was lower than that in WT macrophages (Fig. 4G, H). Inhibition of HO-1 activity with ZnPP also decreased the CD206 expression of macrophages exposed to tumor cell

debris (Fig. 4I, J). HO-1-deficient macrophages treated with cell debris showed decreased mRNA levels of *Il10* compared to the WT macrophages (Fig. 4K, L). Inhibition of HO-1 activity with ZnPP depleted the *Il10* mRNA levels in macrophages co-cultured with tumor cell debris (Fig. 4M, N). HO-1-deficient macrophages exposed to tumor cell debris exhibited a diminished CD36 expression compared to the corresponding WT macrophages (Fig. 4O, P). Finally, the expression of CD36 in macrophages co-cultured with breast cancer cell debris was downregulated in the ZnPP-treated group (Fig. 4Q, R). Taken together, these results suggest that HO-1 signaling induced by tumor cell debris modulates the polarization of macrophages in the TME following chemotherapy.

HO-1 inactivation amplifies the therapeutic efficacy of PTX

To determine whether HO-1 inactivation could enhance the therapeutic efficiency of PTX, I used HO-1 KO mice implanted with 4T1 breast cancer cells (Fig. 5A). It is noticeable that the tumor growth of this model was completely inhibited in HO-1 KO mice treated with PTX (Fig. 5B, C). To further confirm the role of HO-1 in the response to PTX, I injected 4T1 tumor cell-implanted mice with PTX and ZnPP (Fig. 5D). I found that co-treatment of mice with the HO-1 inhibitor plus PTX suppressed tumor

growth more effectively than PTX treatment alone (Fig. 5E, F).

HO-1 inhibition promotes anti-tumor T cell function in response to PTX treatment

In the context of an anti-tumor immune response, sufficient numbers of infiltrating T cell are needed to achieve a favorable clinical outcome (Fridman et al., 2017; Spranger & Gajewski, 2018). Interestingly, there were significantly more $CD8^+$ T cells in tumors of mice treated with PTX plus ZnPP compared to those from mice treated with PTX alone (Fig. 6A, B). As enhanced levels of the chemokines such as CXC-chemokine ligand 9 (CXCL9) and CXC-chemokine ligand 10 (CXCL10) are reportedly associated with amplified numbers of tumor-infiltrating $CD8^+$ T cells (Ugel, De Sanctis, Mandruzzato, & Bronte, 2015), I examined whether HO-1 inhibition could accelerate the infiltration of $CD8^+$ T cells by upregulating expression of chemokines. Indeed, the mRNA levels of *Cxcl9* and *Cxcl10* were higher in tumors from mice treated with PTX plus ZnPP, and this coincided with enhanced $CD8^+$ T cell recruitment (Fig. 6C, D). The functions of cytotoxic T lymphocyte effectors are mediated through secretion of cytokines, such as interferon (IFN)-γ (Durgeau, Virk, Corgnac,

& Mami-Chouaib, 2018). The proportion of T cells producing IFN-γ was significantly increased in mice treated with PTX and ZnPP compared to those treated with PTX alone (Fig. 6E, F). Furthermore, the proportion of $Foxp3^+$ regulatory T cells (Tregs) from 4T1 tumor-bearing mice injected with PTX plus ZnPP was lower than that from 4T1 tumor-bearing mice treated with PTX alone (Fig. 6G). Consistent with the ability of PTX plus ZnPP to increase the anti-tumor immune responses, PTX and ZnPP co-treatment increased the proportion of macrophages phagocytosing breast tumor cell debris to a greater extent than that achieved with PTX alone (Fig. 6H).

HO-1 inactivation-induced M1 TAMs are crucial for the enhanced response to PTX therapy

To further determine whether macrophages are necessary to support the T cell function in PTX and ZnPP co-treatment, I used a clodronate liposome to chemically deplete macrophages (Genard et al., 2017) (Fig. 7A). These results revealed that the tumor-inhibiting efficacy of PTX and ZnPP co-treatment was abrogated in the macrophage depletion group (Fig. 7B, C). Macrophage depletion decreased the intratumoral $CD8^+$ T cell population

(Fig. 7D) and downregulated the expression of *Cxcl9* and *Cxcl10* of tumor from mice treated with PTX and ZnPP (Fig. 7E, F). To evaluate whether inactivation of HO-1 enhanced the therapeutic efficacy of PTX by reprogramming of TAMs, I analyzed markers of TAM phenotypes. As shown in Fig. 7G, the CD86 expression of macrophages was upregulated in mice injected with PTX plus ZnPP compared to that in mice treated with PTX alone. The mRNA levels of *Il10* in $CD11b^{+}$ myeloid cells from 4T1 tumor-bearing mice treated with PTX and ZnPP were reduced compared with those from mice treated with PTX alone (Fig. 7H). These results suggest that inactivation of HO-1 stimulates the conversion of TAMs to the M1 phenotype upon chemotherapy.

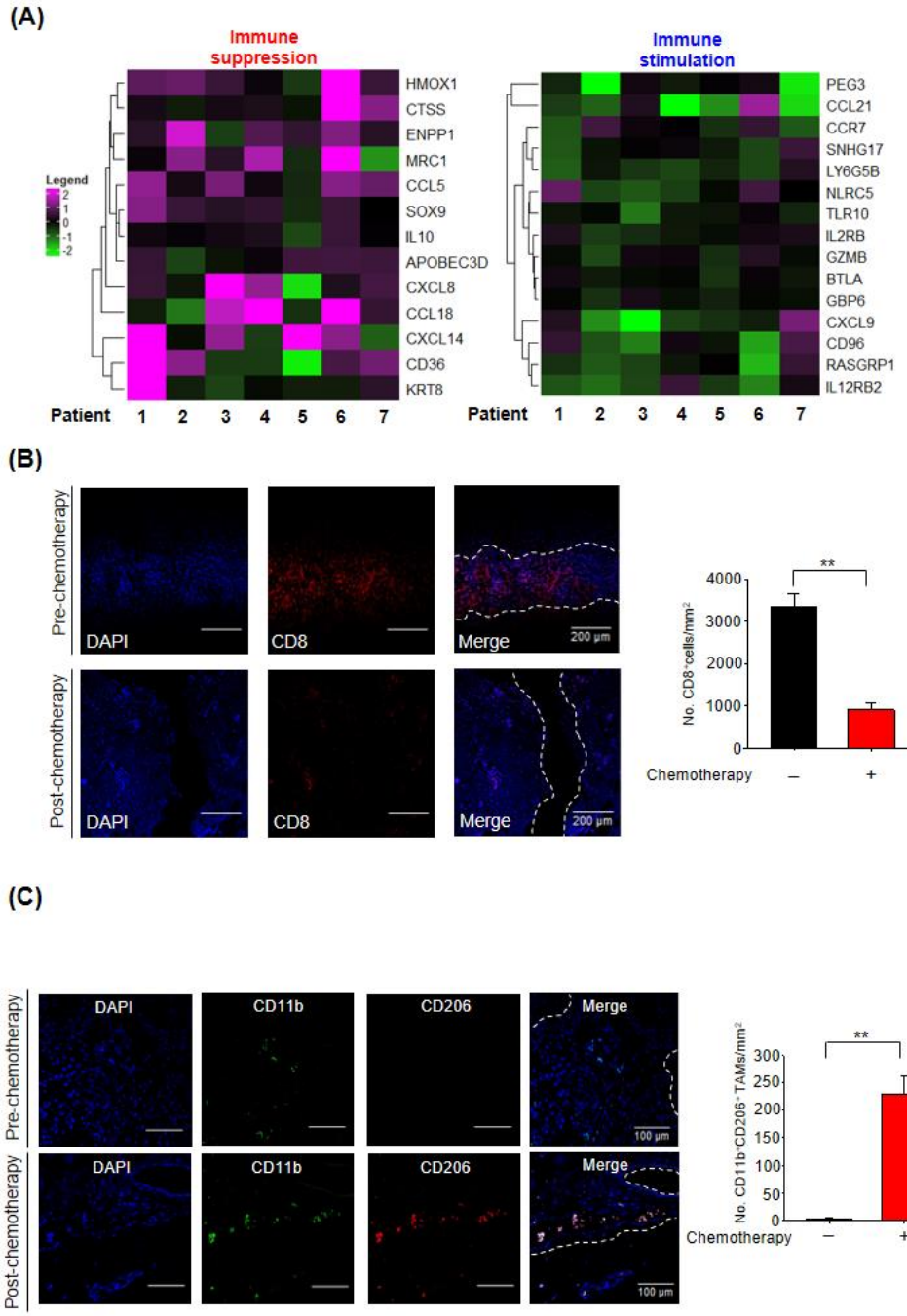
(A)
Immune suppression
Immune stimulation
Legend
2
1
0
-1
-2
HMOX1
CTSS
ENPP1
MRC1
CCL5
SOX9
IL10
APOBEC3D
CXCL8
CCL18
CXCL14
CD36
KRT8
PEG3
CCL21
CCR7
SNHG17
LY6G5B
NLRC5
TLR10
IL2RB
GZMB
BTLA
GBP6
CXCL9
CD96
RASGRP1
IL12RB2
Patient 1 2 3 4 5 6 7
Patient 1 2 3 4 5 6 7
(B)
Pre-chemotherapy
Post-chemotherapy
DAPI
CD8
Merge
200 μm
No. CD8+cells/mm2
4000
3000
2000
1000
0
**
Chemotherapy – +
(C)
Pre-chemotherapy
Post-chemotherapy
DAPI
CD11b
CD206
Merge
100 μm
No. CD11b+CD206+TAMs/mm2
300
250
200
150
100
50
0
**
Chemotherapy – +

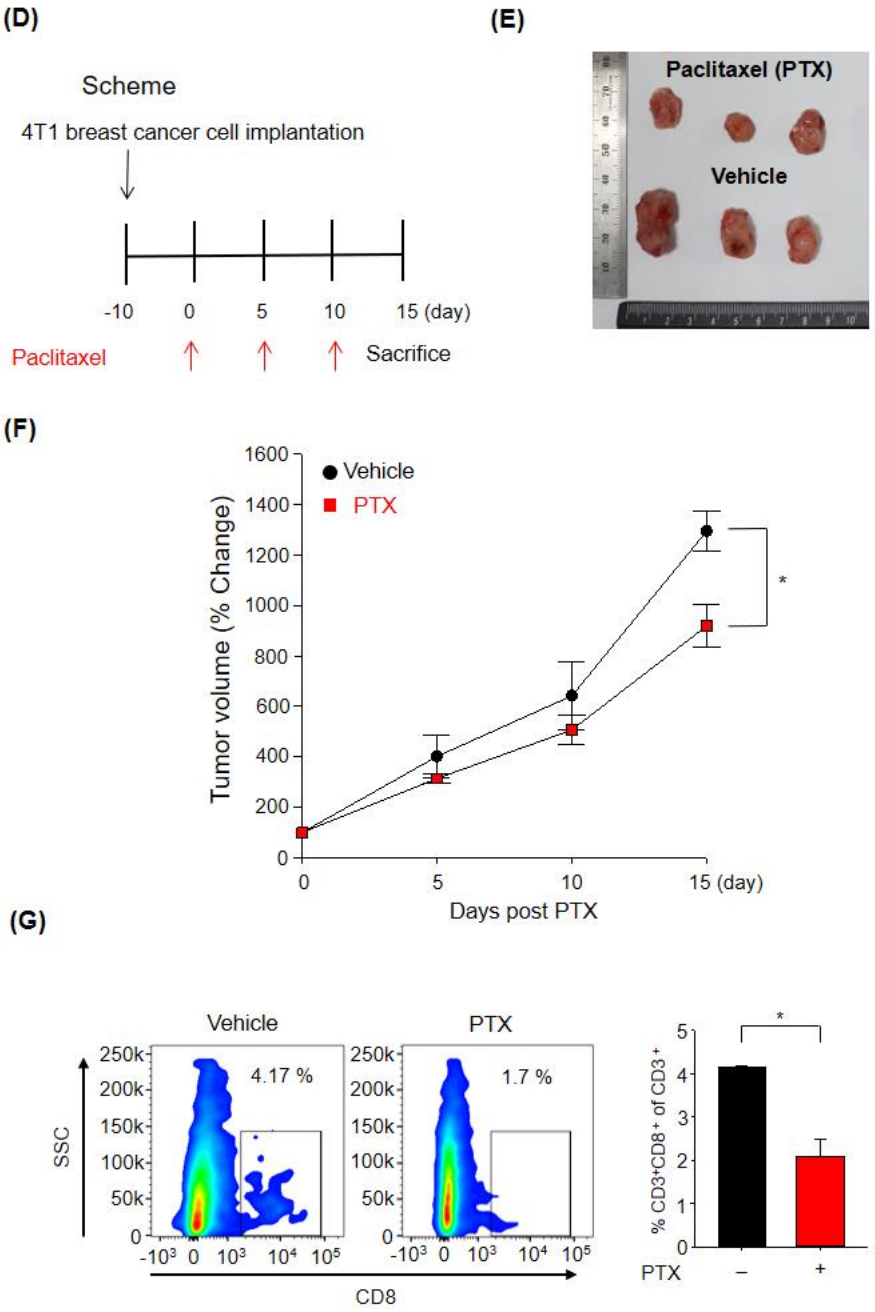
(D)
Scheme
4T1 breast cancer cell implantation
-10
0
5
10
15 (day)
Paclitaxel
Sacrifice
(E)
Paclitaxel (PTX)
Vehicle
(F)
Vehicle
PTX
Tumor volume (% Change)
1600
1400
1200
1000
800
600
400
200
0
*
0
5
10
15 (day)
Days post PTX
(G)
Vehicle
PTX
4.17 %
1.7 %
SSC
CD8
250k
200k
150k
100k
50k
0
-10³ 0 10³ 10⁴ 10⁵
% CD3+CD8+ of CD3+
5
4
3
2
1
0
*
PTX
–
+

(H)

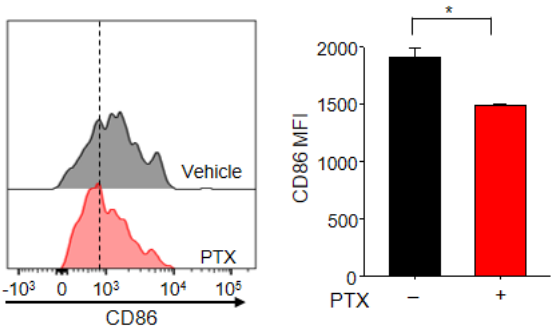
Vehicle
PTX
-10³ 0 10³ 10⁴ 10⁵
CD86
*
2000
1500
1000
500
0
CD86 MFI
PTX
–
+

Figure 1. Chemotherapy alters proportion of tumor-infiltrating immune cells.

(A) Heatmap of genes from breast cancer patients who underwent chemotherapeutic treatments (GSE 43816). (B) Representative images of tumor sections from the patients with breast cancer subjected to chemotherapy following staining for CD8 T cells. (C) Representative images of tumor tissues from breast cancer patients receiving chemotherapy stained for CD206. (D) Mice were implanted subcutaneously in the mammary gland with 4T1 tumor cells. At 10 days after tumor cell injection, the mice were subjected to intraperitoneal injection of vehicle or PTX (5 mg/kg) every 5 day. Mice were sacrificed on day 15 after PTX treatment, and tumors were collected. (E) Representative photographs of tumors in each group. (F) Effect of PTX on growth of implanted 4T1 murine mammary adenocarcinoma. The relative volume change is plotted as the total mean ± SEM. (G) Effects of PTX on proportion of $CD45^+CD3^+CD8^+$ tumor-infiltrating lymphocytes. Whole tumors were dissociated into single cells and flow cytometry was used to identify tumor-infiltrating immune cells. The $CD45^+CD3^+CD8^+$ tumor-infiltrating lymphocyte populations (as percentages) in tumors collected from mice treated with or without PTX were assessed by flow cytometry. (H) The $CD45^+CD11b^+Ly6G^-Ly6C^-$

F4/80^{+} TAM subsets of 4T1 tumors were gated and analyzed for CD86 expression by flow cytometry. The mean fluorescence intensity (MFI) of CD86^{+} TAMs is shown for each group. Data were analyzed by the Student's *t*-test. *p < 0.05, **p < 0.01, and ***p < 0.001.

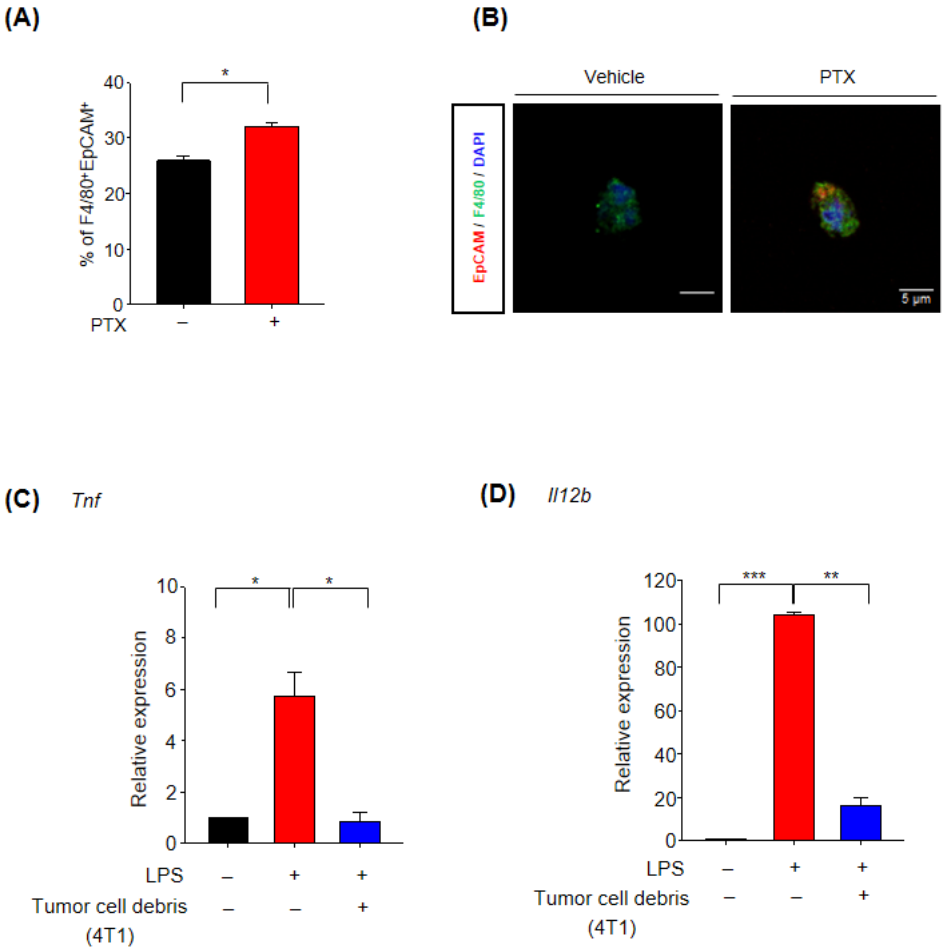
(A)
% of F4/80+EpCAM+
40
30
20
10
0
*
PTX
–
+
(B)
Vehicle
PTX
EpCAM / F4/80 / DAPI
5 μm
(C) Tnf
Relative expression
10
8
6
4
2
0
*
*
LPS
–
+
+
Tumor cell debris
–
–
+
(4T1)
(D) Il12b
Relative expression
120
100
80
60
40
20
0
***
**
LPS
–
+
+
Tumor cell debris
–
–
+
(4T1)

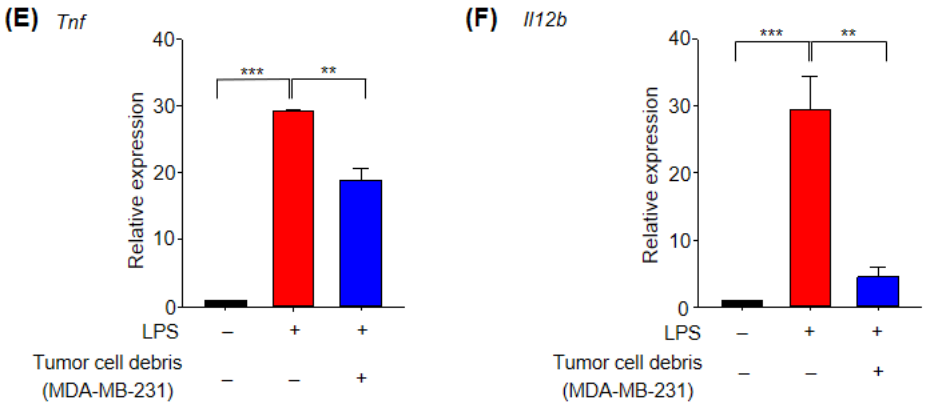
(E) Tnf
Relative expression
40
30
20
10
0
***
**
LPS – + +
Tumor cell debris – – +
(MDA-MB-231)
(F) Il12b
Relative expression
40
30
20
10
0
***
**
LPS – + +
Tumor cell debris – – +
(MDA-MB-231)

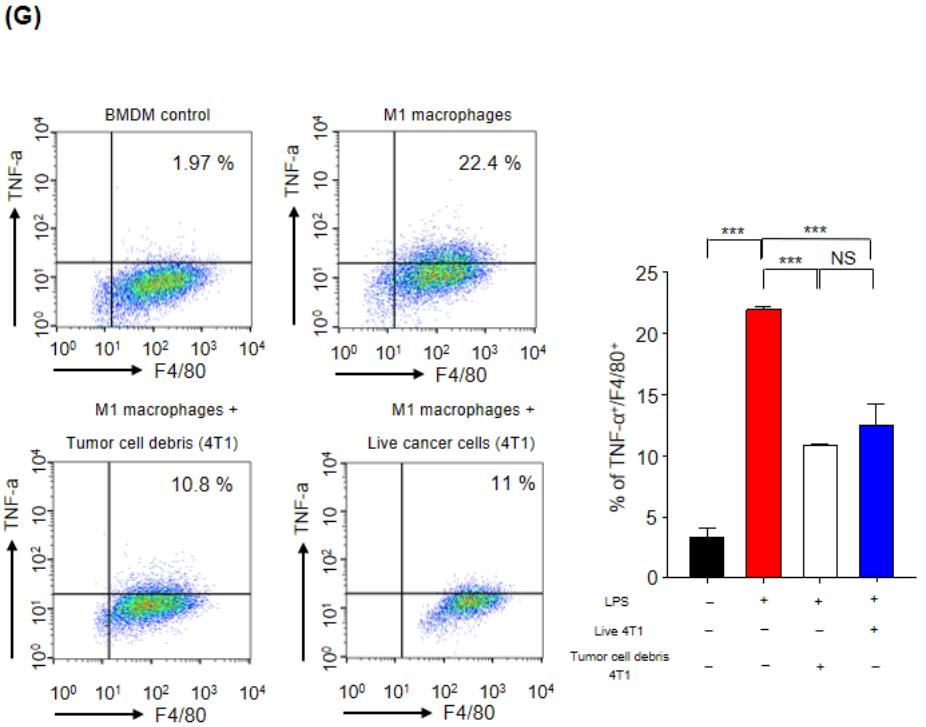
(G)
BMDM control
1.97 %
M1 macrophages
22.4 %
M1 macrophages +
Tumor cell debris (4T1)
10.8 %
M1 macrophages +
Live cancer cells (4T1)
11 %
TNF-a
F4/80
% of TNF-α+/F4/80+
***
***
***
NS
LPS – + + +
Live 4T1 – – – +
Tumor cell debris 4T1 – – + –

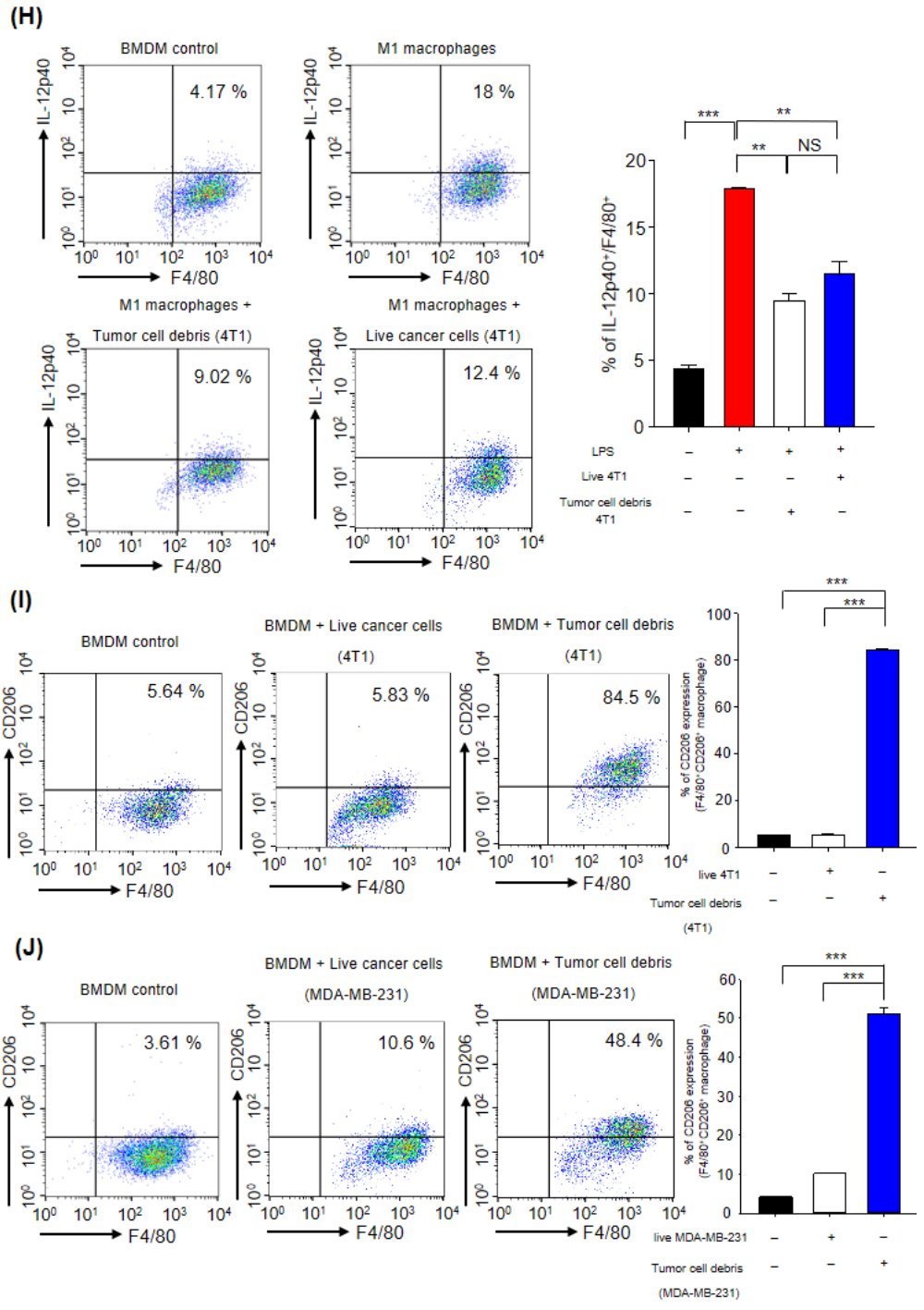
(H)
BMDM control
4.17 %
M1 macrophages
18 %
M1 macrophages +
Tumor cell debris (4T1)
9.02 %
M1 macrophages +
Live cancer cells (4T1)
12.4 %
IL-12p40
F4/80
% of IL-12p40+/F4/80+
***
**
NS
LPS
Live 4T1
Tumor cell debris 4T1
(I)
BMDM control
5.64 %
BMDM + Live cancer cells (4T1)
5.83 %
BMDM + Tumor cell debris (4T1)
84.5 %
CD206
% of CD206 expression (F4/80+CD206+ macrophage)
live 4T1
Tumor cell debris (4T1)
(J)
BMDM control
3.61 %
BMDM + Live cancer cells (MDA-MB-231)
10.6 %
BMDM + Tumor cell debris (MDA-MB-231)
48.4 %
live MDA-MB-231
Tumor cell debris (MDA-MB-231)

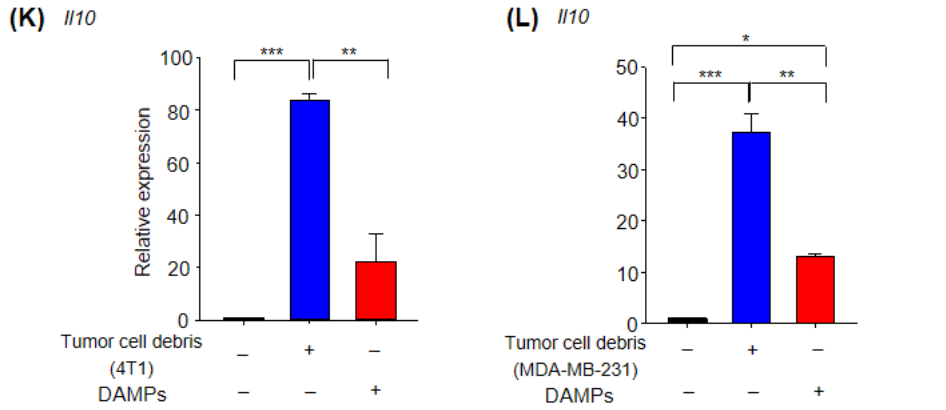
(K) Il10
Relative expression
100
80
60
40
20
0
***
**
Tumor cell debris
(4T1)
DAMPs
– + –
– – +
(L) Il10
50
40
30
20
10
0
*
***
**
Tumor cell debris
(MDA-MB-231)
DAMPs
– + –
– – +

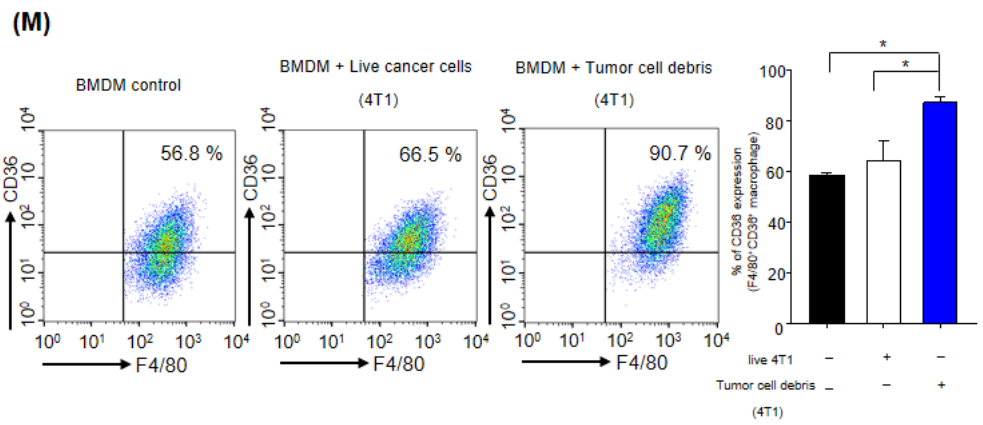
(M)
BMDM control
BMDM + Live cancer cells
(4T1)
BMDM + Tumor cell debris
(4T1)
56.8 %
66.5 %
90.7 %
CD36
F4/80
% of CD36 expression
(F4/80+CD36+ macrophage)
live 4T1
Tumor cell debris
(4T1)

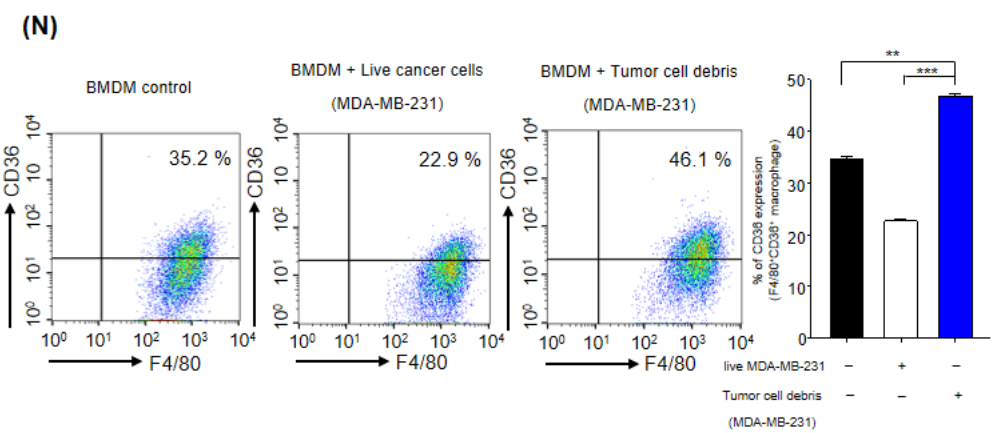
(N)
BMDM control
BMDM + Live cancer cells
(MDA-MB-231)
BMDM + Tumor cell debris
(MDA-MB-231)
35.2 %
22.9 %
46.1 %
CD36
F4/80
% of CD36 expression
(F4/80+CD36+ macrophage)
live MDA-MB-231
Tumor cell debris
(MDA-MB-231)

Figure 2. PTX-generated tumor cell debris contributes to macrophage polarization.

(A) Phagocytosis of breast tumor cell debris was analyzed as the proportion of macrophages found to contain intracellular EpCAM, as assessed by flow cytometry. (B) Whole tumors were processed into single cells. $CD45^+CD11b^+$ myeloid cells were isolated, cytospun onto glass slides, and subjected to immunofluorescence analysis for identification of breast tumor cell debris ($EpCAM^+$) phagocytosed by macrophages ($F4/80^+$). (C, D) BMDMs were treated with 100 ng/ml LPS for 24 h to cause them to skew toward the M1 phenotype. The mRNA expression levels of *Tnf* (C) and *Il12b* (D) in M1-polarized macrophages treated with or without 4T1 cell debris for 30 h were measured by qPCR. (E, F) qPCR analysis of *Tnf* (E) and *Il12b* (F) in M1-polarized macrophages treated with or without MDA-MB-231 cell debris for 30 h. (G, H) M1-polarized macrophages were co-cultured with viable tumor cells or tumor cell debris for 30 h. The percentages of macrophages expressing TNF-α (G) and IL-12p40 (H) were analyzed by flow cytometry. (I) Macrophages were co-cultured with viable 4T1 cells or 4T1 tumor cell debris for 24 h, and the CD206 expression of macrophages was analyzed by flow cytometry. (J) Macrophages were co-cultured with viable MDA-MB-231 tumor cells or MDA-MB-231 tumor cell debris for 24

h, and the proportion of macrophages expressing CD206 was analyzed by flow cytometry. (K) The *Il10* mRNA levels of macrophages incubated for 8 h with or without 4T1 cell debris or DAMPs from 4T1 tumor cell debris were analyzed by qPCR. (L) The mRNA expression of *Il10* in macrophages treated with MDA-MB-231 cell debris or DAMPs from MDA-MB-231 cell debris for 8 h was assessed by qPCR. (M) The expression of CD36 in macrophages co-cultured with viable 4T1 cells or 4T1 tumor cell debris for 24 h was analyzed by flow cytometry. (N) The CD36 expression in macrophages among BMDMs co-cultured with viable MDA-MB-231 cells or MDA-MB-231 tumor cell debris for 24 h was analyzed by flow cytometry. The significance of differences between groups was determined by one-way ANOVA (Tukey's post hoc test) and the Student's *t*-test was used to compare results obtained from the control and experimental conditions. *$p < 0.05$, **$p < 0.01$, and ***$p < 0.001$. NS: not significant.

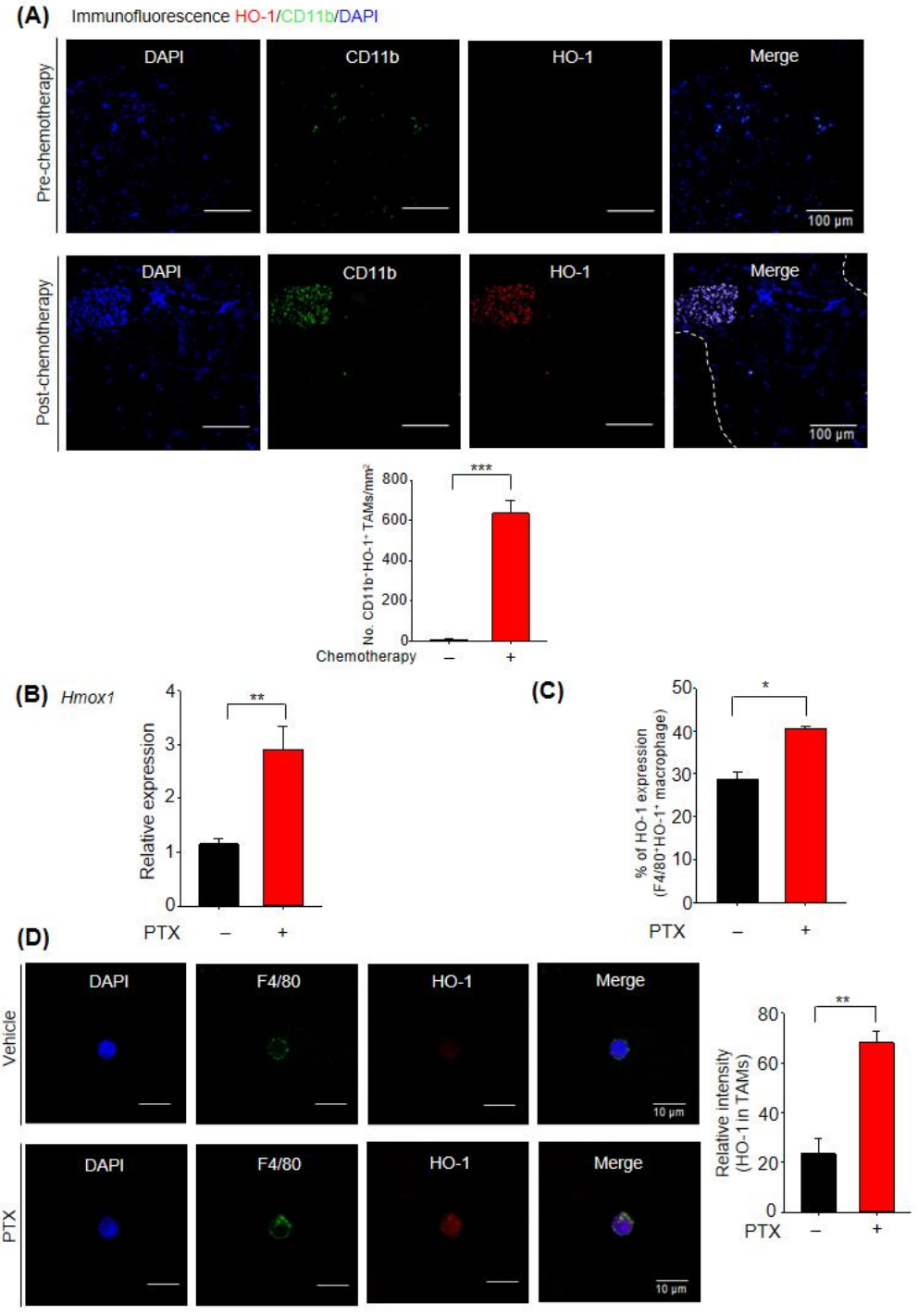
(A)
Immunofluorescence HO-1/CD11b/DAPI
Pre-chemotherapy
Post-chemotherapy
DAPI
CD11b
HO-1
Merge
100 μm
No. CD11b+HO-1+ TAMs/mm2
Chemotherapy
(B)
Hmox1
Relative expression
PTX
(C)
% of HO-1 expression (F4/80+HO-1+ macrophage)
(D)
Vehicle
F4/80
10 μm
Relative intensity (HO-1 in TAMs)

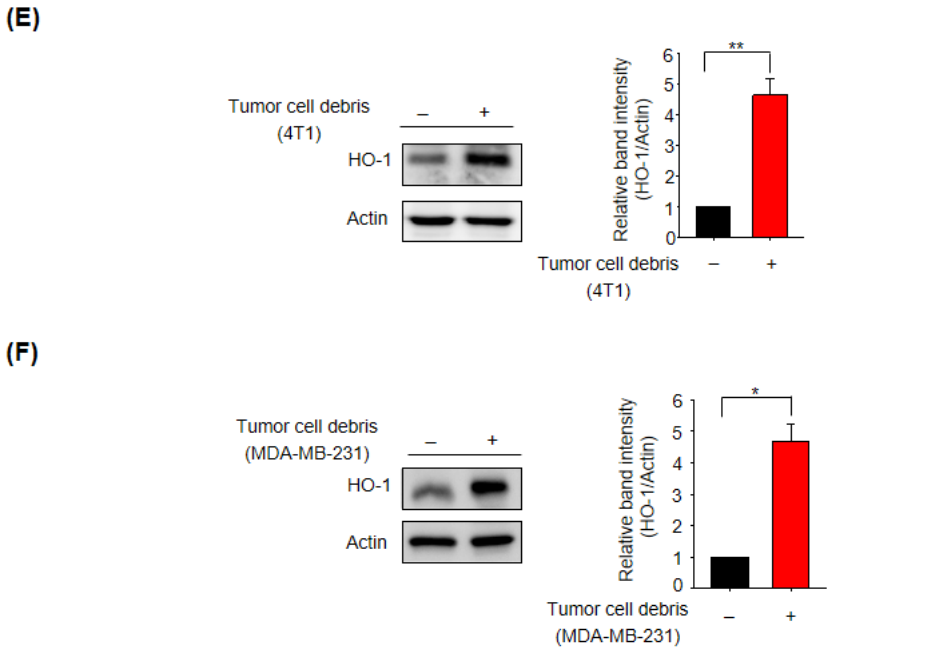
(E)
Tumor cell debris
(4T1)
–
+
HO-1
Actin
Relative band intensity
(HO-1/Actin)
**
Tumor cell debris
(4T1)
(F)
Tumor cell debris
(MDA-MB-231)
HO-1
Actin
*
Tumor cell debris
(MDA-MB-231)

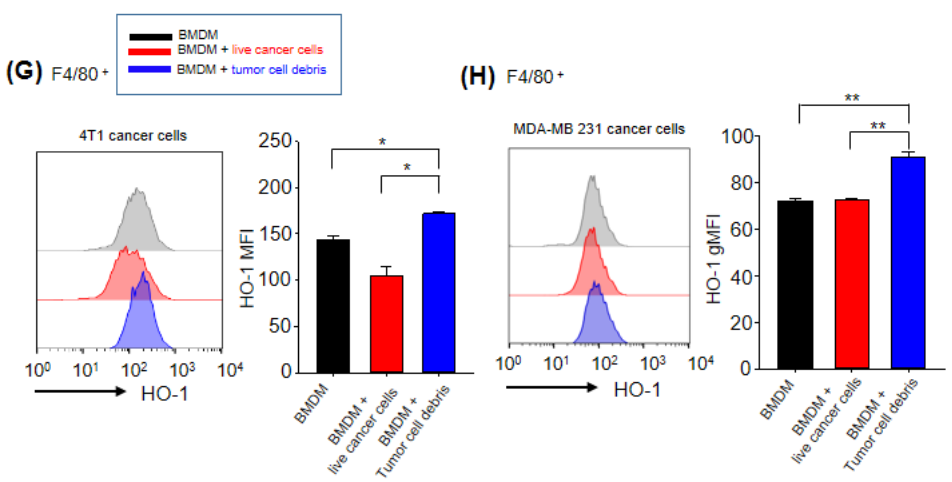
(G) F4/80+
BMDM
BMDM + live cancer cells
BMDM + tumor cell debris
4T1 cancer cells
HO-1
HO-1 MFI
BMDM
BMDM + live cancer cells
BMDM + Tumor cell debris
(H) F4/80+
MDA-MB 231 cancer cells
HO-1
HO-1 gMFI

Figure 3. Phagocytosis of PTX-generated tumor cell debris induces HO-1 expression in macrophages.

(A) Representative images of tumor tissues from breast cancer patients receiving chemotherapy stained with CD11b and HO-1 are shown. (B) Relative mRNA levels of *Hmox1* in $CD45^{+}CD11b^{+}$ tumor-associated myeloid cells isolated from 4T1 tumors were assessed by qPCR. (C) The HO-1 expression levels of TAMs from 4T1 tumor-bearing mice injected with or without PTX were analyzed by flow cytometry. (D) Representative immunofluorescence images of HO-1 expression in TAMs. (E, F) The protein expression levels of HO-1 in macrophages co-incubated for 8 h with tumor cell debris generated from murine 4T1 (E) or human MDA-MB-231 (F) breast cancer cells were measured by Western blot analysis. (G, H) The HO-1 expression levels of macrophages ($F4/80^{+}$) cultured with viable cancer cells or tumor cell debris were analyzed by flow cytometry. Comparisons between the control and experimental groups were performed with the Student's *t*-test. One-way ANOVA (Tukey's post hoc test) was used to determine the significance of differences between groups. $*p < 0.05$, $**p < 0.01$, and $***p < 0.001$.

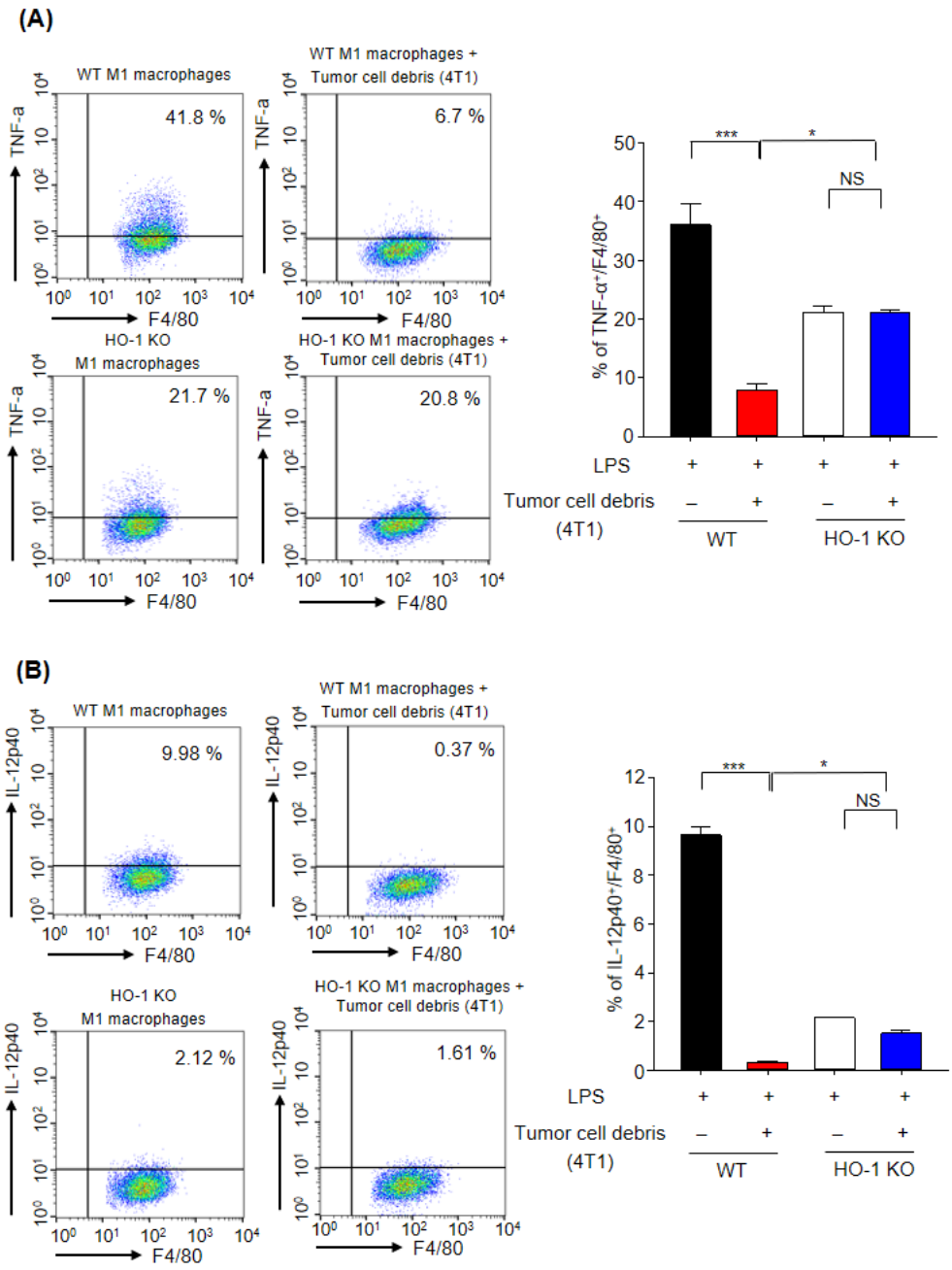
(A)
WT M1 macrophages
41.8 %
WT M1 macrophages +
Tumor cell debris (4T1)
6.7 %
HO-1 KO
M1 macrophages
21.7 %
HO-1 KO M1 macrophages +
Tumor cell debris (4T1)
20.8 %
TNF-a
F4/80
% of TNF-α+/F4/80+
***
*
NS
LPS
Tumor cell debris
(4T1)
WT
HO-1 KO
(B)
WT M1 macrophages
9.98 %
WT M1 macrophages +
Tumor cell debris (4T1)
0.37 %
HO-1 KO
M1 macrophages
2.12 %
HO-1 KO M1 macrophages +
Tumor cell debris (4T1)
1.61 %
IL-12p40
F4/80
% of IL-12p40+/F4/80+
***
*
NS
LPS
Tumor cell debris
(4T1)
WT
HO-1 KO

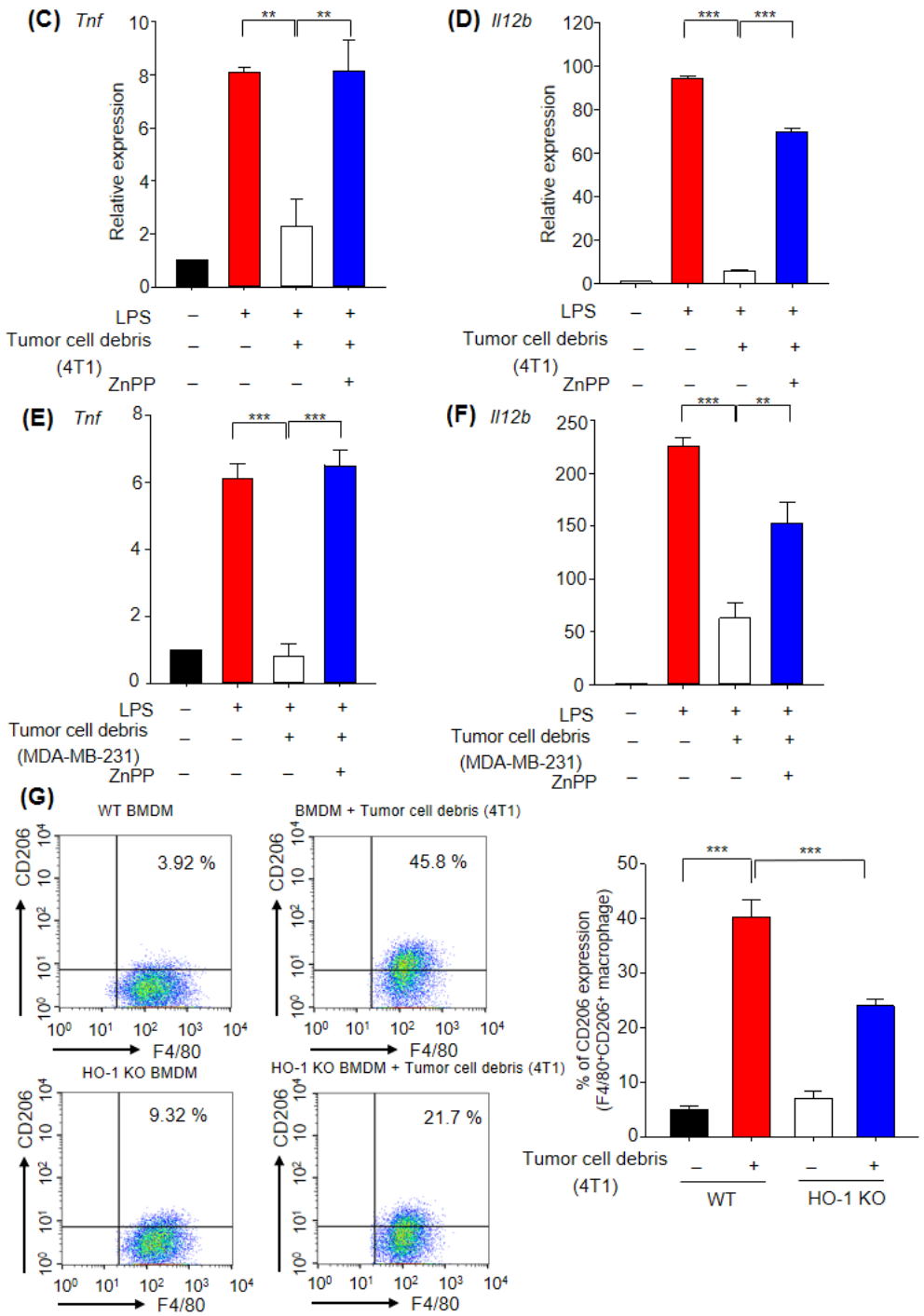
(C) Tnf
Relative expression
LPS
Tumor cell debris
(4T1)
ZnPP
(D) Il12b
Relative expression
LPS
Tumor cell debris
(4T1)
ZnPP
(E) Tnf
LPS
Tumor cell debris
(MDA-MB-231)
ZnPP
(F) Il12b
LPS
Tumor cell debris
(MDA-MB-231)
ZnPP
(G)
WT BMDM
3.92 %
BMDM + Tumor cell debris (4T1)
45.8 %
HO-1 KO BMDM
9.32 %
HO-1 KO BMDM + Tumor cell debris (4T1)
21.7 %
CD206
F4/80
% of CD206 expression
(F4/80+CD206+ macrophage)
Tumor cell debris
(4T1)
WT
HO-1 KO

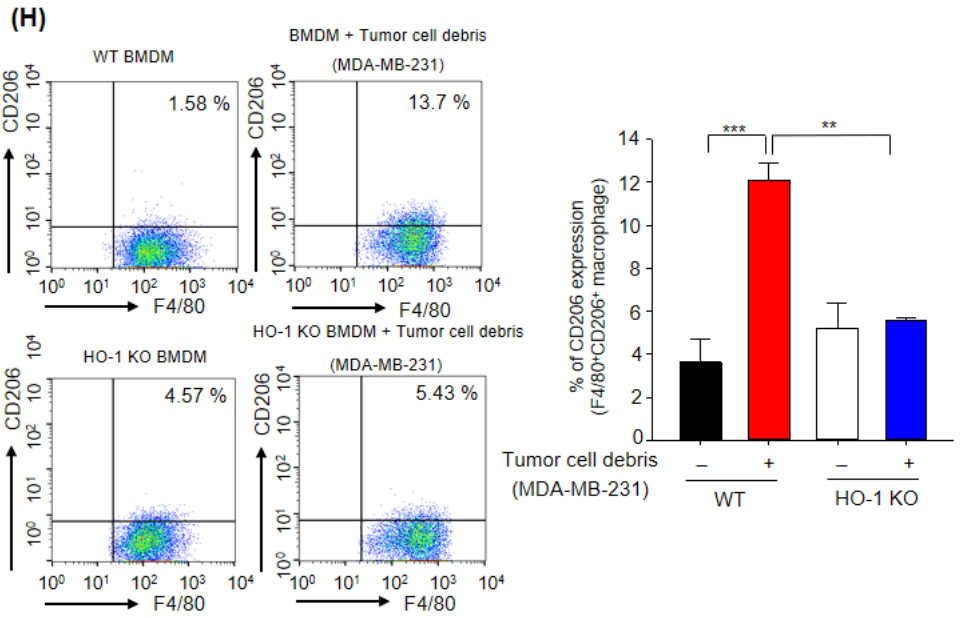
(H)
WT BMDM
1.58 %
BMDM + Tumor cell debris
(MDA-MB-231)
13.7 %
HO-1 KO BMDM
4.57 %
HO-1 KO BMDM + Tumor cell debris
(MDA-MB-231)
5.43 %
CD206
F4/80
% of CD206 expression
(F4/80+CD206+ macrophage)
***
**
Tumor cell debris
(MDA-MB-231)
WT
HO-1 KO

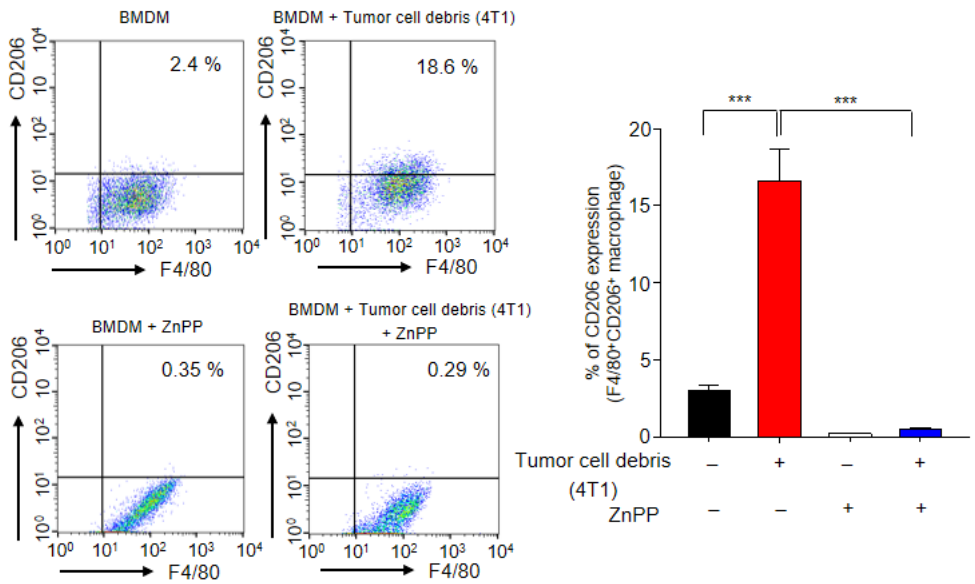
(I)
BMDM
2.4 %
BMDM + Tumor cell debris (4T1)
18.6 %
BMDM + ZnPP
0.35 %
BMDM + Tumor cell debris (4T1)
+ ZnPP
0.29 %
CD206
F4/80
% of CD206 expression
(F4/80+CD206+ macrophage)
***
***
Tumor cell debris
(4T1)
ZnPP

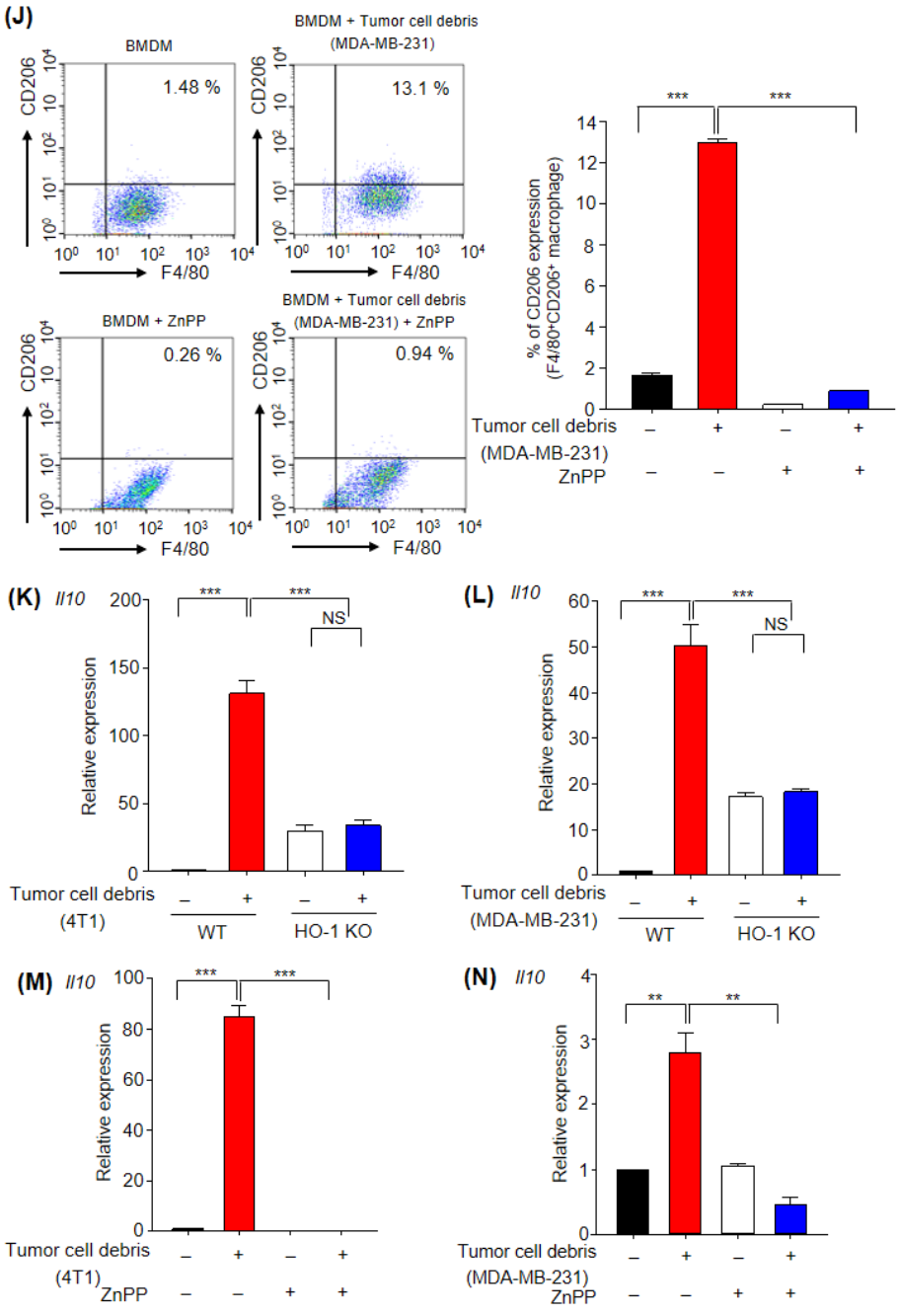
(J)
BMDM
1.48 %
BMDM + Tumor cell debris
(MDA-MB-231)
13.1 %
BMDM + ZnPP
0.26 %
BMDM + Tumor cell debris
(MDA-MB-231) + ZnPP
0.94 %
CD206
F4/80
% of CD206 expression
(F4/80+CD206+ macrophage)
Tumor cell debris
(MDA-MB-231)
ZnPP
(K) Il10
Relative expression
Tumor cell debris
(4T1)
WT
HO-1 KO
NS
(L) Il10
Relative expression
Tumor cell debris
(MDA-MB-231)
WT
HO-1 KO
NS
(M) Il10
Relative expression
Tumor cell debris
(4T1)
ZnPP
(N) Il10
Relative expression
Tumor cell debris
(MDA-MB-231)
ZnPP

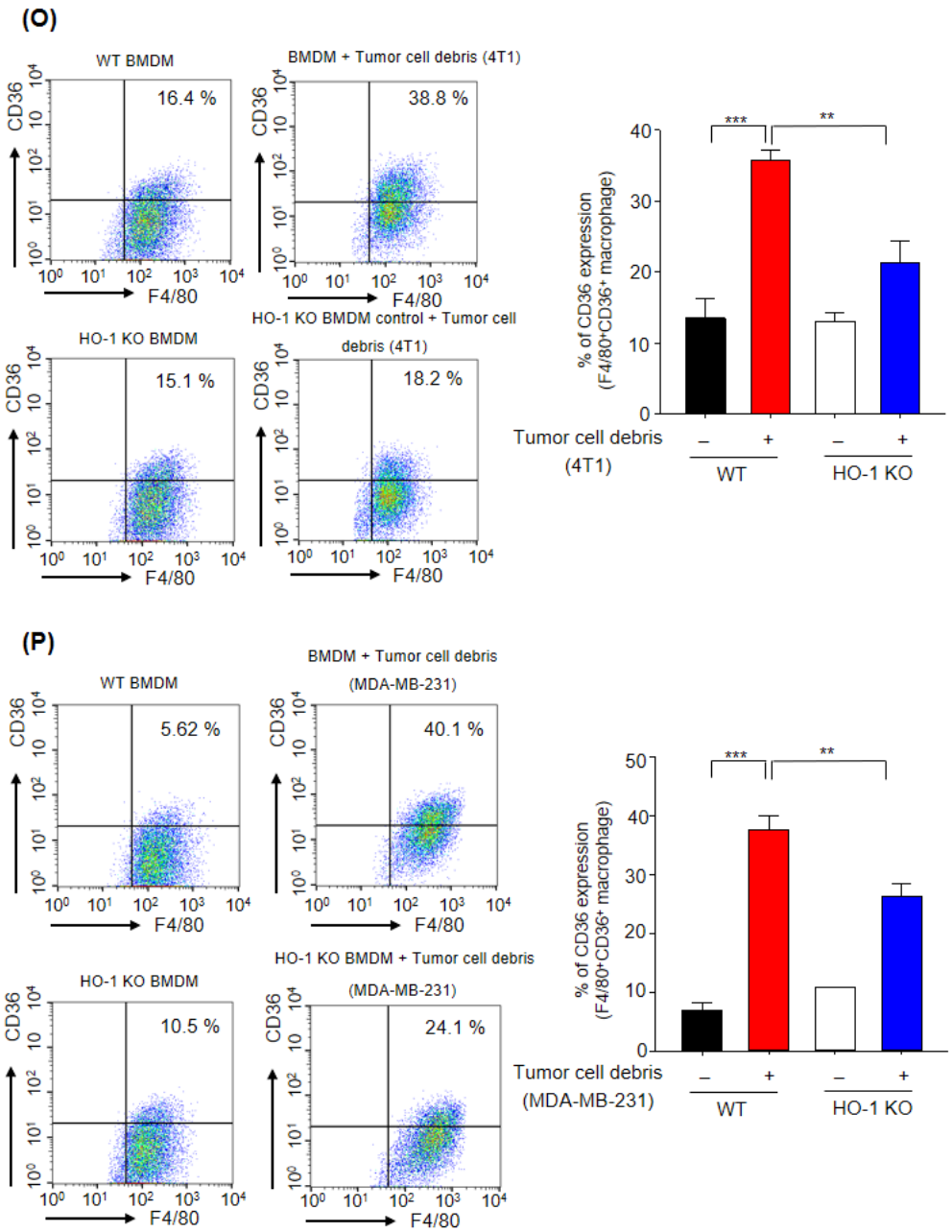
(O)
WT BMDM
16.4 %
BMDM + Tumor cell debris (4T1)
38.8 %
HO-1 KO BMDM
15.1 %
HO-1 KO BMDM control + Tumor cell debris (4T1)
18.2 %
CD36
F4/80
% of CD36 expression (F4/80+CD36+ macrophage)
***
**
Tumor cell debris (4T1)
WT
HO-1 KO
(P)
WT BMDM
5.62 %
BMDM + Tumor cell debris (MDA-MB-231)
40.1 %
HO-1 KO BMDM
10.5 %
HO-1 KO BMDM + Tumor cell debris (MDA-MB-231)
24.1 %
Tumor cell debris (MDA-MB-231)

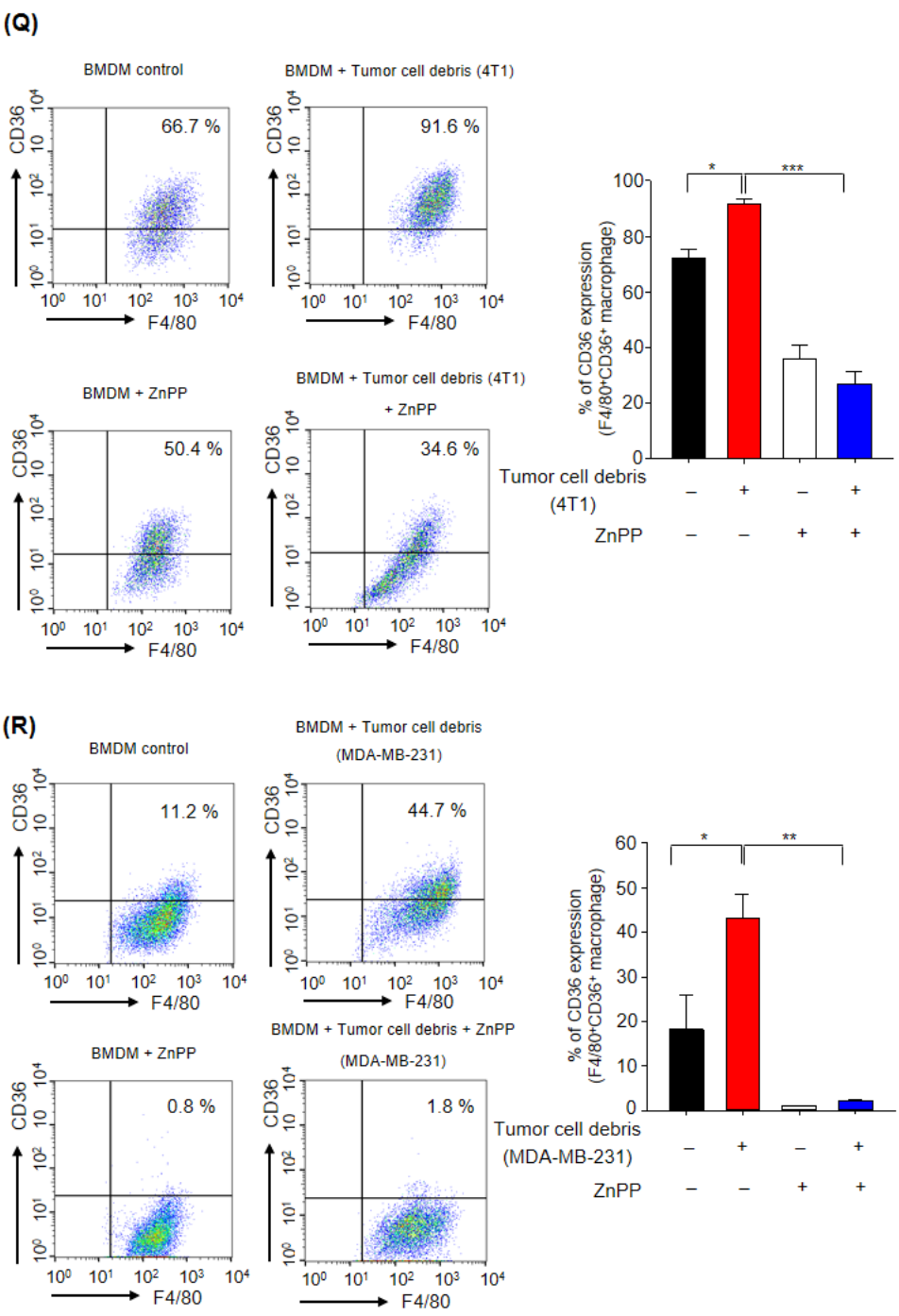
(Q)
BMDM control
66.7 %
BMDM + Tumor cell debris (4T1)
91.6 %
BMDM + ZnPP
50.4 %
BMDM + Tumor cell debris (4T1)
+ ZnPP
34.6 %
CD36
F4/80
% of CD36 expression
(F4/80+CD36+ macrophage)
Tumor cell debris
(4T1)
ZnPP
(R)
BMDM control
11.2 %
BMDM + Tumor cell debris
(MDA-MB-231)
44.7 %
BMDM + ZnPP
0.8 %
BMDM + Tumor cell debris + ZnPP
(MDA-MB-231)
1.8 %
Tumor cell debris
(MDA-MB-231)
ZnPP

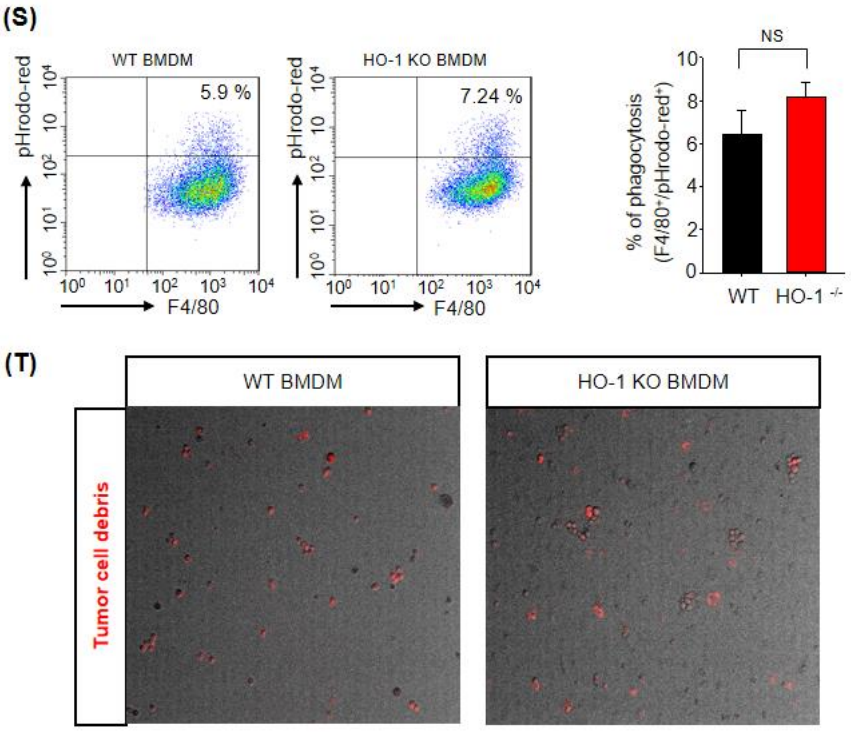
(S)
WT BMDM
5.9 %
HO-1 KO BMDM
7.24 %
pHrodo-red
F4/80
NS
% of phagocytosis
(F4/80+/pHrodo-red+)
WT
HO-1 -/-
(T)
WT BMDM
HO-1 KO BMDM
Tumor cell debris

Figure 4. Tumor cell debris-induced HO-1 expression is crucial for the modulation of macrophage polarization.

(A, B) BMDMs from WT or HO-1 KO mice were treated with LPS (100 ng/ml) for 24 h. The resulting M1-polarized macrophages were co-cultured with 4T1 tumor cell debris for 30 h. The proportion of macrophages expressing TNF-α (A) and IL-12p40 (B) was determined by flow cytometry. (C, D) BMDMs were treated with LPS (100 ng/ml) for 24 h, and the obtained M1-polarized macrophages were incubated with ZnPP (1 μM) or vehicle for 1 h. The mRNA expression levels of *Tnf* (C) and *Il12b* (D) in the above-treated macrophages co-cultured with or without 4T1 cell debris for 30 h were measured by qPCR. (E, F) WT BMDMs were treated with LPS (100 ng/ml) for 24 h. M1-polarized macrophages were pre-treated with ZnPP (1 μM) for 1 h, and co-cultured with or without MDA-MB-231 cell debris for 30 h. The mRNA expression levels of *Tnf* (E) and *Il12b* (F) were measured by qPCR. (G) BMDMs from WT or HO-1 KO mice were co-treated with 4T1 tumor cell debris for 24 h, and the expression of CD206 in macrophages was analyzed by flow cytometry. (H) BMDMs from WT or HO-1 KO mice were co-cultured with or without MDA-MB-231 tumor cell debris for 24 h, and the CD206 expression in macrophages was analyzed by flow cytometry. (I) WT BMDMs pre-treated with ZnPP (10 μM) for 1 h were co-cultured

with or without 4T1 tumor cell debris. After 24 h of incubation, the CD206 expression of macrophages was assessed by flow cytometry. (J) WT BMDMs pre-treated with ZnPP (10 μM) for 1 h were co-cultured with or without MDA-MB-231 tumor cell debris for 24 h, and the CD206 expression of macrophages was analyzed by flow cytometry. (K) BMDMs from WT or HO-1 KO mice were co-cultured with or without 4T1 tumor cell debris for 8 h, and the mRNA levels of *Il10* were analyzed by qPCR. (L) BMDMs from WT or HO-1 KO mice were co-cultured with or without MDA-MB-231 tumor cell debris for 8 h, and the mRNA levels of *Il10* were analyzed by qPCR. (M) WT BMDMs pre-treated with ZnPP (10 μM) for 1 h were co-incubated with or without 4T1 breast cancer cell debris for 8 h, and the mRNA levels of *Il10* were analyzed by qPCR. (N) WT BMDMs pre-treated with ZnPP (10 μM) for 1 h were co-incubated with or without MDA-MB-231 tumor cell debris for 8 h, and the mRNA levels of *Il10* were analyzed by qPCR. (O) BMDMs from WT or HO-1 KO mice treated with tumor cell debris for 24 h, and the expression of CD36 in macrophages was analyzed by flow cytometry. (P) BMDMs from WT or HO-1 KO mice were treated with MDA-MB-231 tumor cell debris for 24 h, and the CD36 expression in macrophages was analyzed by flow cytometry. (Q, R) Macrophages pre-treated with ZnPP (10 μM) for 1 h were co-incubated with or without breast cancer cell debris for 24 h, and the expression of CD36 in macrophages was

assessed by flow cytometry. (S, T) Macrophages from WT or HO-1 KO mice were co-incubated with tumor cell debris. The phagocytosis of cell debris was quantified as the proportion of macrophages ($F4/80^+$) containing intracellular tumor cell debris ($pHrodo^+$), as assessed by flow cytometry (S) and immunofluorescence (T). Data were analyzed with the Student's *t*-test. The significance of differences between experimental groups was determined using one-way ANOVA (Tukey's post hoc test). *$p < 0.05$, **$p < 0.01$, and ***$p < 0.001$. NS: not significant.

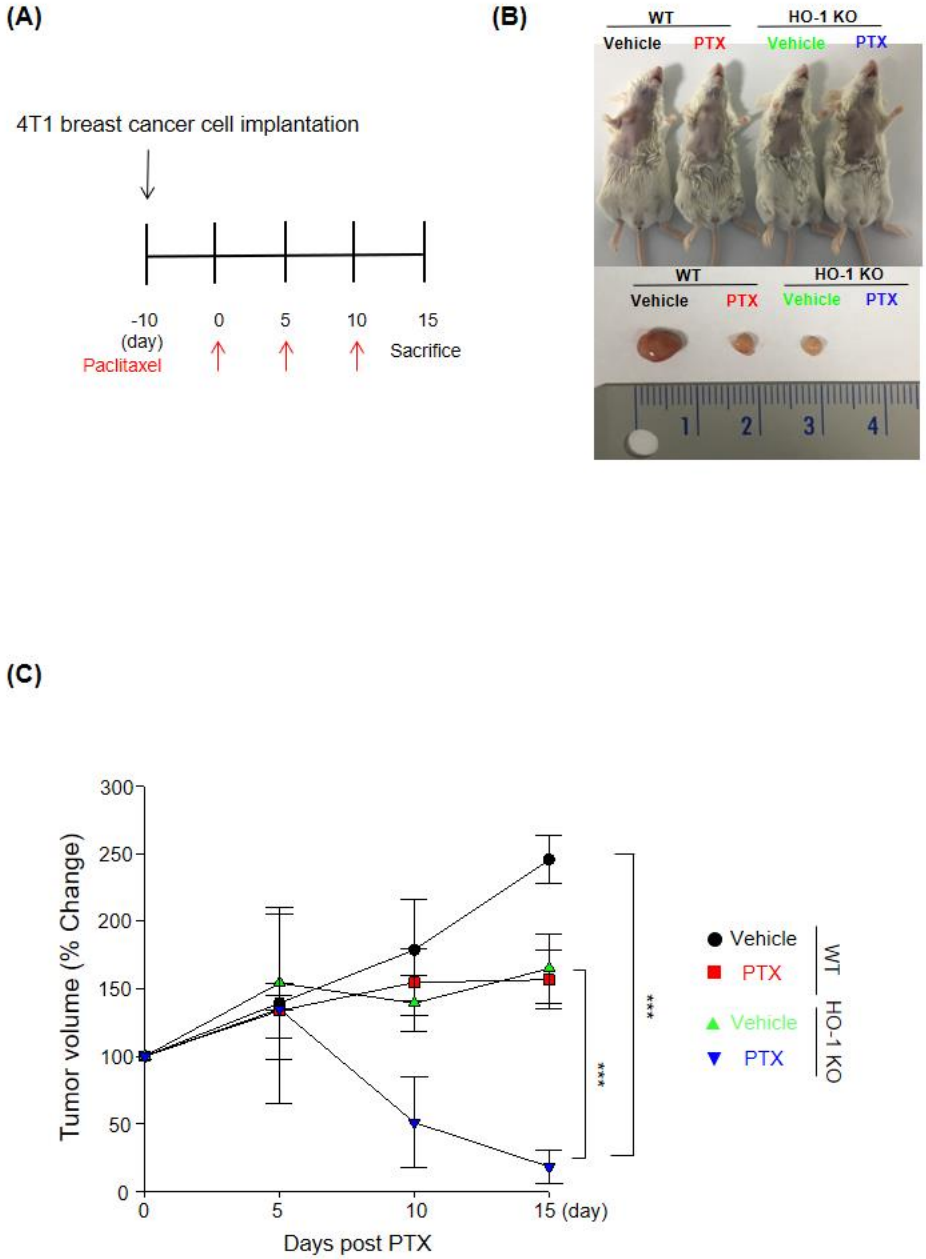
(A)
4T1 breast cancer cell implantation
-10
(day)
Paclitaxel
0
5
10
15
Sacrifice
(B)
WT
HO-1 KO
Vehicle
PTX
Vehicle
PTX
WT
HO-1 KO
Vehicle
PTX
Vehicle
PTX
1
2
3
4
(C)
Tumor volume (% Change)
300
250
200
150
100
50
0
0
5
10
15 (day)
Days post PTX
***
***
Vehicle
PTX
Vehicle
PTX
WT
HO-1 KO

(D)

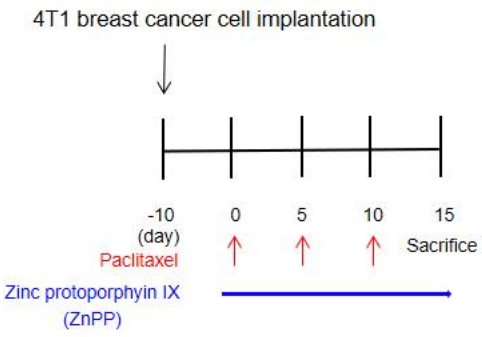
4T1 breast cancer cell implantation
-10
(day)
0
5
10
15
Sacrifice
Paclitaxel
Zinc protoporphyin IX
(ZnPP)

(E)

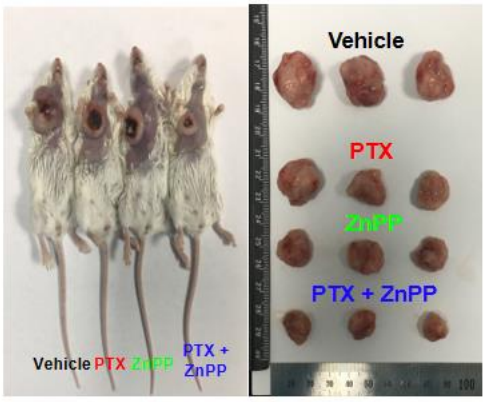
Vehicle
PTX
ZnPP
PTX + ZnPP
Vehicle PTX ZnPP
PTX +
ZnPP

(F)

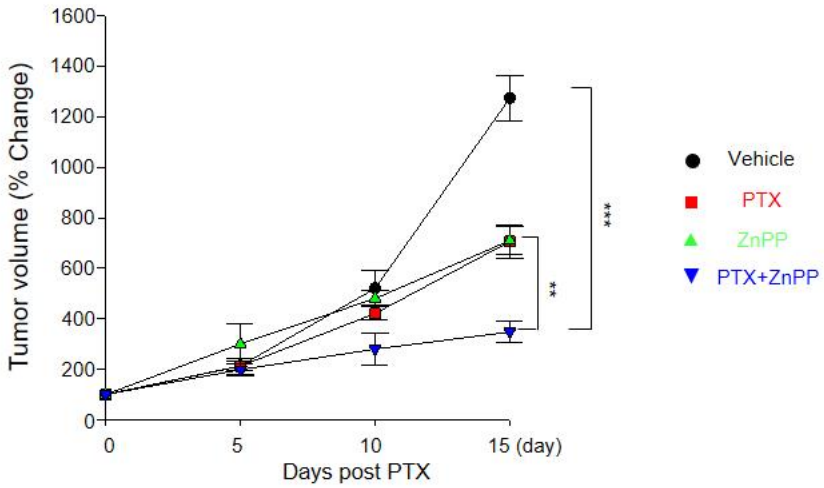
Tumor volume (% Change)
1600
1400
1200
1000
800
600
400
200
0
0
5
10
15 (day)
Days post PTX
**
***
Vehicle
PTX
ZnPP
PTX+ZnPP

Figure 5. Inactivation of HO-1 sensitizes the host response to PTX therapy.

(A) WT or HO-1 KO mice implanted with 4T1 tumors were intraperitoneally injected with vehicle or PTX (5 mg/kg, 5 days). (B) Representative images are shown for each group. (C) Tumor volume was calculated as a relative volume change and plotted as the total mean ± SEM (D) Mice implanted with 4T1 tumor cells received vehicle or PTX (5 mg/kg, 5 days) with or without daily intraperitoneal injection of ZnPP (40 mg/kg). Mice were sacrificed on day 15 after PTX treatment, and tumors were collected. (E) Representative images of tumors are shown for each group. (F) Tumor volume was calculated as a relative change and plotted as the total mean ± SEM. The significance of the differences between experimental groups was determined using one-way ANOVA (Tukey's post hoc test). $^{**}p < 0.01$, and $^{***}p < 0.001$.

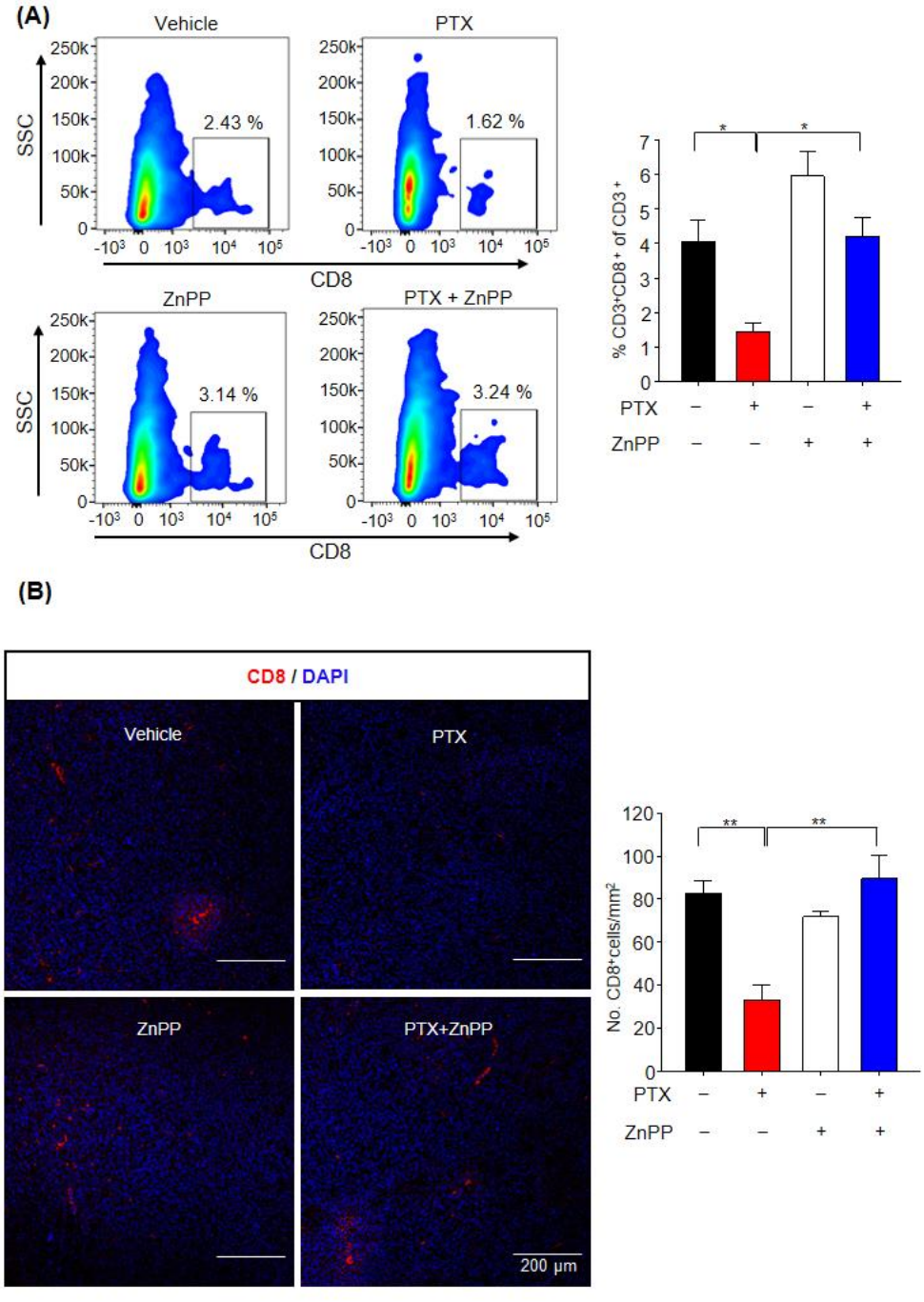
(A)
Vehicle
PTX
ZnPP
PTX + ZnPP
SSC
CD8
2.43 %
1.62 %
3.14 %
3.24 %
% CD3+CD8+ of CD3+
PTX
ZnPP
(B)
CD8 / DAPI
Vehicle
PTX
ZnPP
PTX+ZnPP
200 μm
No. CD8+cells/mm2

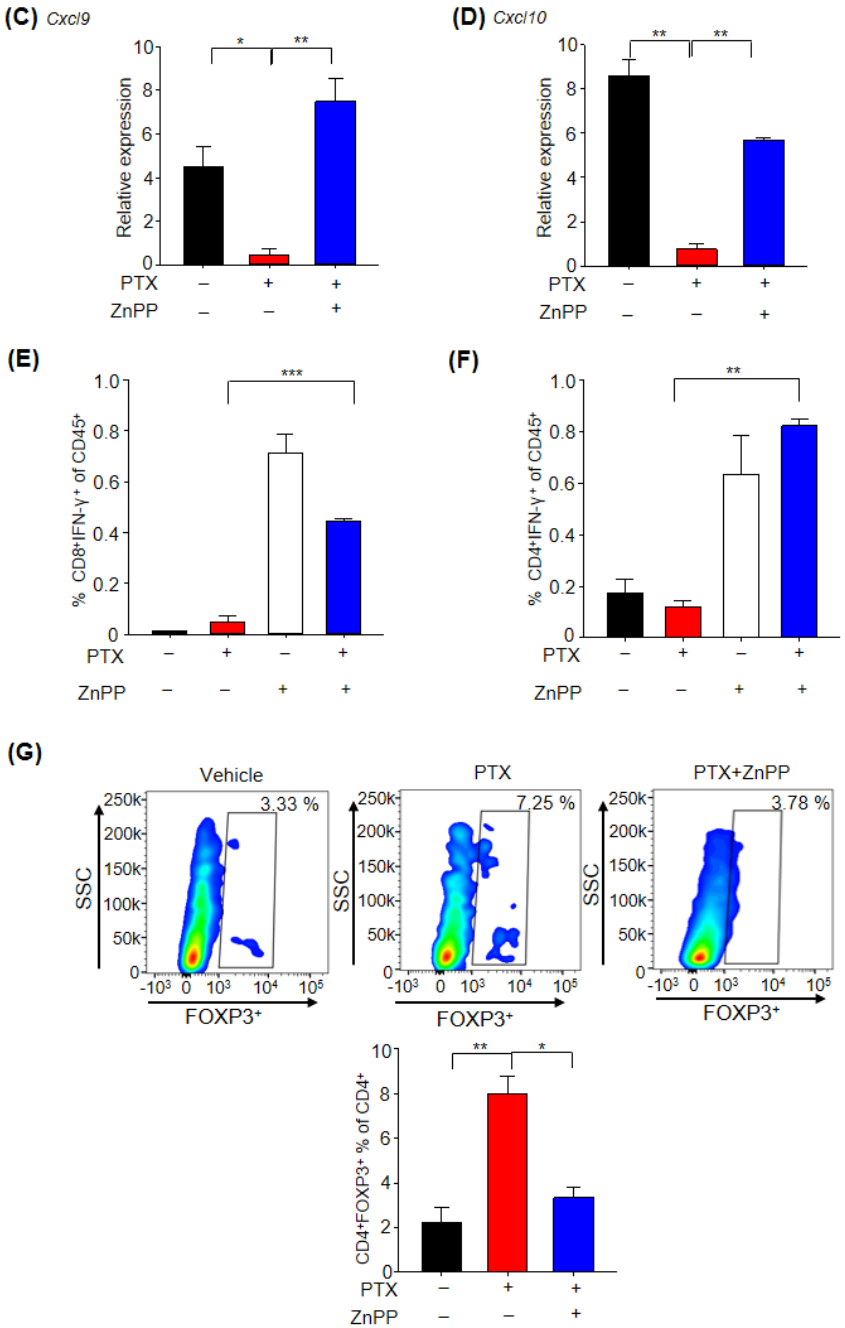
(C) Cxcl9
Relative expression
PTX
ZnPP
(D) Cxcl10
Relative expression
PTX
ZnPP
(E)
% CD8+IFN-γ+ of CD45+
PTX
ZnPP
(F)
% CD4+IFN-γ+ of CD45+
PTX
ZnPP
(G)
Vehicle
PTX
PTX+ZnPP
3.33 %
7.25 %
3.78 %
SSC
FOXP3+
CD4+FOXP3+ % of CD4+
PTX
ZnPP

(H)

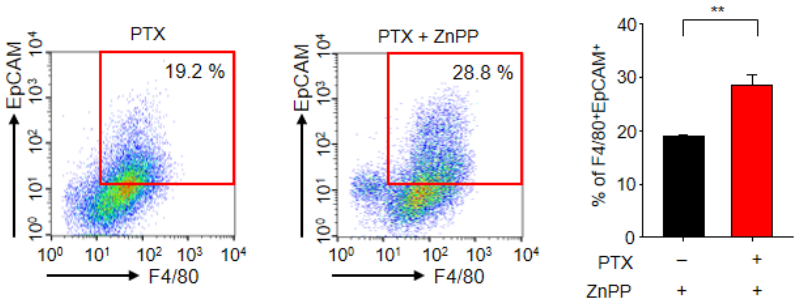
PTX
19.2 %
EpCAM
F4/80
PTX + ZnPP
28.8 %
EpCAM
F4/80
**
% of F4/80+EpCAM+
PTX
ZnPP

Figure 6. HO-1 inhibition increases T cell-mediated anti-tumor immunity in PTX therapy.

(A) $CD45^+CD3^+CD8^+$ tumor-infiltrating lymphocyte populations (as percentages) were identified by flow cytometry. (B) Representative images of tumor sections stained for $CD8^+$ T cells and DAPI are shown (C, D) The whole-tumor mRNA expression levels of *Cxcl9* (C) and *Cxcl10* (D) were analyzed by qPCR. (E) The percentages of IFN-γ^+CD8^+ T cells in $CD45^+$ populations were detected by flow cytometry. (F) The proportions of IFN-γ^+CD4^+ T cells in the $CD45^+$ populations were analyzed by flow cytometry. (G) The percentages of $Foxp3^+CD4^+$ T cells were analyzed by flow cytometry. (H) Engulfment of breast tumor cell debris was analyzed as the proportion of $F4/80^+$ macrophages found to contain intracellular EpCAM (a marker of breast tumor cell debris), as assessed by flow cytometry. Data were analyzed by the Student's *t*-test. The significance of the differences between experimental groups was determined using one-way ANOVA (Tukey's post hoc test). *$p < 0.05$, **$p < 0.01$, and ***$p < 0.001$.

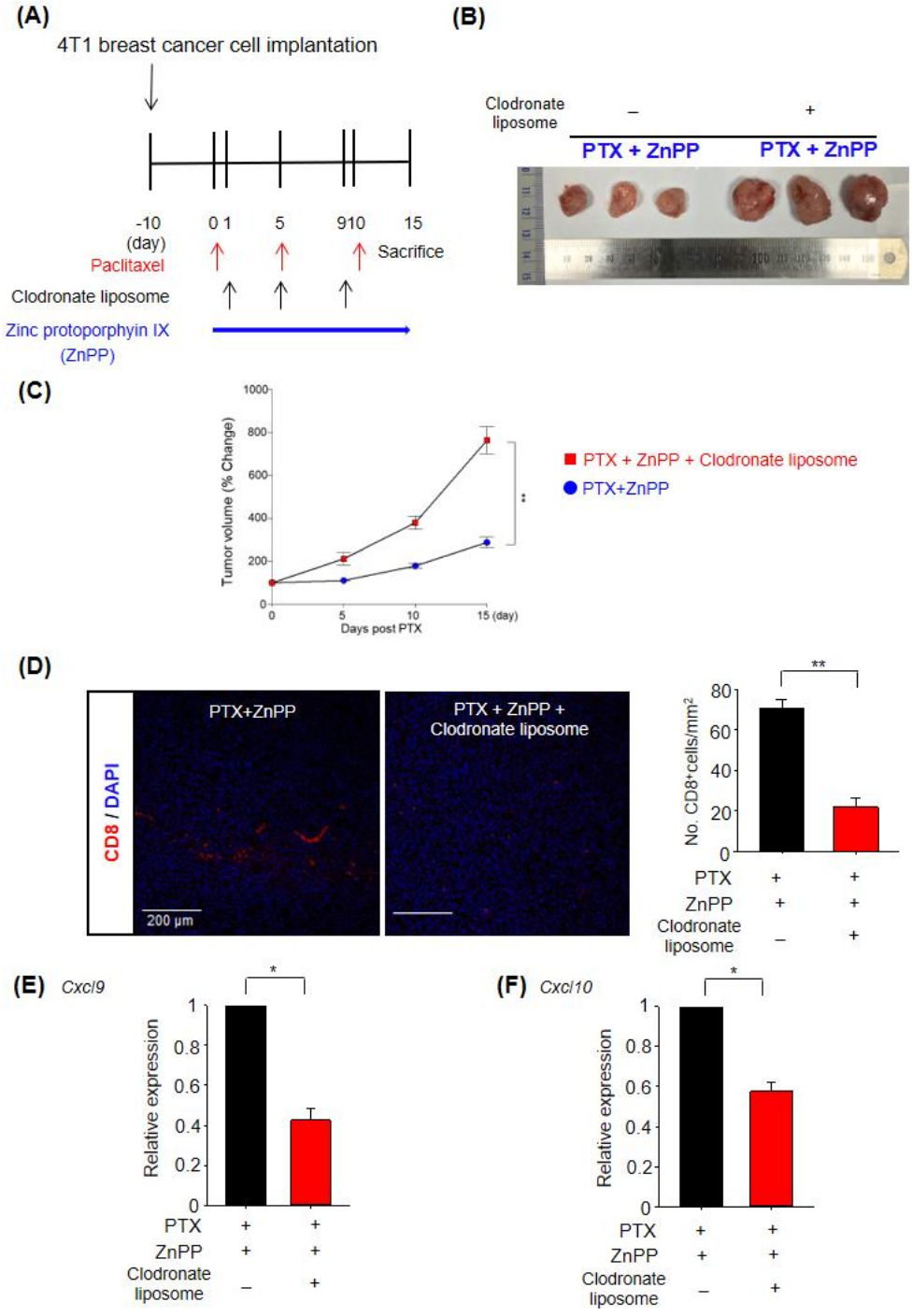
(A)
4T1 breast cancer cell implantation
-10
(day)
0 1
5
910
15
Sacrifice
Paclitaxel
Clodronate liposome
Zinc protoporphyin IX
(ZnPP)
(B)
Clodronate liposome
–
+
PTX + ZnPP
PTX + ZnPP
(C)
Tumor volume (% Change)
Days post PTX
PTX + ZnPP + Clodronate liposome
PTX+ZnPP
(D)
CD8 / DAPI
PTX+ZnPP
PTX + ZnPP + Clodronate liposome
200 μm
No. CD8+cells/mm2
PTX
ZnPP
Clodronate liposome
(E) Cxcl9
Relative expression
(F) Cxcl10
Relative expression

(G)

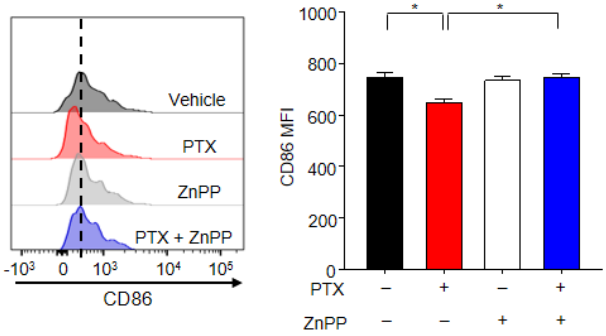
Vehicle
PTX
ZnPP
PTX + ZnPP
-10³ 0 10³ 10⁴ 10⁵
CD86
CD86 MFI
1000
800
600
400
200
0
*
*
PTX – + – +
ZnPP – – + +

(H) *Il10*

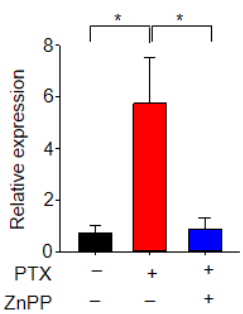
Relative expression
8
6
4
2
0
*
*
PTX – + +
ZnPP – – +

Figure 7. HO-1 inactivation-induced M1 TAMs are required for the enhancement of PTX therapy.

(A) 4T1 breast cancer-bearing mice were injected with vehicle or PTX (5 mg/kg, 5 days) in combination with daily intraperitoneal injection of ZnPP (40 mg/kg). For macrophage depletion, mice were treated with clodronate liposomes every 4 day. (B) Representative photographs of tumors are shown for each group. (C) Tumor volume was calculated as a relative change and plotted as the mean ± SEM. (D) Representative images of tumor sections stained for $CD8^+$ T cells and DAPI are shown. (E, F) The whole-tumor mRNA expression levels of *Cxcl9* and *Cxcl10* were analyzed by qPCR. (G) $CD45^+CD11b^+Ly6G^-Ly6C^-F4/80^+$ TAM subsets of 4T1 tumors were subjected to flow cytometry to measure CD86 expression. (H) The mRNA levels of *Il10* were measured in TAMs. Data were analyzed by Student's *t*-test. The significance of the differences between experimental groups was determined using one-way ANOVA (Tukey's post hoc test). *$p < 0.05$ and **$p < 0.01$.

(A)

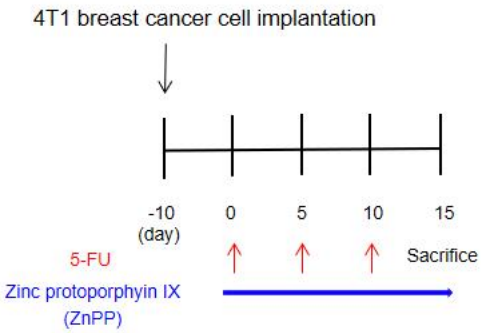
4T1 breast cancer cell implantation
-10
(day)
0
5
10
15
5-FU
Sacrifice
Zinc protoporphyin IX
(ZnPP)

(B)

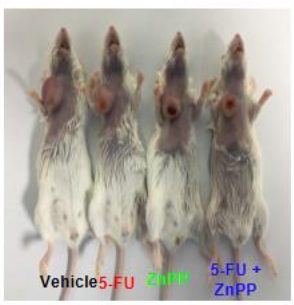
Vehicle
5-FU
ZnPP
5-FU +
ZnPP

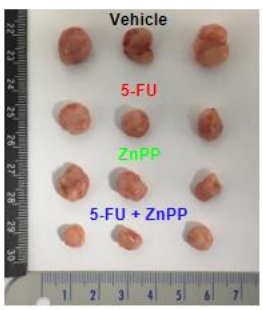
Vehicle
5-FU
ZnPP
5-FU + ZnPP

(C)

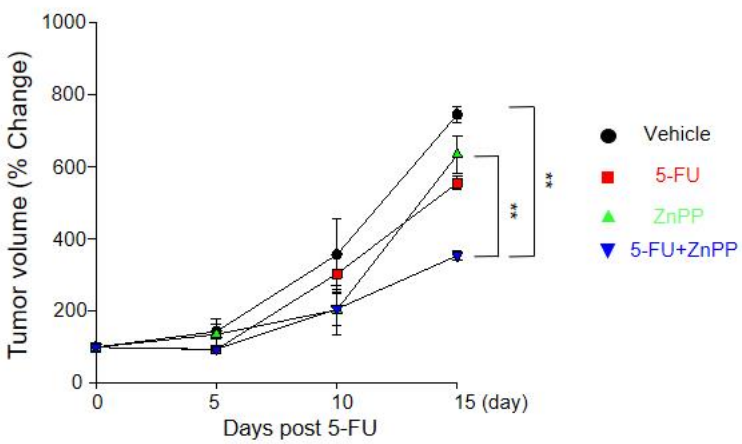
Tumor volume (% Change)
1000
800
600
400
200
0
0
5
10
15 (day)
Days post 5-FU
**
**
Vehicle
5-FU
ZnPP
5-FU+ZnPP

(D)

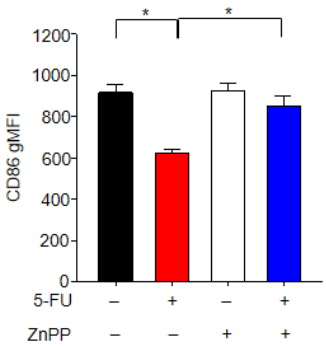
*
*
1200
1000
800
600
400
200
0
CD86 gMFI
5-FU – + – +
ZnPP – – + +

(E)

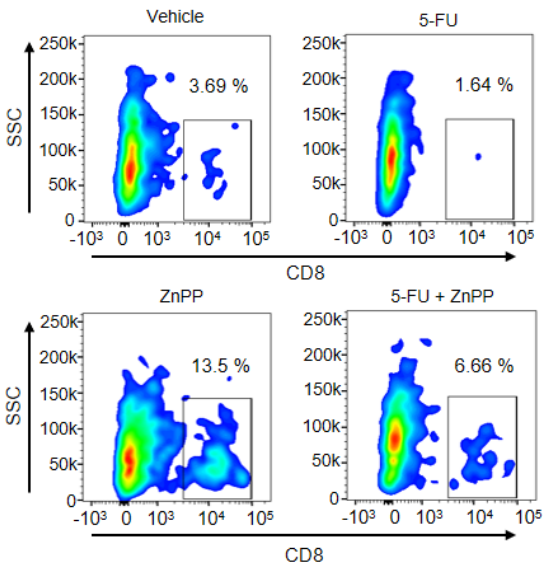
Vehicle
5-FU
ZnPP
5-FU + ZnPP
3.69 %
1.64 %
13.5 %
6.66 %
SSC
CD8
250k
200k
150k
100k
50k
0
-10³ 0 10³ 10⁴ 10⁵

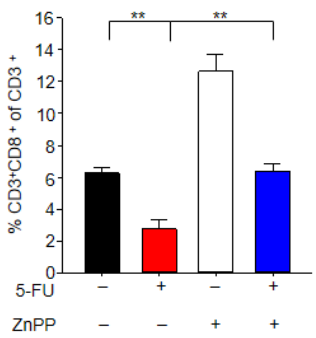
**
**
16
14
12
10
8
6
4
2
0
% CD3+CD8+ of CD3+
5-FU – + – +
ZnPP – – + +

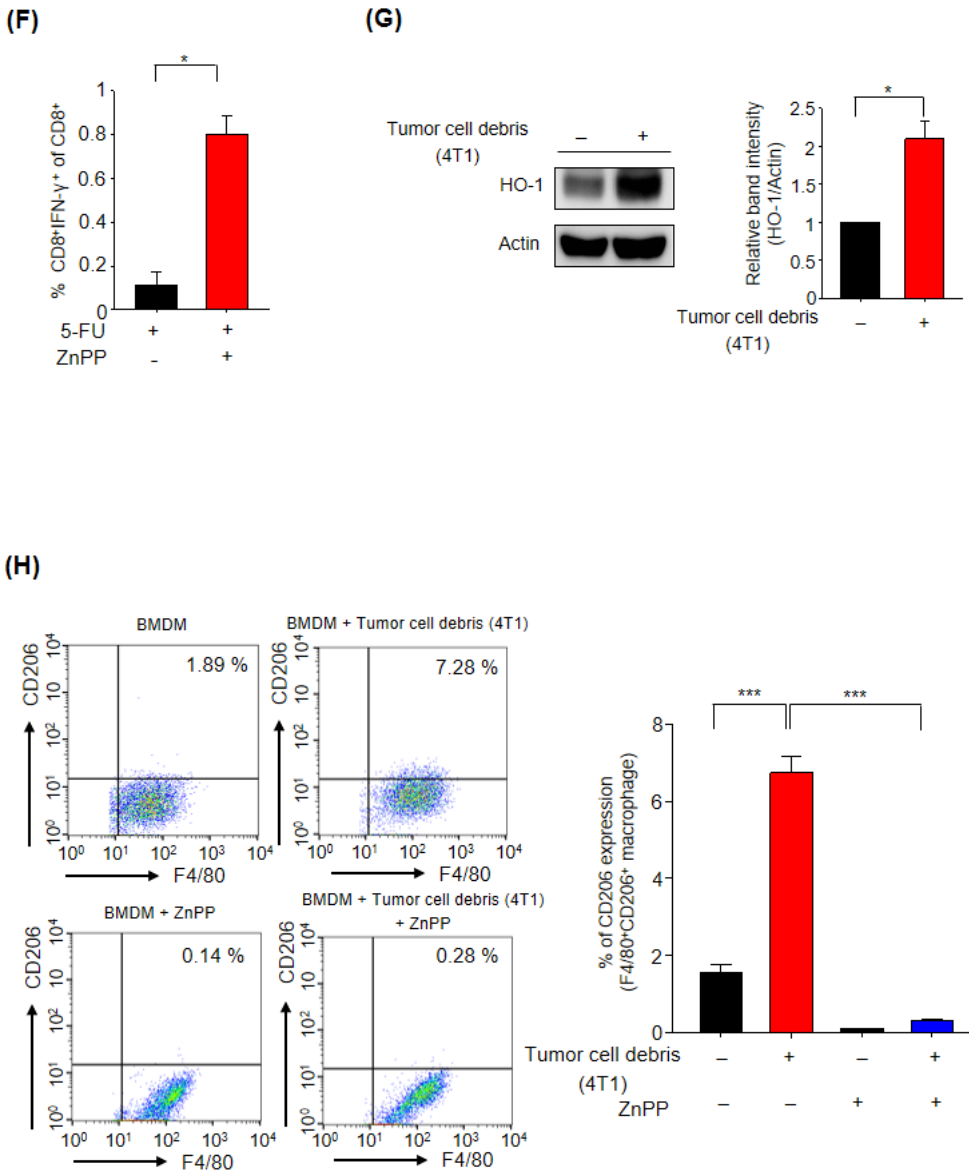
(F)
% CD8+IFN-γ+ of CD8+
5-FU
ZnPP
(G)
Tumor cell debris (4T1)
HO-1
Actin
Relative band intensity (HO-1/Actin)
(H)
BMDM
BMDM + Tumor cell debris (4T1)
BMDM + ZnPP
BMDM + Tumor cell debris (4T1) + ZnPP
CD206
F4/80
1.89 %
7.28 %
0.14 %
0.28 %
% of CD206 expression (F4/80+CD206+ macrophage)
Tumor cell debris (4T1)
ZnPP

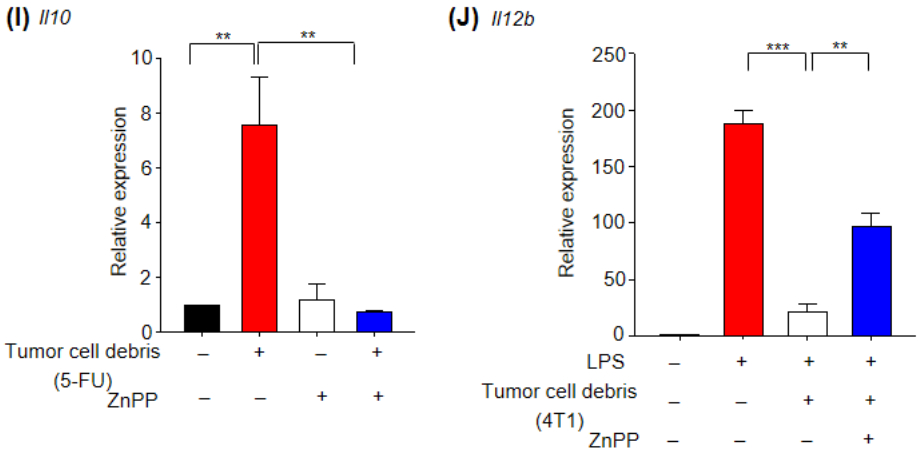
(I) Il10
**
**
Relative expression
10
8
6
4
2
0
Tumor cell debris
(5-FU)
ZnPP
– + – +
– – + +
(J) Il12b
***
**
Relative expression
250
200
150
100
50
0
LPS
Tumor cell debris
(4T1)
ZnPP
– + + +
– – + +
– – – +

Figure 8. The therapeutic efficacy of 5-FU is enhanced by co-treatment of HO-1 inhibitor in a 4T1 breast cancer mouse model.

(A) 4T1 tumor-bearing mice were administrated with vehicle or 5-fluorouracil (5-FU) (40 mg/kg) three times at 5-day intervals, while ZnPP (40 mg/kg) was given once a day. Mice were euthanized on day 15 after 5-FU treatment, and tumors were collected. (B) Representative photographs are shown for each group. (C) Tumor volume was calculated as a relative volume change and plotted as the total mean ± SEM. (D-G) Whole tumors were dissociated into single cells, and flow cytometry was used to identify the tumor-infiltrating immune cells. (D) $CD45^+CD11b^+Ly6G^-Ly6C^-F4/80^+$ TAM subsets of 4T1 tumors were gated and analyzed for CD86 expression by flow cytometry. The MFI of $CD86^+$ TAMs is shown for each group. (E) The percentages of $CD45^+CD3^+CD8^+$ tumor-infiltrating lymphocytes in tumors collected from mice of the various groups were assessed by flow cytometry. (F) The percentages of IFN-γ^+CD8^+ T cells among the $CD8^+$ T cells were determined by flow cytometry. (G) The HO-1 expression levels of macrophages ($F4/80^+$) co-cultured with or without tumor cell debris for 8 h were analyzed by Western blotting. (H) WT BMDMs pre-treated with ZnPP (10 μM) for 1 h were co-incubated with or without 5-FU-generated 4T1 tumor cell debris for 8 h, and the mRNA levels of *Il10* were analyzed

by qPCR. (I) BMDMs pre-treated with ZnPP (10 μM) for 1 h were co-incubated with or without 5-FU-generated 4T1 tumor cell debris for 8 h, and the mRNA levels of *Il10* were analyzed by qPCR. (J) BMDMs were treated with LPS (100 ng/ml) for 24 h, and the obtained M1-polarized macrophages were incubated or with ZnPP (1 μM) for 1 h. The mRNA expression levels of *Il12b* in the above-treated macrophages co-incubated with or without 4T1 cell debris for 30 h were measured by qPCR. Data were analyzed by the Student's *t*-test. The significance of the differences between experimental groups was determined using one-way ANOVA (Tukey's post hoc test). *$p < 0.05$, **$p < 0.01$, and ***$p < 0.001$.

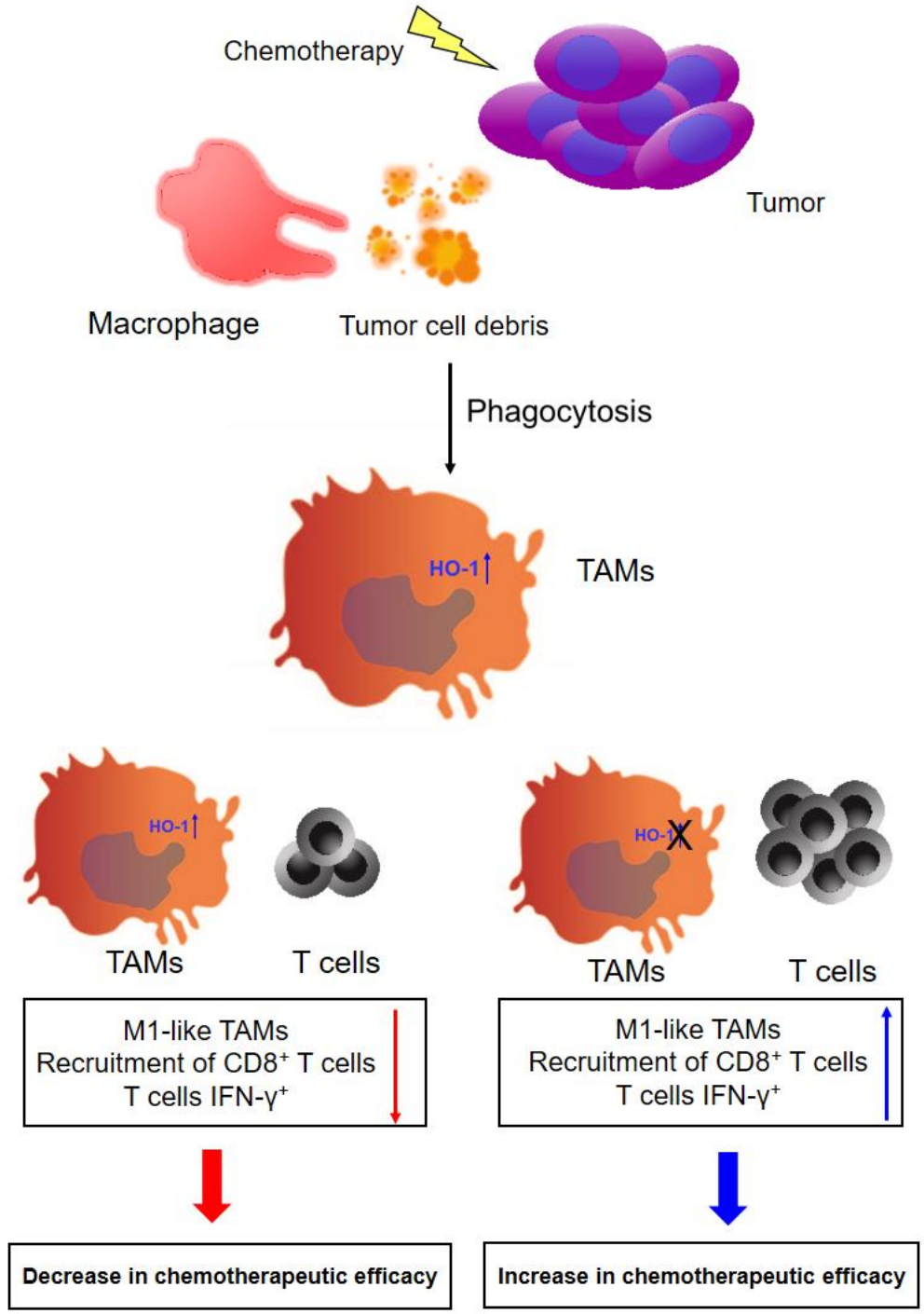
Chemotherapy
Tumor
Macrophage
Tumor cell debris
Phagocytosis
HO-1
TAMs
HO-1
TAMs
T cells
HO-1
TAMs
T cells
M1-like TAMs
Recruitment of CD8+ T cells
T cells IFN-γ+
M1-like TAMs
Recruitment of CD8+ T cells
T cells IFN-γ+
Decrease in chemotherapeutic efficacy
Increase in chemotherapeutic efficacy

Figure 9. Schematic representation of the mechanisms underlying TAM-mediated phagocytosis of tumor cell debris in the TME after chemotherapy.

Phagocytosis of tumor cell debris upregulates the HO-1 expression of macrophages upon chemotherapy. This overexpression of HO-1 regulates the polarization of TAMs in the TME. Therefore, reprogramming of TAMs by HO-1 inactivation is a potential strategy for improving the response to chemotherapy via enhancement of anti-tumor immunity.

4. Discussion

For decades, various anti-tumor therapies have utilized a wide array of strategies in an attempt to eliminate tumors (Sulciner et al., 2017; Weigert, Mora, Sekar, Syed, & Brune, 2016). However such therapies can trigger massive changes in aspects of the immune contexture, including the density, location and composition of tumor-infiltrating immune cells (Becht, Giraldo, Dieu-Nosjean, Sautes-Fridman, & Fridman, 2016; Fridman et al., 2017). Cytotoxic therapy can shift the TME toward an immunosuppressive environment, and thereby developing strategies to maintain a durable anti-tumor immune response during chemotherapy are required (Fridman et al., 2017; Hirata & Sahai, 2017; Ruffell et al., 2014). Therefore, reprogramming the TME to an immunogenic phenotype may potentiate therapeutic efficacy with the goal of tumor regression (Binnewies et al., 2018; Nagarsheth, Wicha, & Zou, 2017).

Chemotherapy-generated tumor cell debris has been shown to stimulate tumor growth, and this has critical implications for cancer therapy (J. Chang et al., 2018; Sulciner et al., 2017). PS presented on the surface of tumor cell debris can contribute to generation of an immunosuppressive TME (Kumar et al., 2017). A chemotherapy-induced immunosuppressive TME has been

shown to regulate macrophage polarization, and this has been associated with the therapeutic response of a tumor (Brown et al., 2017; Ubil et al., 2018). These results suggest that breast tumor cell debris generated during chemotherapy undergoes phagocytosis by macrophages, and this inhibits activation of the anti-tumor immune response-promoting M1 macrophage phenotype. Therefore, chemotherapeutic strategies that focus on killing cancer cells may act as a double-edged sword. In the TME, TAMs are a major source of HO-1, which mediates immune suppression in breast cancer (Arnold, Magiera, Kraman, & Fearon, 2014; Muliaditan et al., 2018). Here, I demonstrate that engulfed breast tumor cell debris stimulates the HO-1 expression of macrophages and thereby inhibits M1 macrophage polarization. Conversely, inactivation of HO-1 in macrophages enhances therapeutic efficacy by polarizing them toward the M1 phenotype. Impairment of LC3-associated phagocytosis (LAP) followed by engulfment of dying cancer cells was previously shown to regulate the polarization of macrophages toward the M1 phenotype (Cunha et al., 2018). This raises the possibility that tumor cell debris-induced HO-1 expression may regulate the immunomodulatory signaling of macrophage polarization via the LAP pathway. Collectively these results suggest that targeting tumor cell debris-induced HO-1 expression in macrophages could be a potential strategy to promote chemotherapeutic efficacy by switching macrophages to an

immune-stimulatory phenotype.

The major approaches currently used to target TAMs for anti-cancer therapy include depleting them or reprogramming to attain an anti-tumor phenotype (Guerriero, 2018; Mantovani et al., 2017). The targeting of PS receptors, which recognize dead tumor cells, has been shown to yield therapeutic effects by reprogramming TAMs to the M1 phenotype (Georgoudaki et al., 2016; Kumar et al., 2017; Stanford et al., 2014). However, blocking PS receptors present on the surface of macrophages could decrease their clearance of dead tumor cells (Stanford et al., 2014), which is crucial for preventing secondary necrosis and subsequent physicochemical stress (Lauber, Ernst, Orth, Herrmann, & Belka, 2012). It has been suggested that it may be unwise to deplete TAMs in combination with cytotoxic anti-tumor therapy due to the potential for aberrant immune responses (Poh & Ernst, 2018; Shree et al., 2011). Thus, it is far more attractive to consider targeting macrophages for anti-cancer therapy while enabling them to maintain ability to efficiently clear dead cancer cells (Shree et al., 2011). I found that HO-1-deficient macrophages did not significantly differ from WT macrophages in their ability to take up tumor cell debris (Fig. 4S, T). Therefore, anti-tumor strategies could potentially target the HO-1-mediated reprogramming of TAMs without altering their clearance efficiency.

Activation of the immunogenic function of M1 TAMs is critical for proper T cell education in the TME (Baer et al., 2016; Daley et al., 2017; Medler, Cotechini, & Coussens, 2015). Typically, M1 TAMs mediate the influx of T cells through production of T cell chemokines (Baer et al., 2016; Mantovani & Allavena, 2015; N. Wang, Liang, & Zen, 2014). Abundant accumulation of M1 TAMs and $CD8^+$ T cells in a tumor has been associated with favorable patient outcomes and thus may be a critical component of anti-tumor therapy (Becht et al., 2016). Here, the increased proportion of M1 TAMs coincided with enhanced anti-tumor T cell responses in a 4T1 tumor model treated with PTX and a HO-1 inhibitor. Previous studies showed that therapeutic inefficacy can be caused by Tregs, which suppress lymphocytic activity via HO-1-mediated mechanisms (Choi, Pae, Jeong, Kim, & Chung, 2005; El Andaloussi & Lesniak, 2007). M2 TAMs play a key role in enhancing the immunosuppressive activity of Tregs through IL-10 (Mantovani et al., 2017). In line with the decreased mRNA levels of *Il10* in TAMs observed herein, I found that the proportion of Tregs was decreased in mice treated with PTX and a HO-1 inhibitor compared to those from mice treated with PTX alone. Together, these findings indicate that the HO-1-mediated conversion of TAMs toward the M1 phenotype contributes to converting an immunosuppressive TME to an immunogenic TME that is capable of undergoing anti-tumor responses during PTX therapy.

Modulation of the ability of conventional chemotherapy-generated tumor cell debris to change the TME could be a novel approach for preventing unwanted therapy-induced effects (J. Chang et al., 2018; Sulciner et al., 2017). Recently other studies showed that 5-FU-generated tumor cell debris stimulates tumor growth (J. Chang et al., 2018). Although I focused on PTX in the present study, I found that 5-FU, which is another first-line chemotherapeutic agent, also showed similar results in a 4T1 breast cancer model. Consistent with the ability of HO-1 inhibition to upregulate the therapeutic efficacy of PTX, I observed that HO-1 inhibition promoted the therapeutic efficacy of 5-FU by upregulating anti-tumor immunity (Fig. 8). Thus, the overexpression of HO-1 triggered by macrophage engulfment of 5-FU-induced tumor cell debris could be a target for the reprogramming of TAMs. Immune checkpoint blockade therapy (e.g., with anti-CTLA-4 and PD-1), which is a firmly established treatment for cancer, acts against a variety of tumor types by enhancing anti-tumor immunity (Sharma & Allison, 2015; Spranger & Gajewski, 2018). However, only a small proportion of patients show a clinical response to this therapy, suggesting that other immune-modulatory treatments might be required to improve this anti-tumor strategy (Georgoudaki et al., 2016; Muliaditan et al., 2018; Spranger & Gajewski, 2018). The failure of immune checkpoint inhibitors is likely to reflect the immunosuppressive nature of the TME (Samanta et al.,

2018). Reprogramming TAMs toward an immune-stimulatory phenotype enhances the activity of immune checkpoint inhibitors (Baer et al., 2016; Georgoudaki et al., 2016; Kaneda et al., 2016). Thus, it will be worthwhile to determine whether the M1 TAMs induced by HO-1 inactivation could improve the response to immune checkpoint inhibitors.

In summary, these findings collectively show that TAM-mediated phagocytosis of breast tumor cell debris diminishes therapeutic efficacy by decreasing the post-chemotherapy proportion of M1 TAMs. Specifically, I reveal that tumor cell debris-induced HO-1 expression in macrophages is critical to their polarization upon chemotherapy, and that inhibition of HO-1 overexpression in TAMs can create a robust anti-tumor immune response to potentiate the efficacy of chemotherapy.

5. References

Alaoui-Jamali, M. A., Bismar, T. A., Gupta, A., Szarek, W. A., Su, J., Song, W., . . . Schipper, H. M. (2009). A novel experimental heme oxygenase-1-targeted therapy for hormone-refractory prostate cancer. *Cancer Res, 69*(20), 8017-8024. doi:10.1158/0008-5472.can-09-0419

Anampa, J., Makower, D., & Sparano, J. A. (2015). Progress in adjuvant chemotherapy for breast cancer: an overview. *BMC Med, 13*, 195. doi:10.1186/s12916-015-0439-8

Arnold, J. N., Magiera, L., Kraman, M., & Fearon, D. T. (2014). Tumoral immune suppression by macrophages expressing fibroblast activation protein-alpha and heme oxygenase-1. *Cancer Immunol Res, 2*(2), 121-126. doi:10.1158/2326-6066.cir-13-0150

Baer, C., Squadrito, M. L., Laoui, D., Thompson, D., Hansen, S. K., Kiialainen, A., . . . De Palma, M. (2016). Suppression of microRNA activity amplifies IFN-gamma-induced macrophage activation and promotes anti-tumour immunity. *Nat Cell Biol, 18*(7), 790-802. doi:10.1038/ncb3371

Becht, E., Giraldo, N. A., Dieu-Nosjean, M. C., Sautes-Fridman, C., &

Fridman, W. H. (2016). Cancer immune contexture and immunotherapy. *Curr Opin Immunol, 39*, 7-13. doi:10.1016/j.coi.2015.11.009

Binnewies, M., Roberts, E. W., Kersten, K., Chan, V., Fearon, D. F., Merad, M., . . . Krummel, M. F. (2018). Understanding the tumor immune microenvironment (TIME) for effective therapy. *Nat Med, 24*(5), 541-550. doi:10.1038/s41591-018-0014-x

Biswas, S. K., & Mantovani, A. (2010). Macrophage plasticity and interaction with lymphocyte subsets: cancer as a paradigm. *Nat Immunol, 11*(10), 889-896. doi:10.1038/ni.1937

Brown, J. M., Recht, L., & Strober, S. (2017). The Promise of Targeting Macrophages in Cancer Therapy. *Clin Cancer Res, 23*(13), 3241-3250. doi:10.1158/1078-0432.ccr-16-3122

Cassetta, L., Noy, R., Swierczak, A., Sugano, G., Smith, H., Wiechmann, L., & Pollard, J. W. (2016). Isolation of Mouse and Human Tumor-Associated Macrophages. *Adv Exp Med Biol, 899*, 211-229. doi:10.1007/978-3-319-26666-4_12

Chang, J., Bhasin, S. S., Bielenberg, D. R., Sukhatme, V. P., Bhasin, M., Huang, S., . . . Panigrahy, D. (2018). Chemotherapy-generated cell debris stimulates colon carcinoma tumor growth via osteopontin. *Faseb j*, fj201800019RR. doi:10.1096/fj.201800019RR

Chang, Y. S., Jalgaonkar, S. P., Middleton, J. D., & Hai, T. (2017). Stress-inducible gene Atf3 in the noncancer host cells contributes to chemotherapy-exacerbated breast cancer metastasis. *Proc Natl Acad Sci U S A, 114*(34), E7159-e7168. doi:10.1073/pnas.1700455114

Choi, B. M., Pae, H. O., Jeong, Y. R., Kim, Y. M., & Chung, H. T. (2005). Critical role of heme oxygenase-1 in Foxp3-mediated immune suppression. *Biochem Biophys Res Commun, 327*(4), 1066-1071. doi:10.1016/j.bbrc.2004.12.106

Coffelt, S. B., & de Visser, K. E. (2015). Immune-mediated mechanisms influencing the efficacy of anticancer therapies. *Trends Immunol, 36*(4), 198-216. doi:10.1016/j.it.2015.02.006

Cunha, L. D., Yang, M., Carter, R., Guy, C., Harris, L., Crawford, J. C., . . . Green, D. R. (2018). LC3-Associated Phagocytosis in Myeloid Cells Promotes Tumor Immune Tolerance. *Cell*. doi:10.1016/j.cell.2018.08.061

Daley, D., Mani, V. R., Mohan, N., Akkad, N., Pandian, G., Savadkar, S., . . . Miller, G. (2017). NLRP3 signaling drives macrophage-induced adaptive immune suppression in pancreatic carcinoma. *J Exp Med, 214*(6), 1711-1724. doi:10.1084/jem.20161707

DeNardo, D. G., Brennan, D. J., Rexhepaj, E., Ruffell, B., Shiao, S. L., Madden, S. F., . . . Coussens, L. M. (2011). Leukocyte complexity

predicts breast cancer survival and functionally regulates response to chemotherapy. *Cancer Discov, 1*(1), 54-67. doi:10.1158/2159-8274.cd-10-0028

Di Biase, S., Lee, C., Brandhorst, S., Manes, B., Buono, R., Cheng, C. W., . . . Longo, V. D. (2016). Fasting-Mimicking Diet Reduces HO-1 to Promote T Cell-Mediated Tumor Cytotoxicity. *Cancer Cell, 30*(1), 136-146. doi:10.1016/j.ccell.2016.06.005

Dijkgraaf, E. M., Heusinkveld, M., Tummers, B., Vogelpoel, L. T., Goedemans, R., Jha, V., . . . van der Burg, S. H. (2013). Chemotherapy alters monocyte differentiation to favor generation of cancer-supporting M2 macrophages in the tumor microenvironment. *Cancer Res, 73*(8), 2480-2492. doi:10.1158/0008-5472.can-12-3542

Du, X. L., Key, C. R., Osborne, C., Mahnken, J. D., & Goodwin, J. S. (2003). Discrepancy between consensus recommendations and actual community use of adjuvant chemotherapy in women with breast cancer. *Ann Intern Med, 138*(2), 90-97.

Durgeau, A., Virk, Y., Corgnac, S., & Mami-Chouaib, F. (2018). Recent Advances in Targeting CD8 T-Cell Immunity for More Effective Cancer Immunotherapy. *Front Immunol, 9*, 14. doi:10.3389/fimmu.2018.00014

El Andaloussi, A., & Lesniak, M. S. (2007). CD4+ CD25+ FoxP3+ T-cell

infiltration and heme oxygenase-1 expression correlate with tumor grade in human gliomas. *J Neurooncol, 83*(2), 145-152. doi:10.1007/s11060-006-9314-y

Engblom, C., Pfirschke, C., & Pittet, M. J. (2016). The role of myeloid cells in cancer therapies. *Nat Rev Cancer, 16*(7), 447-462. doi:10.1038/nrc.2016.54

Fang, J., Sawa, T., Akaike, T., Greish, K., & Maeda, H. (2004). Enhancement of chemotherapeutic response of tumor cells by a heme oxygenase inhibitor, pegylated zinc protoporphyrin. *Int J Cancer, 109*(1), 1-8. doi:10.1002/ijc.11644

Fridman, W. H., Zitvogel, L., Sautes-Fridman, C., & Kroemer, G. (2017). The immune contexture in cancer prognosis and treatment. *Nat Rev Clin Oncol, 14*(12), 717-734. doi:10.1038/nrclinonc.2017.101

Galluzzi, L., Senovilla, L., Zitvogel, L., & Kroemer, G. (2012). The secret ally: immunostimulation by anticancer drugs. *Nat Rev Drug Discov, 11*(3), 215-233. doi:10.1038/nrd3626

Genard, G., Lucas, S., & Michiels, C. (2017). Reprogramming of Tumor-Associated Macrophages with Anticancer Therapies: Radiotherapy versus Chemo- and Immunotherapies. *Front Immunol, 8*, 828. doi:10.3389/fimmu.2017.00828

Georgoudaki, A. M., Prokopec, K. E., Boura, V. F., Hellqvist, E., Sohn, S.,

Ostling, J., . . . Karlsson, M. C. (2016). Reprogramming Tumor-Associated Macrophages by Antibody Targeting Inhibits Cancer Progression and Metastasis. *Cell Rep, 15*(9), 2000-2011. doi:10.1016/j.celrep.2016.04.084

Gorrini, C., Harris, I. S., & Mak, T. W. (2013). Modulation of oxidative stress as an anticancer strategy. *Nat Rev Drug Discov, 12*(12), 931-947. doi:10.1038/nrd4002

Gregory, C. D., & Pound, J. D. (2011). Cell death in the neighbourhood: direct microenvironmental effects of apoptosis in normal and neoplastic tissues. *J Pathol, 223*(2), 177-194. doi:10.1002/path.2792

Gruosso, T., Mieulet, V., Cardon, M., Bourachot, B., Kieffer, Y., Devun, F., . . . Mechta-Grigoriou, F. (2016). Chronic oxidative stress promotes H2AX protein degradation and enhances chemosensitivity in breast cancer patients. *EMBO Mol Med, 8*(5), 527-549. doi:10.15252/emmm.201505891

Guerriero, J. L. (2018). Macrophages: The Road Less Traveled, Changing Anticancer Therapy. *Trends Mol Med, 24*(5), 472-489. doi:10.1016/j.molmed.2018.03.006

Halin Bergstrom, S., Nilsson, M., Adamo, H., Thysell, E., Jernberg, E., Stattin, P., . . . Bergh, A. (2016). Extratumoral Heme Oxygenase-1 (HO-1) Expressing Macrophages Likely Promote Primary and Metastatic Prostate Tumor Growth. *PLoS One, 11*(6), e0157280.

doi:10.1371/journal.pone.0157280

Hernandez, C., Huebener, P., & Schwabe, R. F. (2016). Damage-associated molecular patterns in cancer: A double-edged sword. *Oncogene, 35*(46), 5931-5941. doi:10.1038/onc.2016.104

Hirata, E., & Sahai, E. (2017). Tumor Microenvironment and Differential Responses to Therapy. *Cold Spring Harb Perspect Med, 7*(7). doi:10.1101/cshperspect.a026781

Hopper, C. P., Meinel, L., Steiger, C., & Otterbein, L. E. (2018). Where is the Clinical Breakthrough of Heme Oxygenase-1 / Carbon Monoxide Therapeutics? *Curr Pharm Des, 24*(20), 2264-2282. doi:10.2174/1381612824666180723161811

Hughes, R., Qian, B. Z., Rowan, C., Muthana, M., Keklikoglou, I., Olson, O. C., . . . Lewis, C. E. (2015). Perivascular M2 Macrophages Stimulate Tumor Relapse after Chemotherapy. *Cancer Res, 75*(17), 3479-3491. doi:10.1158/0008-5472.can-14-3587

Kaneda, M. M., Messer, K. S., Ralainirina, N., Li, H., Leem, C. J., Gorjestani, S., . . . Varner, J. A. (2016). PI3Kgamma is a molecular switch that controls immune suppression. *Nature, 539*(7629), 437-442. doi:10.1038/nature19834

Karagiannis, G. S., Pastoriza, J. M., Wang, Y., Harney, A. S., Entenberg, D., Pignatelli, J., . . . Oktay, M. H. (2017). Neoadjuvant chemotherapy

induces breast cancer metastasis through a TMEM-mediated mechanism. *Sci Transl Med, 9*(397). doi:10.1126/scitranslmed.aan0026

Kumar, S., Calianese, D., & Birge, R. B. (2017). Efferocytosis of dying cells differentially modulate immunological outcomes in tumor microenvironment. *Immunol Rev, 280*(1), 149-164. doi:10.1111/imr.12587

Lauber, K., Ernst, A., Orth, M., Herrmann, M., & Belka, C. (2012). Dying cell clearance and its impact on the outcome of tumor radiotherapy. *Frontiers in Oncology, 2*, 116. doi:10.3389/fonc.2012.00116

Lewis, C. E., & Pollard, J. W. (2006). Distinct role of macrophages in different tumor microenvironments. *Cancer Res, 66*(2), 605-612. doi:10.1158/0008-5472.can-05-4005

Li, X., Lewis, M. T., Huang, J., Gutierrez, C., Osborne, C. K., Wu, M. F., . . . Chang, J. C. (2008). Intrinsic resistance of tumorigenic breast cancer cells to chemotherapy. *J Natl Cancer Inst, 100*(9), 672-679. doi:10.1093/jnci/djn123

Maman, S., & Witz, I. P. (2018). A history of exploring cancer in context. *Nat Rev Cancer, 18*(6), 359-376. doi:10.1038/s41568-018-0006-7

Mantovani, A., & Allavena, P. (2015). The interaction of anticancer therapies with tumor-associated macrophages. *J Exp Med, 212*(4), 435-445.

doi:10.1084/jem.20150295

Mantovani, A., Marchesi, F., Malesci, A., Laghi, L., & Allavena, P. (2017). Tumour-associated macrophages as treatment targets in oncology. *Nat Rev Clin Oncol, 14*(7), 399-416. doi:10.1038/nrclinonc.2016.217

McCoy, M. J., Lake, R. A., van der Most, R. G., Dick, I. M., & Nowak, A. K. (2012). Post-chemotherapy T-cell recovery is a marker of improved survival in patients with advanced thoracic malignancies. *Br J Cancer, 107*(7), 1107-1115. doi:10.1038/bjc.2012.362

Medler, T. R., Cotechini, T., & Coussens, L. M. (2015). Immune response to cancer therapy: mounting an effective antitumor response and mechanisms of resistance. *Trends Cancer, 1*(1), 66-75. doi:10.1016/j.trecan.2015.07.008

Metz, R., DuHadaway, J. B., Rust, S., Munn, D. H., Muller, A. J., Mautino, M., & Prendergast, G. C. (2010). Zinc protoporphyrin-IX stimulates tumor immunity by disrupting the immunosuppressive enzyme indoleamine 2,3-dioxygenase. *Molecular cancer therapeutics, 9*(6), 1864-1871. doi:10.1158/1535-7163.MCT-10-0185

Miyake, M., Fujimoto, K., Anai, S., Ohnishi, S., Nakai, Y., Inoue, T., . . . Hirao, Y. (2010). Inhibition of heme oxygenase-1 enhances the cytotoxic effect of gemcitabine in urothelial cancer cells. *Anticancer*

Res, 30(6), 2145-2152.

Muliaditan, T., Opzoomer, J. W., Caron, J., Okesola, M., Kosti, P., Lall, S., . . . Arnold, J. N. (2018). Repurposing tin mesoporphyrin as an immune checkpoint inhibitor shows therapeutic efficacy in preclinical models of cancer. *Clin Cancer Res*. doi:10.1158/1078-0432.ccr-17-2587

Na, H. K., & Surh, Y. J. (2014). Oncogenic potential of Nrf2 and its principal target protein heme oxygenase-1. *Free Radic Biol Med, 67*, 353-365. doi:10.1016/j.freeradbiomed.2013.10.819

Nagarsheth, N., Wicha, M. S., & Zou, W. (2017). Chemokines in the cancer microenvironment and their relevance in cancer immunotherapy. *Nat Rev Immunol, 17*(9), 559-572. doi:10.1038/nri.2017.49

Naito, Y., Takagi, T., & Higashimura, Y. (2014). Heme oxygenase-1 and anti-inflammatory M2 macrophages. *Arch Biochem Biophys, 564*, 83-88. doi:10.1016/j.abb.2014.09.005

Nitti, M., Piras, S., Marinari, U. M., Moretta, L., Pronzato, M. A., & Furfaro, A. L. (2017). HO-1 Induction in Cancer Progression: A Matter of Cell Adaptation. *Antioxidants, 6*(2), 29. doi:10.3390/antiox6020029

Niu, Z., Shi, Q., Zhang, W., Shu, Y., Yang, N., Chen, B., . . . Shen, P. (2017). Caspase-1 cleaves PPARgamma for potentiating the pro-tumor action of TAMs. *Nat Commun, 8*(1), 766. doi:10.1038/s41467-017-00523-6

Onyema, O. O., Decoster, L., Njemini, R., Forti, L. N., Bautmans, I., De Waele, M., & Mets, T. (2015). Chemotherapy-induced changes and immunosenescence of CD8+ T-cells in patients with breast cancer. *Anticancer Res, 35*(3), 1481-1489.

Pachynski, R. K., Scholz, A., Monnier, J., Butcher, E. C., & Zabel, B. A. (2015). Evaluation of Tumor-infiltrating Leukocyte Subsets in a Subcutaneous Tumor Model. *J Vis Exp*(98). doi:10.3791/52657

Poh, A. R., & Ernst, M. (2018). Targeting Macrophages in Cancer: From Bench to Bedside. *Front Oncol, 8*, 49. doi:10.3389/fonc.2018.00049

Pulaski, B. A., & Ostrand-Rosenberg, S. (2001). Mouse 4T1 breast tumor model. *Curr Protoc Immunol, Chapter 20*, Unit 20.22. doi:10.1002/0471142735.im2002s39

Pyonteck, S. M., Akkari, L., Schuhmacher, A. J., Bowman, R. L., Sevenich, L., Quail, D. F., . . . Joyce, J. A. (2013). CSF-1R inhibition alters macrophage polarization and blocks glioma progression. *Nat Med, 19*(10), 1264-1272. doi:10.1038/nm.3337

Ringleb, J., Strack, E., Angioni, C., Geisslinger, G., Steinhilber, D., Weigert, A., & Brune, B. (2017). Apoptotic Cancer Cells Suppress 5-Lipoxygenase in Tumor-Associated Macrophages. *J Immunol*. doi:10.4049/jimmunol.1700609

Roca, H., Jones, J. D., Purica, M. C., Weidner, S., Koh, A. J., Kuo, R., . . .

McCauley, L. K. (2017). Apoptosis-induced CXCL5 accelerates inflammation and growth of prostate tumor metastases in bone. *J Clin Invest*. doi:10.1172/jci92466

Ruffell, B., Chang-Strachan, D., Chan, V., Rosenbusch, A., Ho, C. M., Pryer, N., . . . Coussens, L. M. (2014). Macrophage IL-10 blocks CD8+ T cell-dependent responses to chemotherapy by suppressing IL-12 expression in intratumoral dendritic cells. *Cancer Cell, 26*(5), 623-637. doi:10.1016/j.ccell.2014.09.006

Rugo, H. S., Barry, W. T., Moreno-Aspitia, A., Lyss, A. P., Cirrincione, C., Leung, E., . . . Winer, E. P. (2015). Randomized Phase III Trial of Paclitaxel Once Per Week Compared With Nanoparticle Albumin-Bound Nab-Paclitaxel Once Per Week or Ixabepilone With Bevacizumab As First-Line Chemotherapy for Locally Recurrent or Metastatic Breast Cancer: CALGB 40502/NCCTG N063H (Alliance). *J Clin Oncol, 33*(21), 2361-2369. doi:10.1200/jco.2014.59.5298

Samanta, D., Park, Y., Ni, X., Li, H., Zahnow, C. A., Gabrielson, E., . . . Semenza, G. L. (2018). Chemotherapy induces enrichment of CD47(+)/CD73(+)/PDL1(+) immune evasive triple-negative breast cancer cells. *Proc Natl Acad Sci U S A, 115*(6), E1239-e1248. doi:10.1073/pnas.1718197115

Sharma, P., & Allison, J. P. (2015). The future of immune checkpoint therapy. *Science, 348*(6230), 56-61. doi:10.1126/science.aaa8172

Shree, T., Olson, O. C., Elie, B. T., Kester, J. C., Garfall, A. L., Simpson, K., . . . Joyce, J. A. (2011). Macrophages and cathepsin proteases blunt chemotherapeutic response in breast cancer. *Genes Dev, 25*(23), 2465-2479. doi:10.1101/gad.180331.111

Spranger, S., & Gajewski, T. F. (2018). Impact of oncogenic pathways on evasion of antitumour immune responses. *Nat Rev Cancer*. doi:10.1038/nrc.2017.117

Stanford, J. C., Young, C., Hicks, D., Owens, P., Williams, A., Vaught, D. B., . . . Cook, R. S. (2014). Efferocytosis produces a prometastatic landscape during postpartum mammary gland involution. *J Clin Invest, 124*(11), 4737-4752. doi:10.1172/jci76375

Sulciner, M. L., Serhan, C. N., Gilligan, M. M., Mudge, D. K., Chang, J., Gartung, A., . . . Panigrahy, D. (2017). Resolvins suppress tumor growth and enhance cancer therapy. *J Exp Med*. doi:10.1084/jem.20170681

Tong, C. W. S., Wu, M., Cho, W. C. S., & To, K. K. W. (2018). Recent Advances in the Treatment of Breast Cancer. *Frontiers in Oncology, 8*, 227-227. doi:10.3389/fonc.2018.00227

Ubil, E., Caskey, L., Holtzhausen, A., Hunter, D., Story, C., & Earp, H. S.

(2018). Tumor-secreted Pros1 inhibits macrophage M1 polarization to reduce antitumor immune response. *J Clin Invest, 128*(6), 2356-2369. doi:10.1172/jci97354

Ugel, S., De Sanctis, F., Mandruzzato, S., & Bronte, V. (2015). Tumor-induced myeloid deviation: when myeloid-derived suppressor cells meet tumor-associated macrophages. *J Clin Invest, 125*(9), 3365-3376. doi:10.1172/jci80006

Verma, R., Foster, R. E., Horgan, K., Mounsey, K., Nixon, H., Smalle, N., . . . Carter, C. R. (2016). Lymphocyte depletion and repopulation after chemotherapy for primary breast cancer. *Breast Cancer Res, 18*(1), 10. doi:10.1186/s13058-015-0669-x

Vijayan, V., Wagener, F., & Immenschuh, S. (2018). The macrophage heme-heme oxygenase-1 system and its role in inflammation. *Biochem Pharmacol*. doi:10.1016/j.bcp.2018.02.010

Voss, J., Ford, C. A., Petrova, S., Melville, L., Paterson, M., Pound, J. D., . . . Gregory, C. D. (2017). Modulation of macrophage antitumor potential by apoptotic lymphoma cells. *Cell Death Differ, 24*(6), 971-983. doi:10.1038/cdd.2016.132

Wang, H.-W., & Joyce, J. A. (2010). Alternative activation of tumor-associated macrophages by IL-4: Priming for protumoral functions. *Cell Cycle, 9*(24), 4824-4835. doi:10.4161/cc.9.24.14322

Wang, N., Liang, H., & Zen, K. (2014). Molecular mechanisms that influence the macrophage m1-m2 polarization balance. *Front Immunol, 5*, 614. doi:10.3389/fimmu.2014.00614

Weigert, A., Mora, J., Sekar, D., Syed, S., & Brune, B. (2016). Killing Is Not Enough: How Apoptosis Hijacks Tumor-Associated Macrophages to Promote Cancer Progression. *Adv Exp Med Biol, 930*, 205-239. doi:10.1007/978-3-319-39406-0_9

Zhao, Y., Zhang, C., Gao, L., Yu, X., Lai, J., Lu, D., . . . Liu, Z. (2017). Chemotherapy-Induced Macrophage Infiltration into Tumors Enhances Nanographene-Based Photodynamic Therapy. *Cancer Res, 77*(21), 6021-6032. doi:10.1158/0008-5472.can-17-1655

Appendix

Taurine chloramine potentiates phagocytic activity of peritoneal macrophages through upregulation of dectin-1 mediated by heme oxygenase-1-derived carbon monoxide

1. Abstract

Timely resolution of inflammation that occurs following microbial infection or tissue damage is an important physiologic process to maintain or restore host homeostasis. Taurine chloramine (TauCl) is formed as a consequence of reaction between taurine and hypochlorite in leukocytes, and it is especially abundant in activated neutrophils that encounter oxidative burst. As neutrophils undergo apoptosis, TauCl is released to extracellular matrix at inflamed sites, thereby affecting coexisting macrophages in the inflammatory microenvironment. In this study, I investigated the role of TauCl in phagocytosis by macrophages upon fungal infection. I found that exogenous TauCl substantially increased the phagocytic activity of macrophages through upregulation of dectin-1, a receptor for fungal β-1,3-glucans, which is presents on the surface of macrophages. The previous studies demonstrated the induction of heme oxygenase-1 (HO-1) expression in murine peritoneal macrophages treated with TauCl. Knocking out HO-1 or pharmacologic inhibition of HO-1 with zinc protoporphyin IX, abrogated the TauCl-induced dectin-1 expression and subsequent phagocytosis of macrophage. Furthermore, carbon monoxide (CO), a by-product of the HO-1-catalyzed reaction, induced dectin-1 expression and potentiated phagocytic capability of macrophages, which appeared to be mediated

through peroxisome proliferator-activated receptor gamma (PPAR-γ) up-regulation. Taken together, induction of HO-1 expression and subsequent CO production by TauCl are essential for phagocytosis of fungi by macrophages. These results suggest that TauCl plays important roles in host defense against fungal infection and has therapeutic potential in the management of inflammatory diseases.

2. Introduction

Detection of infected microbial pathogens and stimulation of innate immune responses by phagocytes are critical for maintaining or restoring host homeostasis (Billings et al., 2016; Brubaker, Bonham, Zanoni, & Kagan, 2015; David M Underhill & Helen S Goodridge, 2012). Phagocytes, such as macrophages, play major roles in host defense against microbial infections by removing the pathogens through modulation of the immune responses. When microbial infection occurs, both macrophages as well as neutrophils are recruited to the inflamed site from circulating blood to detect, kill and engulf the pathogens. Macrophages then initiate an immune response for microbial clearance through their pattern recognition receptors (PRRs). Among the various infections caused by different microbial species, fungal infections are prevalent due to increasing immunosuppressive medical treatment (Gordon D Brown, Denning, Gow, et al., 2012; Gordon D Brown, Denning, & Levitz, 2012).

Acute inflammatory response to fungal infection is accompanied by production of endogenous mediators (Charles N Serhan, Chiang, Dalli, & Levy, 2015) that are involved in resolution of acute inflammation (N. Chiang, de la Rosa, Libreros, & Serhan, 2017; C. N. Serhan, 2017). Upon microbial infection, recruited neutrophils overproduce reactive oxygen species (ROS)

and hypochlorous acid (HOCl) that protect the host from pathogens by oxidizing microbes. However, the overproduced these reactive species may cause oxidative stress and chronic inflammation in host. Therefore, timely neutralization of these oxidants is essentially required to maintain homeostasis (Smith, 1994; Weiss, 1989). Taurine, a semi-essential sulfur-containing β-amino acid, is present at high concentrations in most cells of all animal species (Sturman, 1993). Notably, taurine which is abundant in neutrophils reacts stoichiometrically with HOCl to produce taurine chloramine (TauCl) (Weiss, Klein, Slivka, & Wei, 1982). Once the activated neutrophils undergo apoptosis, TauCl is released to the infected microenvironment where the recruited macrophages accumulate. TauCl then acts as a local autacoid to the abundant macrophages at the inflamed site. Although TauCl has bactericidal and fungicidal activity (Waldemar Gottardi & Nagl, 2005; Chaekyun Kim & Cha, 2014; Lackner et al., 2015), the underlying molecular mechanisms are poorly understood.

To clear fungal invasion, macrophages accumulated at the inflammation site must detect and engulf the fungi through phagocytic receptors that recognize fungal-cell specific surface molecules called pathogen associated molecular patterns (PAMPs) (Erwig & Gow, 2016). Dectin-1 is one of the PRRs that recognizes β-1,3-glucans which constitute the major cell wall of multiple pathogenic fungi including *Candida albicans*. Dectin-1 plays a

central role in the host defense against fungal infection through peroxisome proliferator-activated receptor gamma (PPAR-γ) activation (Galès et al., 2010). Upon the recognition of fungal cell wall carbohydrates, the transmembrane receptor dectin-1 mediates phagocytosis of fungi and initiates an acute inflammatory response by producing inflammatory cytokines (Gordon D Brown, 2006; Goodridge et al., 2011). The loss of dectin-1 provokes devastating or aberrant immune response which leads to an inability of macrophages to engulf fungi (Dambuza & Brown, 2015). The mechanisms by which the expression of dectin-1 in macrophages affects the clearance of fungal infection still remains unresolved. Here, I demonstrated that TauCl could promote phagocytic activity of macrophages through upregulation of dectin-1 mediated by the stress-responsive protein HO-1 overexpression upon fungal infection.

3. Materials and Methods

Materials

TauCl as a crystalline sodium salt (molecular weight 181.57) was prepared according to the previously published method (Waldemar Gottardi & Nagl, 2002). Dulbecco's modified Eagle's medium (DMEM), penicillin, streptomycin and fetal bovine serum (FBS) were obtained from Gibco-BRL (Grand Island, NY, USA). Taurine, CORM-3, yeast malt **(**YM) broth**,** fluorescein isothiocyanate (FITC), GW9662, hemoglobin (Hb) and antibodies against actin were purchased from Sigma-Aldrich Co. (St. Louis, MO, USA). Red blood cell lysis buffer was a product from iNtRON biotechnology. Curdlan was purchased from invivogen (San Francisco, CA, USA). Primary antibodies against PPAR-γ and ZnPP were supplied by Santa Cruz Biotechnology, Inc. (Santa Cruz, Dallas, TX, USA). Anti-HO-1 was the product of stressgen (Ann, Arbor, MI, USA), and anti-rabbit and anti-mouse horseradish peroxidase-conjugated secondary antibodies were provided by Zymed Laboratories Inc. (San Francisco, CA, USA). Polyvinylidene difluoride (PVDF) membranes were supplied from Gelman Laboratory (Ann, Arbor, MI, USA). Enhanced chemiluminescent (ECL) detection kit was obtained from Amersham Pharmacia Biotech

(Buckinghamshire, UK).

Mice

C57BL/6 mice (6~9weeks old) were purchased from Central Lab Animal Inc. (Seoul, South Korea) HO-1 KO mice, in which HO-1 gene is abolished by targeted gene knockout, were used for experiment. HO-1 KO mice were provided by Dr. M.A. Perrella (Harvard Medical School). All the animals were maintained according to the institutional animal care guidelines. Animal experimental procedures were approved by the institutional animal care and use committee at Seoul National University. IACUC number: SNU-160718-2

Cell culture

The primary peritoneal macrophages were obtained from mice following intraperitoneal thioglycollate injection (Murray et al., 2014). Murine macrophage RAW264.7 cells were purchased from American Type Culture collection (ATCC, Manassas, VA, USA). RAW264.7 cells and peritoneal macrophages were cultured in DMEM, with 10% FBS, 100 μg/ml streptomycin and 100 U/ml penicillin. Cells were maintained at 37 ℃ in a

humidified atmosphere of 5% CO_2 and 95% O_2.

Survival test

C. albicans was cultured on a yeast mold plate at 25°C for 1 day and a single colony was inoculated into 10 mL YM broth at 30°C for 24 h. *C. albicans* ($1x10^9$) was injected into mice peritoneum. Intraperitoneal administration of vehicle or TauCl was performed 3 times a week. Mouse survival (%) was assessed twice daily.

Phagocytosis assay

C. albicans and curdlan were stained by using 1mg/ml FITC in carbonate-bicarbonate buffer (pH 9.6). *C. albicans* ($1x10^6$) and curdlan (2.5 mg per mouse) were administered intraperitoneally followed by injection of vehicle or TauCl (20 mg/kg, intraperitoneally), and mice were sacrificed 12 h later. Peritoneal leukocytes were harvested by washing with 3 ml of PBS containing 3 mM ethylene diamine tetra acetate (EDTA). For phagocytosis *in vivo*, exudate cells were labelled with allophycocyanin (APC)-conjugated anti-F4/80-antibody (macrophages marker). All samples were analyzed by using BD FACS Calibur™ Flow Cytometer (BD, Franklin Lakes, NJ, USA)

and Flow jo (Tree star). Dead cells were excluded by 7-aminoactinomycin D (7AAD) (Biolegend, San Diego, CA, USA) staining.

Flow cytometry analysis

The cells were washed with PBS containing 0.5% bovine serum albumin (BSA). To block non-specific antibody binding, the cells were pre-treated with unlabeled isotype control Abs, and then stained with CD16/32 antibody was performed to block non-specific binding to Fc receptors. Fluorescence-conjugated dectin-1 and F4/80 (eBioscience, San Diego, CA, USA) were added to samples by incubation on ice for 30 min. After washing the cells with PBS, dectin-1 expression was analyzed by flow cytometry. To confirm the level of PPAR-γ in inner cells, cells were fixed with 2% formaldehyde in PBS for 30 min at room temperature. A permeabilization of cells was proceeded with 0.2 % Tween-20 in PBS for 15 min at room temperature, and blocked with 2 % BSA in PBS for 30 min. Anti- PPAR-γ antibodies in PBS containing 2% BSA were applied for 1 h at 4 ℃. After washing with PBS, cells were incubated with FITC-conjugated secondary antibody for 1 h. Dead cells were excluded by 7-aminoactinomycin D (7AAD) (Biolegend, San Diego, CA, USA) staining. All samples were analyzed by using BD FACS Calibur™ Flow Cytometer (BD, Franklin Lakes, NJ, USA) and Flow

jo (Tree star).

Reverse transcription PCR (RT-PCR)

Total RNA was isolated from macrophages using TRIzol™ (Invitrogen, Carlsbad, CA, USA) according to the manufacturer's instruction. To generate cDNA, total RNA was reverse transcribed by using murine leukemia virus reverse transcriptase (Promega, Madison, WI, USA). Amplification of genes was performed by PCR analysis using SolgTM 2x Taq PCR Smart Mix (Solgent, Daejeon**,** South Korea) according to instruction from the manufactures. The PCR products were analyzed with 2% agarose gel and stained with SYBR® Green for visualization. The mRNA levels were normalized to GAPDH. The primer pairs of the expected products were as follows

Gene symbol	Primer sequence
C-type lectin domain family 7 member a (*Clec7a*)	5'-GGCGACACAATTCAGGGAGA-3' 5'-TGGGGAACTGCATTTCTGACT-3'
Pparg	5'-GCTCCACACTATGAAGACATTCCA-3' 5'-CGGCAGTTAAGATCACACCTATCA-3'
Gapdh	5'-TGTGAACGGATTTGGCGTA-3' 5'-GGTCTCGCTCCTGGAAGATG-3'

Western blot analysis

Whole cell extracts were prepared by suspending the cells in the cell lysis buffer (Cell signaling technology, Danvers, USA) containing protease inhibitors (Roche, Switzerland) for 1 h on ice, followed by centrifugation for 15 min at 12,000 g. The protein concentration was determined by using the BCA protein assay reagents (Pierce, Rockford, IL, USA). The protein samples were solubilized with SDS-polyacrylamide gel electrophoresis sample loading buffer and boiled for 5 min. Protein were electrophoresed on sodium dodecyl sulfate polyacrylamide gel electrophoresis (SDS-PAGE) and transferred to PVDF membranes. The membranes were blocked with 5 % fat-free dry milk in PBST (PBS containing 0.1% Tween-20) buffer for 1 h at room temperature and incubated with primary antibody diluted at 1:1000 in 3% fat-free dry milk-PBST overnight at 4℃. After washing to remove primary antibodies, the blots were incubated with horseradish peroxidase-conjugated secondary antibody. The immunoblot was incubated with the ECL according to the manufacturer's instruction and visualized with LAS 4000 (Fujifilm Life Science, Tokyo, Japan).

Transfection with Pparg siRNA

Pparg siRNA (Bioneer, Daejeon, South Korea) was transfected into RAW264.7 cells with lipofectamine RNAi-MAX reagents (Invitrogen Life Technologies, Carlsbad, CA, USA) according to the manufacturer's instructions.

Immunocytochemistry analysis

Peritoneal macrophages from mice treated with curdlan-FITC were fixed with 2% formaldehyde. The cells were washed in PBS and blocked with 3% BSA in TBST. Anti-F4/80 was applied for overnight at 4℃ and then washed in PBS. Fluorophore-conjugated secondary antibodies were incubated for another 1 h at room temperature. Samples were imaged at 20x using an Eclipse Ti-U inverted microscope integrated by an NIS-Elements imaging software (Nikon, Japan).

Statistical analysis

All data were presented as mean ± SE and statistical analysis were completed in sigmaplot 12. Statistical significance was performed using Student's *t* test. The criterion for statistical significance was $^{*}p < 0.05$, $^{**}p < 0.01$, and $^{***}p < 0.001$.

4. Results

TauCl potentiates host defense to fungal infection

In this study, I aimed to investigate the effect of TauCl on the phagocytic function of macrophages to elucidate its role in the host defense against fungal infection. First, I examined whether TauCl administration could protect mice from fungal infection. Injection of a lethal dose of *C. albicans* to the peritoneum of mice resulted in severe systemic toxicity, leading to a robust reduction in the survival rate (Fig. 1A). The lethal effects of this fungal pathogen were ameliorated by intraperitoneal administration of TauCl.

TauCl promotes phagocytic efficiency of peritoneal macrophages in a fungal infection

To investigate the role of TauCl in host defense to fungal infection, I examined the possibility that TauCl could potentiate phagocytic activity of macrophages. Phagocytosis is a key process, particularly macrophages, to eliminate pathogens after recognition by surface receptors (W. Kim et al., 2015; David M Underhill & Helen S Goodridge, 2012). To assess the effect of TauCl on phagocytosis by macrophages, I used an *in vivo* phagocytosis

assay by intraperitoneal injection of *C. albicans*-FITC. As illustrated in Fig. 2A, exogenous injection of TauCl to mice increased the phagocytic activity of macrophages (Fig. 2A). To further confirm the effects of TauCl on phagocytosis of macrophages, I evaluated the phagocytic activity using a cognate ligand of fungi, curdlan, a β-1,3-glucan polymer derived from *Alcaligenes faecalis* (Greenblatt, Aliprantis, Hu, & Glimcher, 2010; Kumar et al., 2009; Nembrini, Marsland, & Kopf, 2009; Trinath et al., 2014). As curdlan has a specific affinity for dectin-1, it has been used as a model pure β-1,3-glucan recognized by macrophages and dendritic cells in studying host immune response to fungal infection (Ferwerda, Meyer-Wentrup, Kullberg, Netea, & Adema, 2008). Administration of curdlan led to infiltration of leukocytes to the mouse peritoneum which peaked at 6 h (Maruyama et al., 2005). I treated the mice with TauCl at 6 h following curdlan administration. The assessment of phagocytic activity of peritoneal macrophages (PMs) was then performed 12 h after treatment of TauCl. The proportion of PMs labeled with F4/80 and engulfing curdlan-FITC was selectively assessed by flow cytometry. PMs from mice treated with TauCl showed a higher proportion of macrophages carrying out engulfment of curdlan ($F4/80^{+}$curdlan-$FITC^{+}$) than those from mice injected curdlan-FITC alone (Fig. 2B). I also confirmed the TauCl-induced phagocytic activity of macrophages by immunofluorescence staining. TauCl administration potentiated phagocytic

activity of macrophages in curdlan-challenged mice (Fig. 2C).

TauCl increases dectin-1 expression in macrophages of mice infected with fungal pathogens

Upon recognition of pathogens by phagocytic receptors, macrophages stimulate ingestion of fungal particles. Macrophages then initiate an immune response for microbial clearance through their PRRs. A deficiency of these receptors on macrophages causes a more severe infection owing to inability to activate phagocytic functions (Kawai & Akira, 2011). Dectin-1 is a representative PRR that recognizes β-1,3-glucans of fungi (Gordon D Brown, 2006; Goodridge et al., 2011). To determine whether TauCl promotes the phagocytic activity of macrophages through upregulation of PRR expression, I examined the proportion of dectin-1expressed macrophages which play a decisive role in the clearance of fungi. I measured the expression of dectin-1 in PMs of mice upon *C. albicans* infection. TauCl treatment increased the expression of dectin-1 in macrophages (Fig. 3A). Like *C. albicans*, administration of curdlan alone caused a modest increase in the proportion of dectin-1 expressing PMs as a host adaptive response to acute inflammation (Fig. 3B). However, the proportion of macrophages expressing dectin-1 was further increased in the curdlan plus TauCl treated

group (Fig. 3B). In general, the amounts of residual PMs are not sufficient for use in biochemical analysis. Thioglycollate broth is a medium that is widely used to enrich macrophages (Murray et al., 2014). To examine the potent role of chlorination of taurine in upregulation of dectin-1 expression, mice pretreated with thioglycollate were administrated phosphate buffered saline (PBS), taurine or TauCl. Compared with TauCl, the same concentration of its parent molecule, taurine exerted much weaker effect on dectin-1 expression (Fig. 3C). Consistent with the increased protein level, expression of dectin-1 mRNA, C-type lectin domain family 7 member A (*clec7a*) was also elevated in PMs of mice treated with TauCl (Fig. 3D). I also measured the protein and mRNA levels of dectin-1 in the thioglycollate-elicited PMs treated *ex vivo* with TauCl for 36 h. TauCl treatment increased dectin-1 expression at both protein (Fig. 3E) and mRNA level (Fig. 3F). Altogether, these data suggest that TauCl contributes to the phagocytosis of fungi through upregulation of dectin-1 in macrophages.

TauCl-induced HO-1 expression is critical for upregulation of dectin-1 expression in macrophages in a murine peritonitis

Considering a prominent role of HO-1 in cellular protection against inflammatory insults (Ryter & Choi, 2016), I attempted to determine

whether the TauCl-induced HO-1 expression (C. Kim, Jang, Cho, Agarawal, & Cha, 2010; W. Kim et al., 2015) could contribute to dectin-1 upregulation to promote phagocytic activity of macrophages. I verified the role of HO-1 in TauCl-induced dectin-1 expression by use of HO-1 knockout mice. TauCl treatment further increased the dectin-1 expression in macrophages during curdlan-induced peritonitis. The expression of dectin-1 induced by TauCl was abrogated in HO-1 knockout mice (Fig. 4A). Consistent with this finding, inhibition of HO activity by zinc protoporphyrin IX (ZnPP) attenuated TauCl-induced enhancement of dectin-1 expression (Fig. 4B).

TauCl-induced HO-1 expression is essential for enhanced phagocytic activity of macrophages in a murine peritonitis

PMs from HO-1 deficient mice treated with TauCl showed a significantly lower phagocytic activity (Fig. 5A) compared to those from the wild type mice upon TauCl treatment. Likewise, pharmacologic inhibition of HO activity with ZnPP abrogated the TauCl-induced stimulation of phagocytic activity of macrophages (Fig. 5B). These findings suggest that HO-1 overexpression contributes substantially to the TauCl-mediated potentiation of phagocytic activity of macrophages.

CO enhances phagocytic activity of murine macrophages through upregulation of dectin-1 expression

CO is a gaseous byproduct of the HO-1-catalyzed reaction and has been known to have strong anti-inflammatory activity. I attempted to confirm the involvement of CO in TauCl-induced upregulation of dectin-1 by using hemoglobin (Hb) as a scavenger of CO. Scavenging CO resulted in marked decrease in the proportion of dectin-1 expressing macrophages treated with TauCl (Fig. 6A). To further verify the critical role of CO in enhancement of phagocytic activity through dectin-1 in macrophages, I utilized CO-releasing molecule-3 (CORM-3). Mice pretreated with thioglycollate were injected with PBS or CORM-3. The proportion of dectin-1 expressing PMs from mice treated with CORM-3 was further elevated (Fig. 6B). As shown in Fig. 7A, the PMs from mice treated with curdlan-FITC plus CORM-3 exhibited increased phagocytic activity compared to those from mice injected curdlan-FITC alone. CORM-3 also induced upregulation of dectin-1 expression in cultured murine PMs (Fig. 7B).

TauCl-induced HO-1 expression upregulates dectin-1 expression through PPAR-γ activation

It has been documented that PPAR-γ is a transcription factor that regulates the expression of dectin-1 in macrophages (Galès et al., 2010; Lefèvre et al., 2015). Upregulation of dectin-1 expression via activation of PPAR-γ augments antifungal host defense (Gales et al., 2010). This prompted us to determine whether the TauCl-induced HO-1 expression and subsequent dectin-1 upregulation could be mediated via PPAR-γ in PMs. PMs obtained from mice treated with TauCl showed the significantly elevated PPAR-γ expression in curdlan-induced peritonitis (Fig. 8A). To further determine whether TauCl-induced dectin-1 expression was mediated by PPAR-γ, I utilized a PPAR-γ antagonist GW9662. When the mice were cotreated with GW9662 and curdlan, TauCl failed to increase dectin-1 expression in PMs (Fig. 8B). Likewise, GW9662 injection abrogated TauCl-induced phagocytic activity of PMs (Fig. 8C). In addition, suppression of PPAR-γ with GW9662 resulted in blockade of dectin-1 upregulation in macrophages treated with TauCl (Fig. 8D). When the transcriptional expression of PPAR-γ was silenced in RAW 264.7 cells by use of siRNA, TauCl barely induced the expression of dectin-1 at both transcriptional (Fig. 8E) and translational level (Fig. 8F). These results suggest that PPAR-γ mediates the upregulation of TauCl-induced dectin-1 expression in macrophages. To further confirm that the increase of HO-1 by TauCl is responsible for the PPAR-γ upregulation in macrophages, TauCl was intraperitoneally administered with

thioglycollate in mice. PMs obtained from TauCl-treated mice showed enhanced expression of PPAR-γ as well as HO-1 (Fig. 9A). Pharmacologic inhibition of HO activity attenuated upregulation of TauCl-induced PPAR-γ expression in PMs (Fig. 9B). In contrast, intraperitoneal injection of CORM-3 induced the expression of PPAR-γ in PMs (Fig. 9C).

(A)

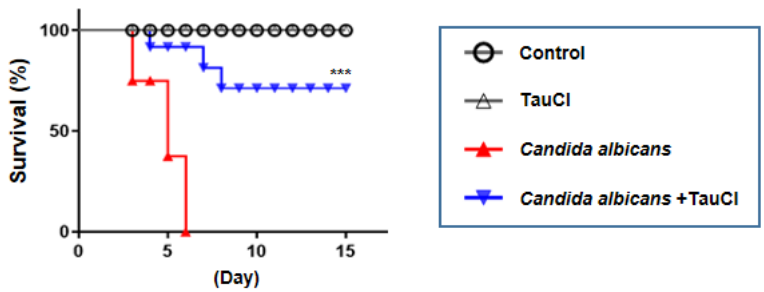
100
50
0
Survival (%)
0
5
10
15
(Day)
***
Control
TauCl
Candida albicans
Candida albicans +TauCl

Figure 1. TauCl enhances host defense from fungal infection

(A) Mice infected with *Candida albicans* ($1x10^9$ yeasts/mouse, n=9/group) were treated with or without TauCl (20 mg/kg) intraperitoneally. Mouse survival (%) was monitored twice daily. P value to infected group without TauCl treatment. ***$p<0.001$

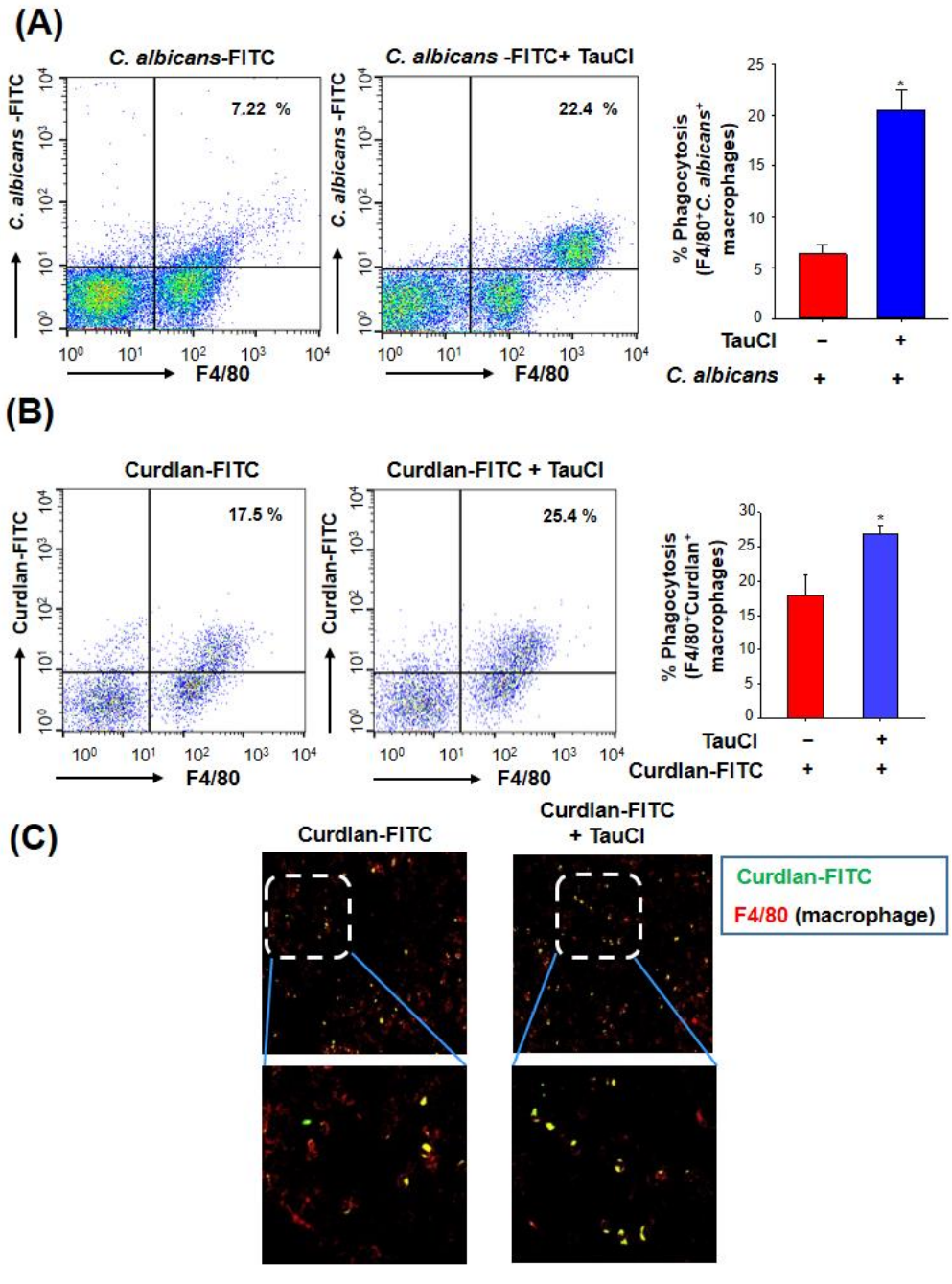
(A)
C. albicans-FITC
C. albicans -FITC+ TauCl
7.22 %
22.4 %
C. albicans -FITC
F4/80
% Phagocytosis (F4/80+C. albicans+ macrophages)
TauCl
C. albicans
(B)
Curdlan-FITC
Curdlan-FITC + TauCl
17.5 %
25.4 %
% Phagocytosis (F4/80+Curdlan+ macrophages)
Curdlan-FITC
(C)
Curdlan-FITC + TauCl
Curdlan-FITC
F4/80 (macrophage)

Figure 2. TauCl enhances phagocytic activity of macrophages in a murine peritonitis model

(A) Phagocytic activity of PMs from mice treated with vehicle or TauCl (20 mg/kg, i.p.) was measured. The proportion of macrophages ($F4/80^+$) engulfing *C. albicans*-FITC was assessed by flow cytometry. (B) Mice were challenged with 2.5 mg of curdlan-FITC (from *Alcaligenes faecalis*) for 6 h followed by intraperitoneal administration of vehicle or TauCl (20 mg/kg). After 12 h, mice were sacrificed, and peritoneal exudates were collected. The proportion of macrophages engulfing curdlan-FITC ($F4/80^+$curdlan-$FITC^+$) was identified by flow cytometry. (C) Phagocytosis was detected by immunostaining using anti-F4/80 (*red*; macrophages marker) and curdlan-FITC (*green*). A representative fluorescence micrograph shows macrophages (*red*) engulfing curdlan-FITC (*green*). Data were analyzed by Student's *t*-test, $*p<0.05$.

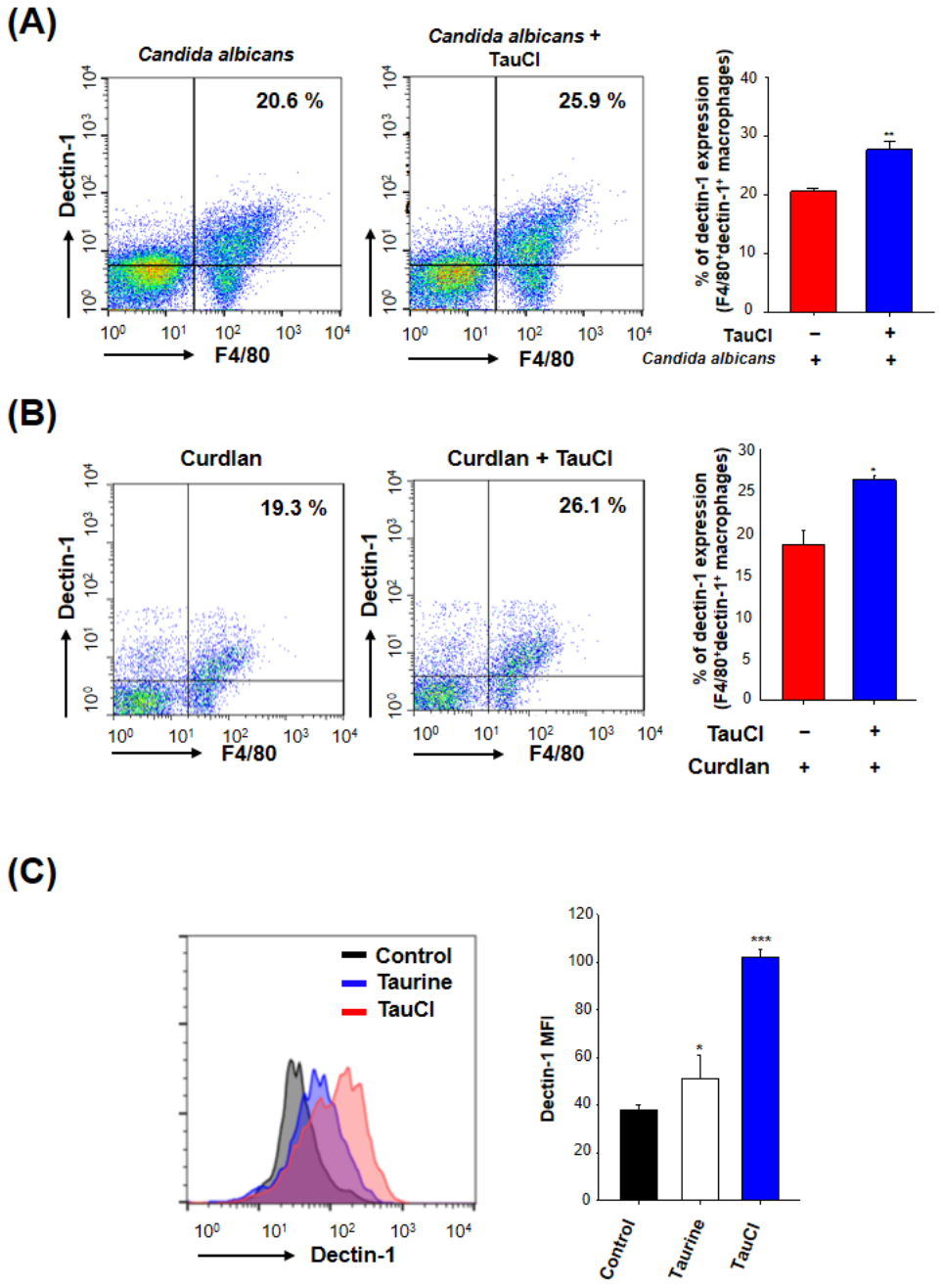
(A)
Candida albicans
20.6 %
Candida albicans + TauCl
25.9 %
Dectin-1
F4/80
% of dectin-1 expression (F4/80+dectin-1+ macrophages)
TauCl
Candida albicans
(B)
Curdlan
19.3 %
Curdlan + TauCl
26.1 %
Curdlan
(C)
Control
Taurine
TauCl
Dectin-1 MFI

(D)

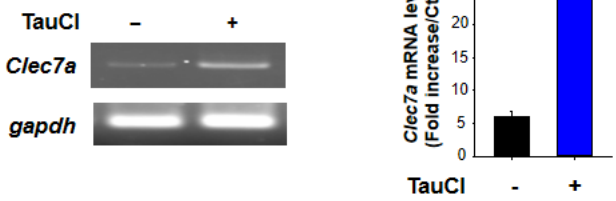
TauCl
–
+
Clec7a
gapdh
Clec7a mRNA level (Fold increase/Ctrl)
30
25
20
15
10
5
0
**
TauCl
-
+

(E)

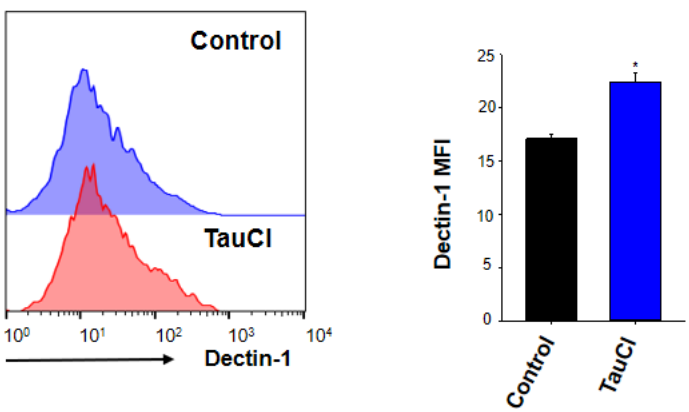
Control
TauCl
10⁰
10¹
10²
10³
10⁴
Dectin-1
Dectin-1 MFI
25
20
15
10
5
0
*
Control
TauCl

(F)

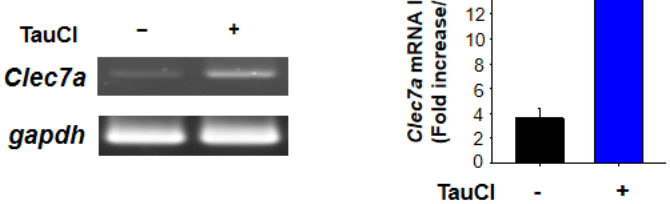
TauCl
–
+
Clec7a
gapdh
Clec7a mRNA level (Fold increase/Ctrl)
18
16
14
12
10
8
6
4
2
0
**
TauCl
-
+

Figure 3. TauCl augments phagocytosis through upregulation of dectin-1 expression in PMs

(A) The level of dectin-1 on PMs in *C. albicans* infection was detected by flow cytometry. (B) The proportion of PMs expressing dectin-1 in the curdlan-induced murine peritonitis model was quantified by flow cytometry. (C, D) The expression of TauCl-induced dectin-1 in the thioglycollate-elicited PMs were analyzed by flow cytometry and RT-PCR. *Clec7a*, dectin-1 mRNA (E, F) Protein and mRNA levels of dectin-1 in the harvested primary macrophages treated with vehicle or TauCl (0.5 mM) for 36 h were measured. All data were analyzed by Student's *t*-test, $*p<0.05$, $**p<0.01$ and $***p<0.001$.

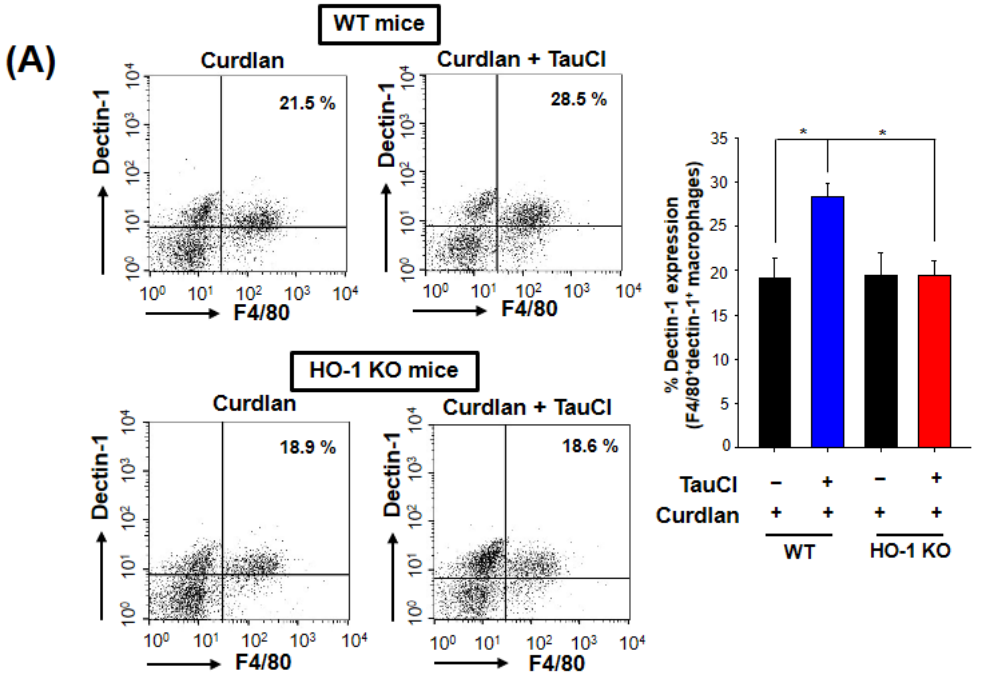
(A)
WT mice
Curdlan
Curdlan + TauCl
21.5 %
28.5 %
Dectin-1
F4/80
HO-1 KO mice
18.9 %
18.6 %
% Dectin-1 expression
(F4/80+dectin-1+ macrophages)
TauCl
Curdlan
WT
HO-1 KO

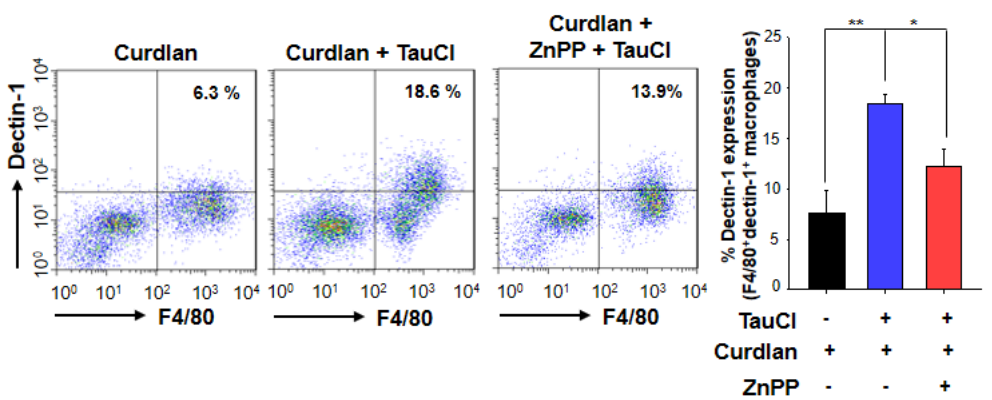
(B)
Curdlan
Curdlan + TauCl
Curdlan +
ZnPP + TauCl
6.3 %
18.6 %
13.9%
Dectin-1
F4/80
% Dectin-1 expression
(F4/80+dectin-1+ macrophages)
TauCl
Curdlan
ZnPP

Figure 4. TauCl-induced HO-1 expression is important to upregulation of dectin-1 expression

(A) The proportion of dectin-1 expressing PMs from WT and HO-1 KO mice was compared by flow cytometry. (B) Mice treated with curdlan-FITC (2.5 mg/mouse) for 6 h were given an i.p. injection of vehicle or the HO-1 inhibitor, ZnPP (25 mg/kg) 1 h prior to the TauCl (20 mg/kg) treatment. The proportion of dectin-1 expressing PMs from mice was determined by flow cytometry.

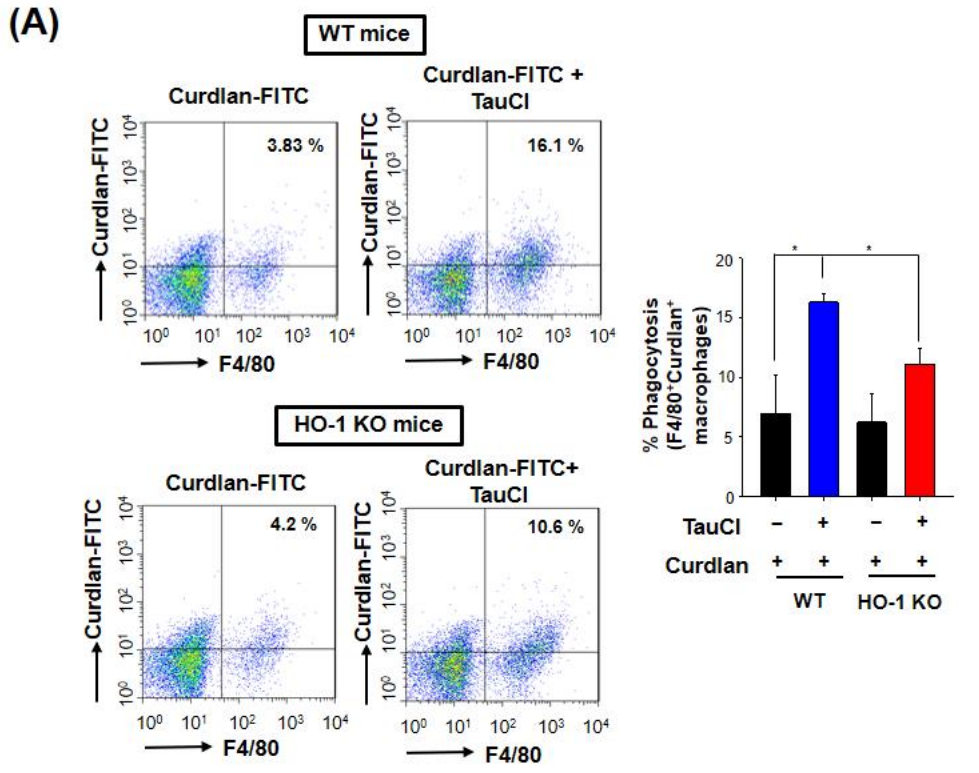
(A)
WT mice
Curdlan-FITC
Curdlan-FITC + TauCl
3.83 %
16.1 %
Curdlan-FITC
F4/80
HO-1 KO mice
Curdlan-FITC
Curdlan-FITC+ TauCl
4.2 %
10.6 %
% Phagocytosis (F4/80+Curdlan+ macrophages)
TauCl
Curdlan
WT
HO-1 KO

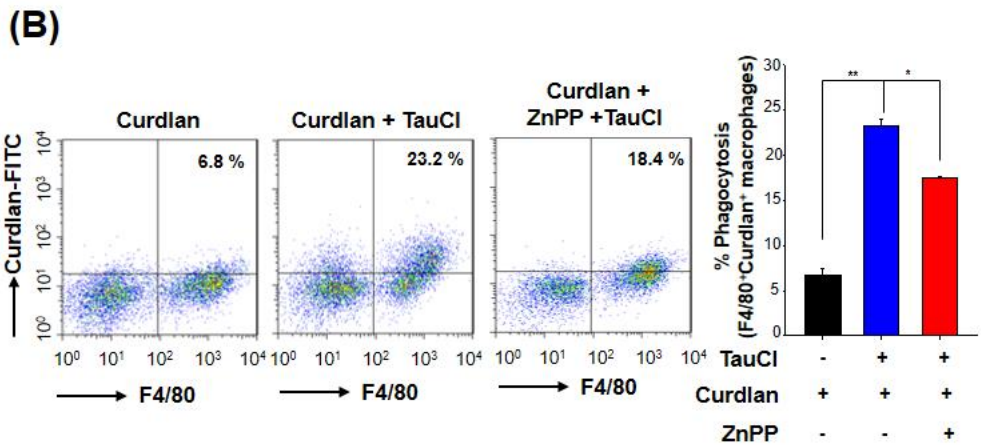
(B)
Curdlan
Curdlan + TauCl
Curdlan + ZnPP +TauCl
6.8 %
23.2 %
18.4 %
Curdlan-FITC
F4/80
% Phagocytosis (F4/80+Curdlan+ macrophages)
TauCl
Curdlan
ZnPP

Figure 5. TauCl-induced HO-1 expression is critical for stimulating phagocytosis by macrophages

(A) Phagocytic activity of macrophages was determined by flow cytometry as described in Materials and Methods. (B) The proportion of macrophages ingesting curdlan-FITC ($F4/80^{+}$curdlan-$FITC^{+}$) was determined by flow cytometry. Histograms represent quantification of flow cytometry. All data were analyzed by Student's *t*-test, $*p<0.05$, $**p<0.01$ and $***p<0.001$.

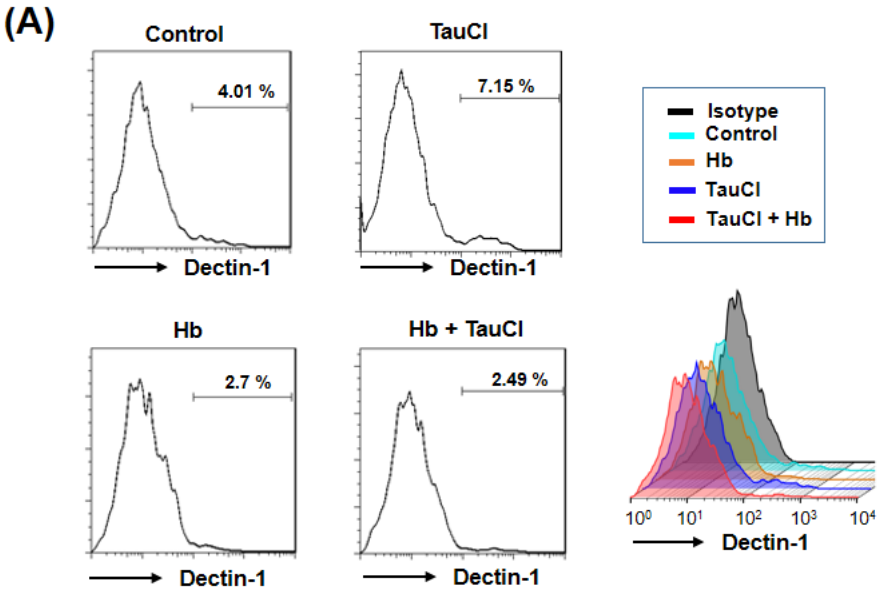
(A)
Control
4.01 %
Dectin-1
TauCl
7.15 %
Dectin-1
Isotype
Control
Hb
TauCl
TauCl + Hb
Hb
2.7 %
Dectin-1
Hb + TauCl
2.49 %
Dectin-1
10^0 10^1 10^2 10^3 10^4
Dectin-1

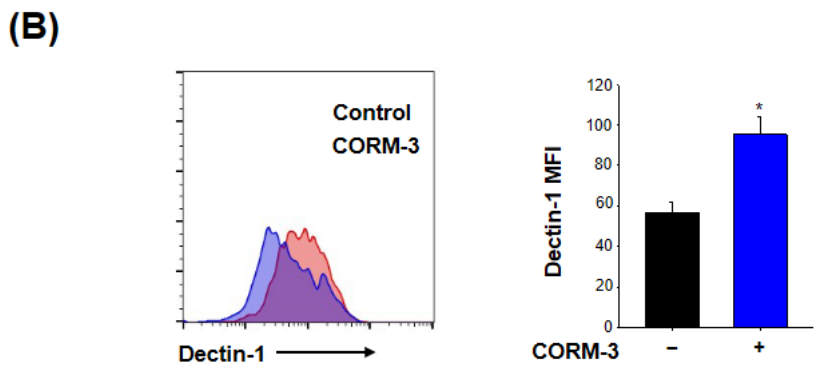
(B)
Control
CORM-3
Dectin-1
Dectin-1 MFI
120
100
80
60
40
20
0
*
CORM-3
–
+

Figure 6. TauCl-induced CO production plays a role in upregulation of dectin-1 expression in macrophages

(A) Representative flow cytometry data illustrate dectin-1 expression of macrophages co-treated with TauCl (0.5mM) and Hb (10 μM) as a CO scavenger for 36 h. (B) Histograms represent dectin-1 expression in PMs from mice injected with thioglycollate alone or thioglycollate plus CORM-3 (10 mg/kg). All data were analyzed by Student's *t*-test, **p*<0.05.

(A)

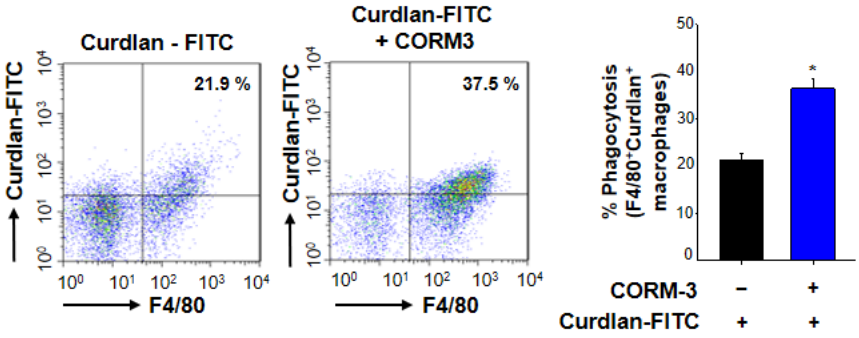
Curdlan - FITC
21.9 %
Curdlan-FITC
F4/80
Curdlan-FITC
+ CORM3
37.5 %
Curdlan-FITC
F4/80
% Phagocytosis
(F4/80+Curdlan+
macrophages)
CORM-3 – +
Curdlan-FITC + +

(B)

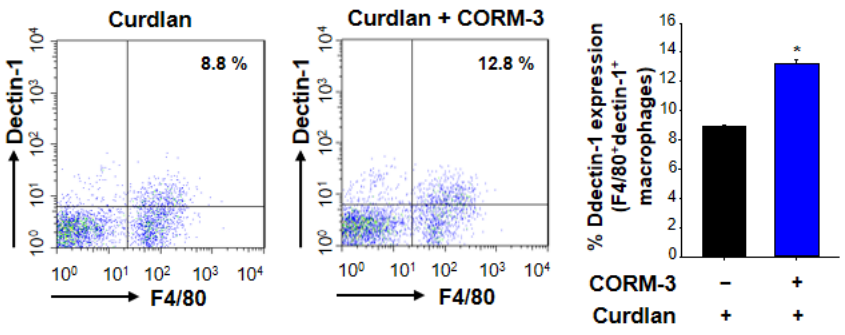
Curdlan
8.8 %
Dectin-1
F4/80
Curdlan + CORM-3
12.8 %
Dectin-1
F4/80
% Ddectin-1 expression
(F4/80+dectin-1+
macrophages)
CORM-3 – +
Curdlan + +

Figure 7. CO increases phagocytosis through dectin-1 expression

(A) Mice were pre-treated with CORM-3 (10 mg/kg) 3 times per week prior to i.p. injection of curdlan-FITC (2.5mg/kg/mouse). After 18 h, mice were sacrificed, and peritoneal exudates were collected. The engulfment of curdlan-FITC by macrophages ($F4/80^{+}$curdlan-$FITC^{+}$) was detected by flow cytometry. (B) Dot-plot represents dectin-1 expression of PMs derived from mice treated with curdlan. All data were analyzed by Student's *t*-test, $*p<0.05$.

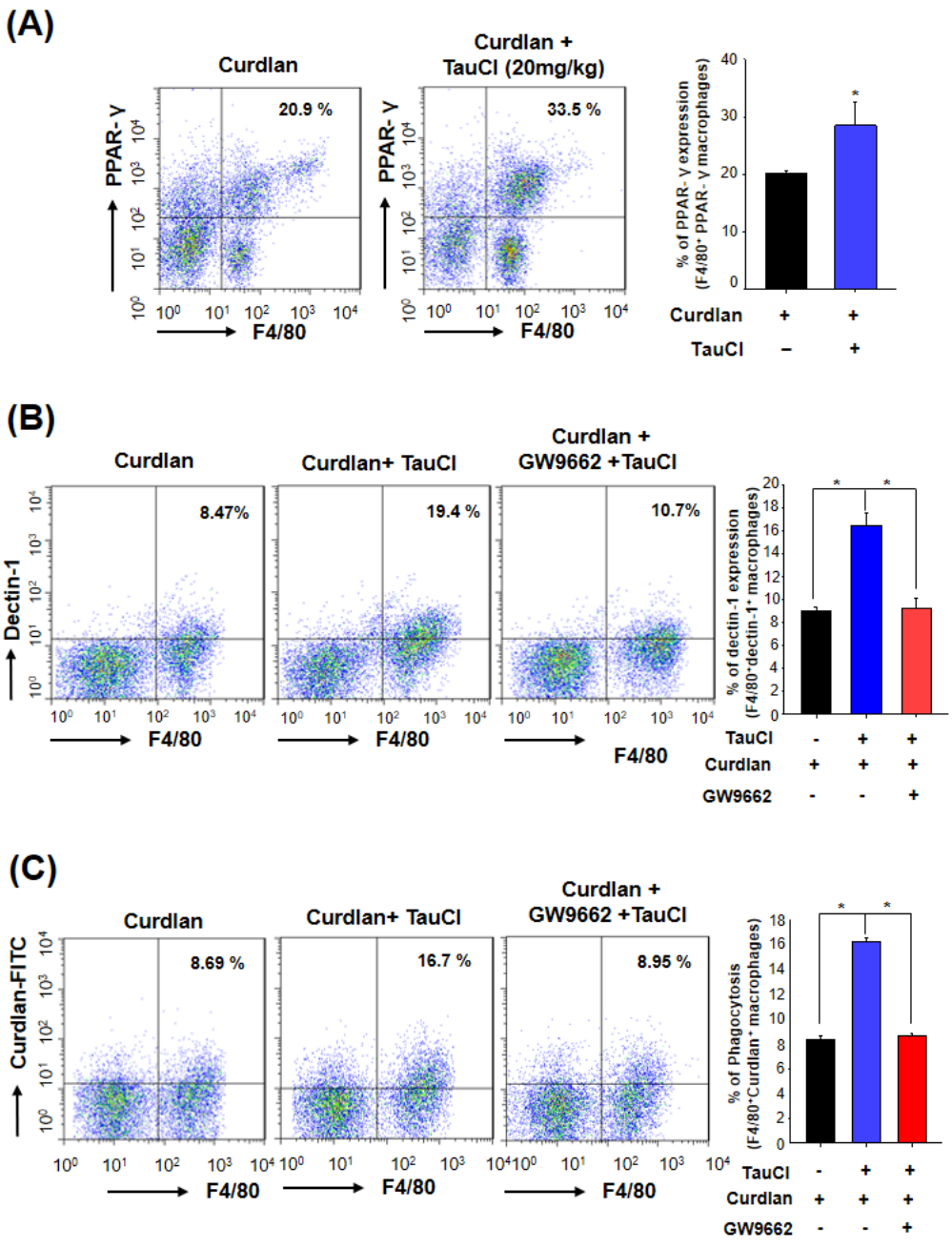
(A)
Curdlan
Curdlan + TauCl (20mg/kg)
20.9 %
33.5 %
PPAR- γ
F4/80
% of PPAR- γ expression (F4/80+ PPAR- γ macrophages)
Curdlan + +
TauCl – +
(B)
Curdlan
Curdlan+ TauCl
Curdlan + GW9662 +TauCl
8.47%
19.4 %
10.7%
Dectin-1
F4/80
% of dectin-1 expression (F4/80+dectin-1+ macrophages)
TauCl - + +
Curdlan + + +
GW9662 - - +
(C)
Curdlan
Curdlan+ TauCl
Curdlan + GW9662 +TauCl
8.69 %
16.7 %
8.95 %
Curdlan-FITC
F4/80
% of Phagocytosis (F4/80+Curdlan+ macrophages)
TauCl - + +
Curdlan + + +
GW9662 - - +

(D)

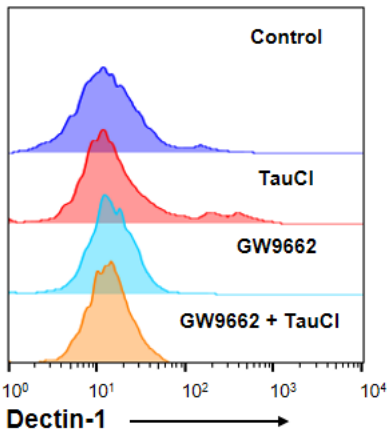
Control
TauCl
GW9662
GW9662 + TauCl
10^0 10^1 10^2 10^3 10^4
Dectin-1

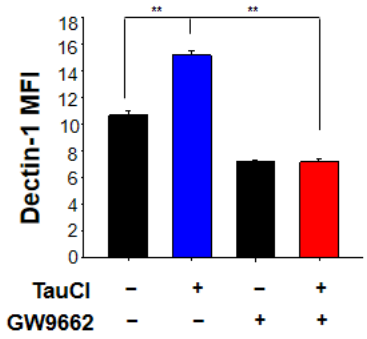
Dectin-1 MFI
18
16
14
12
10
8
6
4
2
0
**
**
TauCl – + – +
GW9662 – – + +

(E)

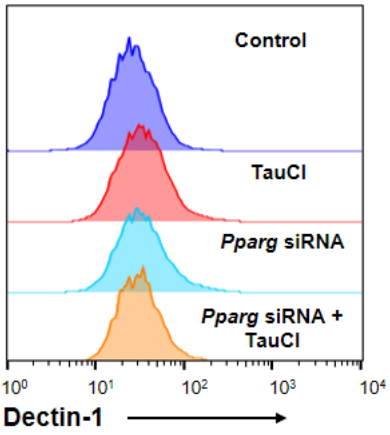
Control
TauCl
Pparg siRNA
Pparg siRNA + TauCl
10^0 10^1 10^2 10^3 10^4
Dectin-1

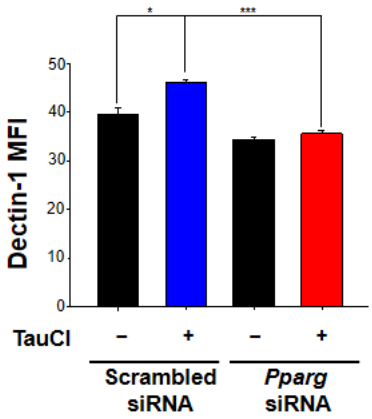
Dectin-1 MFI
50
40
30
20
10
0
*
***
TauCl – + – +
Scrambled siRNA
Pparg siRNA

(F)

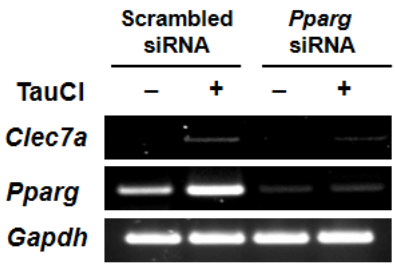
Scrambled siRNA
Pparg siRNA
TauCl – + – +
Clec7a
Pparg
Gapdh

Figure 8. TauCl upregulates dectin-1 expression via PPAR-γ in macrophages

(A) PPAR-γ expression of PMs from mice treated with curdlan was determined by flow cytometry. (B) Mice treated with curdlan-FITC (2.5mg/mouse) for 6 h were given an i.p. injection of vehicle or GW9662 (3 mg/kg), a PPAR-γ inhibitor, 1 h before TauCl (20 mg/kg) treatment. The proportion of PMs expressing dectin-1 was determined by flow cytometry. (C) Phagocytic activity of macrophages was measured by flow cytometry. (D) The dectin-1 level of PMs co-treated with TauCl and GW9662 (5 μM) was determined by flow cytometry. (E, F) RAW264.7 cells were transfected with scrambled or *PPAR-γ* siRNA for 24 h followed by treatment with TauCl for an additional 36 hr. The protein (E) and mRNA (F) levels of dectin-1 were measured by flow cytometry and RT-PCR, respectively. All data were analyzed by a Student's *t*-test, $*p<0.05$, $**p<0.01$ and $***p<0.001$.

(A)

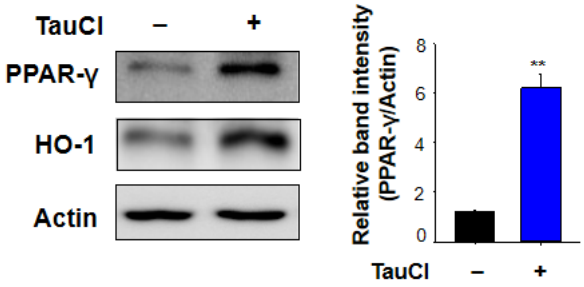
TauCl – +
PPAR-γ
HO-1
Actin
Relative band intensity (PPAR-γ/Actin)
8
6
4
2
0
**
TauCl – +

(B)

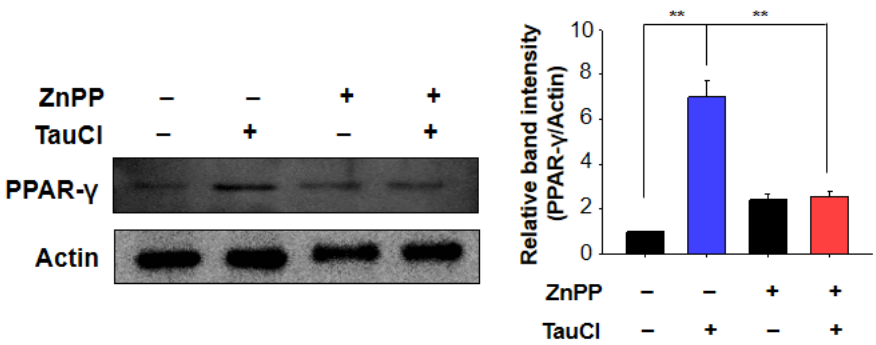
ZnPP – – + +
TauCl – + – +
PPAR-γ
Actin
Relative band intensity (PPAR-γ/Actin)
10
8
6
4
2
0
** **
ZnPP – – + +
TauCl – + – +

(C)

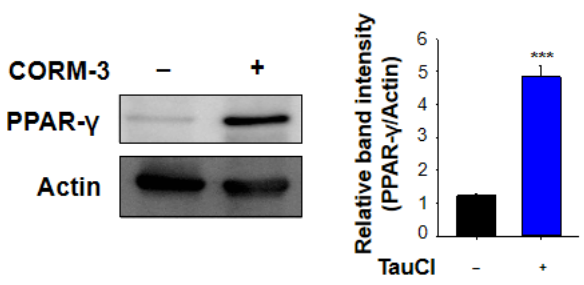
CORM-3 – +
PPAR-γ
Actin
Relative band intensity (PPAR-γ/Actin)
6
5
4
3
2
1
0
***
TauCl – +

Figure 9. HO-1 induction by TauCl is required for dectin-1 upregulation by PPAR-γ in macrophages

(A) Mice were treated with thioglycollate and TauCl as described in Materials and Methods. The protein expression levels of PPAR-γ and HO-1 in macrophages were assessed by Western blot analysis. (B) To determine whether HO-1 activation is required for PPAR-γ induction by TauCl, mice were co-treated with TauCl (20 mg/kg) and ZnPP (25 mg/kg). After 3 days, mice were sacrificed to collect PMs. The PPAR-γ protein level of macrophages was measured by Western blot analysis. (C) To verify that CO, as a by-product of HO-1 reaction, is required for PPAR-γ expression in macrophages, mice were co-injected with thioglycollate and CORM-3. The protein level of PPAR-γ was measured by Western blot analysis. All data were analyzed by Student's *t*-test $^{**}p<0.01$ and $^{***}p<0.001$.

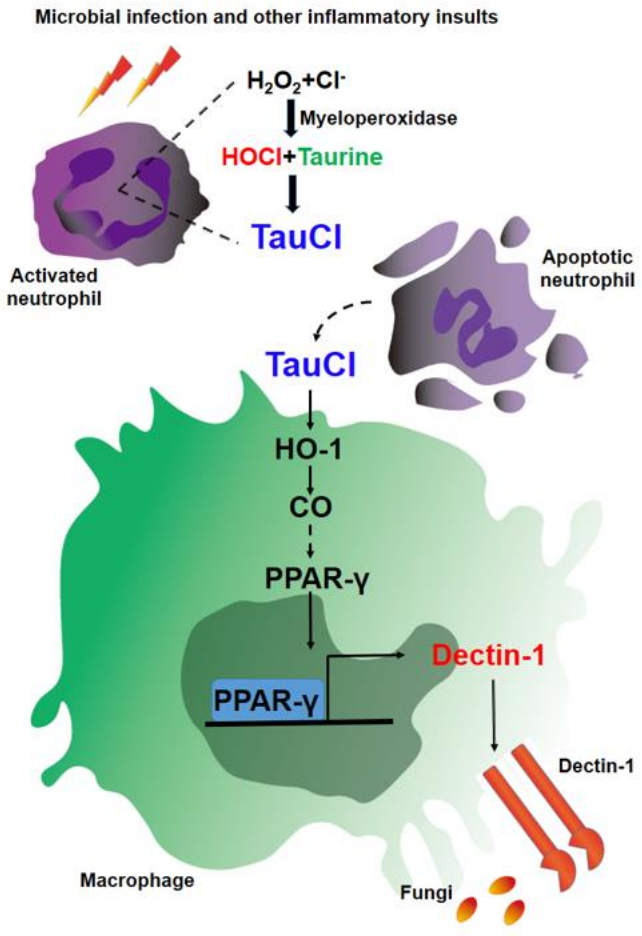
Microbial infection and other inflammatory insults
H_2O_2+Cl^-
Myeloperoxidase
HOCl+Taurine
TauCl
Activated neutrophil
Apoptotic neutrophil
TauCl
HO-1
CO
PPAR-γ
PPAR-γ
Dectin-1
Dectin-1
Macrophage
Fungi

Figure 10. A proposed mechanism underlying TauCl-induced phagocytosis

TauCl is endogenously produced by activated neutrophils in inflammatory microenvironment, which can stimulate the phagocytic activity of macrophages through induction of HO-1 expression and subsequently CO production. This, in turn, leads to PPAR-γ activation and dectin-1 upregulation.

5. Discussion

Every human has fungi as part of their microbiota which can be pathogenic factors when systemic immunity of host is changed. It is becoming of great importance to understand the underlying mechanisms by which host immunity plays a crucial role in the prevention and resolution of fungal infection (G. D. Brown, 2011). Phagocytes, such as macrophages, are important to clear of pathogens through their PRRs, which detect the microbial PAMPs (Charles N Serhan et al., 2015; Winkler et al., 2016). In order to eliminate the pathogens efficiently, the macrophages are required to stimulate the expression of the phagocytic receptor (David M Underhill & Helen S Goodridge, 2012). During acute inflammation response, endogenous pro-resolving mediators are produced to facilitate phagocytic actions of macrophages required for timely resolution of inflammation (Nan Chiang et al., 2012; C. N. Serhan, 2017).

TauCl, a metabolite of taurine produced by activated neutrophils, is released to the site of inflammation. TauCl is a long-lived mild oxidant that inhibits invasion of pathogens (Lackner et al., 2015). TauCl kills pathogens directly by transferring the chlorine atom to the amino group to the pathogen membrane (Waldemar Gottardi & Nagl, 2005). The subsequent formation of a chlorine cover made up of covalent N-Cl bonds impairs the viability of

pathogens including bacteria and fungi (W. Gottardi, Debabov, & Nagl, 2013). Several studies suggest that TauCl functions as an endogenous signaling molecule that regulates the generation of pro- and anti-inflammatory mediators in macrophages at the inflamed site (Chaekyun Kim & Cha, 2014; J. Marcinkiewicz, Grabowska, Bereta, & Stelmaszynska, 1995). I have previously demonstrated that TauCl enhances the efferocytic activity of macrophages (W. Kim et al., 2015). A TauCl-derived increase of HO-1 activity is associated with the upregulation of scavenger receptors expressed on the surface of macrophages, which facilitates recognition and engulfment of apoptotic neutrophils in the inflammatory microenvironment (W. Kim et al., 2015). In this study, I demonstrate that TauCl facilitates clearance of pathogens through potentiation of phagocytic activity of macrophages.

Phagocytic receptors promote phagocytosis following recognition of particulate targets on pathogens. The pathogenic fungal β-1,3-glucans are recognized by dectin-1, a PRR expressed on macrophages (D. M. Underhill & H. S. Goodridge, 2012). I found that TauCl exerts phagocytosis through the upregulation of dectin-1 which recognizes fungal β-1,3-glucans. Phagocytosis presents engulfed antigens efficiently to initiate an adaptive immune response (D. M. Underhill & H. S. Goodridge, 2012). Dectin-1 regulates several Th17-associated cytokines which influence the

differentiation of activated CD4+ T-cells (Drummond & Brown, 2011; LeibundGut-Landmann et al., 2007). Thus, it seems that TauCl-mediated stimulation of phagocytosis could enhance anti-fungal effects through activation of the immune responses.

Acute inflammation that occurs upon microbial infection gives rise to transient induction of HO-1 that possesses an anti-inflammatory capability. The enhanced HO-1 expression protects the host tissue from injuries caused by pathogens through multiple mechanisms (Pamplona et al., 2007). In line with this notion, HO-1 knockdown increases susceptibility to microbial infection, which is associated with inability of the macrophages to protect the host from pathogens (Wegiel et al., 2014). TauCl has been shown to exert cytoprotective and anti-inflammatory effects through HO-1 upregulation (Chaekyun Kim & Cha, 2014; Janusz Marcinkiewicz & Kontny, 2014). This prompted me to speculate that HO-1 upregulation in macrophages might be critical for its anti-fungal activity. In spite of the several studies demonstrating that elevated HO-1 expression enhances bacterial clearance (Bilban et al., 2006; Onyiah et al., 2013), little is known about the molecular mechanisms by which HO-1 induction stimulates phagocytosis. In the present study, I found that TauCl-induced HO-1 overexpression plays an important role in phagocytosis through dectin-1 upregulation.

CO generated as a consequence of HO-1 induction is an important

molecule that acts as an anti-inflammatory substance and a pro-resolving mediator (Fullerton & Gilroy, 2016; C. N. Serhan, 2017). Although CO is relatively inert gas in biological systems, it can maintain cellular protection against inflammatory insults (H. J. Kim et al., 2017). The present study indicates that HO-1-derived CO production by TauCl can upregulate dectin-1 expression and thereby stimulates fungal clearance by macrophages. Recent studies suggest that fungal antigen recognition by dectin-1 leads to LC3-associated phagocytosis (LAP) (Tam et al., 2016). Initiation of LAP accelerates internalization of microbial particles and phagosome maturation for degradation of the phagosome contents (Vernon & Tang, 2013). HO-1 induction and subsequent CO production are potentially involved in autophagy for enhancement of host protection (Lee et al., 2014; Yun, Cho, & Lee, 2014). It will be worthwhile determining whether TauCl-induced CO production is involved in LAP acceleration by dectin-1 during fungal clearance.

PPAR-γ plays an essential role in inflammation by regulating expression of phagocytic receptors of macrophages, such as dectin-1 (Galès et al., 2010; Odegaard et al., 2007). PPAR-γ is also required for the alternative activation of macrophages which is considered to mediate anti-inflammatory effects. Activation of PPAR-γ promotes uptake and killing of *C. albicans* by macrophages (Coste et al., 2003). The upregulation of dectin-1 by PPAR-γ

ligands in macrophages promotes phagocytosis and triggers resolution of candidiasis (Coste et al., 2008; Galès et al., 2010; Lefèvre et al., 2015; Lefevre et al., 2010). Moreover, dectin-1 activation by a particulate yeast-derived β-glucan resulted in conversion of polarized immunosuppressive M2 macrophages into an M1-like phenotype with potent immune-stimulating activity (Liu et al., 2015). In this study, I found that TauCl-induced HO-1 expression upregulates dectin-1 through PPAR-γ in macrophages. Several studies have suggested that HO-1-derived CO enhances PPAR-γ activity, thereby regulating inflammatory processes (Bilban et al., 2006; Hoetzel et al., 2008). CO facilitates the termination of acute inflammation by stimulating production of pro-resolving lipid mediators production (Tsoyi et al., 2016). PPAR-γ is a member of the nuclear receptors of lipid ligand-inducible transcription factors (Ahmadian et al., 2013). I speculate that CO produced as a consequence of TauCl-induced HO-1 upregulation may trigger activation of PPAR-γ. Further studies will be necessary to elucidate how TauCl-induced CO production enhances PPAR-γ elevation.

In conclusion, TauCl released from apoptotic neutrophils in the inflamed site enhances phagocytic activity of macrophages by stimulating expression of HO-1 and subsequently dectin-1 (Fig. 8). Specifically, CO, a byproduct of the HO-1-catalyzed reaction, plays a critical role as a putative signaling

molecule in mediating TauCl-induced phagocytosis. These results suggest that TauCl, a metabolite of taurine produced in the inflammatory microenvironment, has a powerful therapeutic potential to act as a modulator of phagocytic activity in the inflammatory disorders.

6. References

Ahmadian, M., Suh, J. M., Hah, N., Liddle, C., Atkins, A. R., Downes, M., & Evans, R. M. (2013). PPAR [gamma] signaling and metabolism: the good, the bad and the future. *Nature medicine, 99*(5), 557-566.

Bilban, M., Bach, F. H., Otterbein, S. L., Ifedigbo, E., de Costa d'Avila, J., Esterbauer, H., . . . Wagner, O. (2006). Carbon monoxide orchestrates a protective response through PPARγ. *Immunity, 24*(5), 601-610.

Billings, E. A., Lee, C. S., Owen, K. A., D'Souza, R. S., Ravichandran, K. S., & Casanova, J. E. (2016). The adhesion GPCR BAI1 mediates macrophage ROS production and microbicidal activity against Gram-negative bacteria. *Sci Signal, 9*(413), ra14. doi:10.1126/scisignal.aac6250

Brown, G. D. (2006). Dectin-1: a signalling non-TLR pattern-recognition receptor. *Nature Reviews Immunology, 6*(1), 33-43.

Brown, G. D. (2011). Innate antifungal immunity: the key role of phagocytes. *Annu Rev Immunol, 29*, 1-21. doi:10.1146/annurev-immunol-030409-101229

Brown, G. D., Denning, D. W., Gow, N. A., Levitz, S. M., Netea, M. G., & White, T. C. (2012). Hidden killers: human fungal infections. *Science translational medicine, 4*(165), 165rv113-165rv113.

Brown, G. D., Denning, D. W., & Levitz, S. M. (2012). Tackling human fungal infections. *Science, 336*(6082), 647-647.

Brubaker, S. W., Bonham, K. S., Zanoni, I., & Kagan, J. C. (2015). Innate immune pattern recognition: a cell biological perspective. *Annual review of immunology, 33*, 257-290.

Chiang, N., de la Rosa, X., Libreros, S., & Serhan, C. N. (2017). Novel Resolvin D2 Receptor Axis in Infectious Inflammation. *J Immunol,*

198(2), 842-851. doi:10.4049/jimmunol.1601650

Chiang, N., Fredman, G., Bäckhed, F., Oh, S. F., Vickery, T., Schmidt, B. A., & Serhan, C. N. (2012). Infection regulates pro-resolving mediators that lower antibiotic requirements. *Nature, 484*(7395), 524-528.

Coste, A., Dubourdeau, M., Linas, M. D., Cassaing, S., Lepert, J. C., Balard, P., . . . Pipy, B. (2003). PPARgamma promotes mannose receptor gene expression in murine macrophages and contributes to the induction of this receptor by IL-13. *Immunity, 19*(3), 329-339.

Coste, A., Lagane, C., Filipe, C., Authier, H., Gales, A., Bernad, J., . . . Pipy, B. (2008). IL-13 attenuates gastrointestinal candidiasis in normal and immunodeficient RAG-2(-/-) mice via peroxisome proliferator-activated receptor-gamma activation. *J Immunol, 180*(7), 4939-4947.

Dambuza, I. M., & Brown, G. D. (2015). C-type lectins in immunity: recent developments. *Current opinion in immunology, 32*, 21-27.

Drummond, R. A., & Brown, G. D. (2011). The role of Dectin-1 in the host defence against fungal infections. *Curr Opin Microbiol, 14*(4), 392-399. doi:10.1016/j.mib.2011.07.001

Erwig, L. P., & Gow, N. A. (2016). Interactions of fungal pathogens with phagocytes. *Nature Reviews Microbiology, 14*(3), 163-176.

Ferwerda, G., Meyer-Wentrup, F., Kullberg, B. J., Netea, M. G., & Adema, G. J. (2008). Dectin-1 synergizes with TLR2 and TLR4 for cytokine production in human primary monocytes and macrophages. *Cell Microbiol, 10*(10), 2058-2066. doi:10.1111/j.1462-5822.2008.01188.x

Fullerton, J. N., & Gilroy, D. W. (2016). Resolution of inflammation: a new therapeutic frontier. *Nature Reviews Drug Discovery*.

Galès, A., Conduché, A., Bernad, J., Lefevre, L., Olagnier, D., Béraud, M., . . . Coste, A. (2010). PPARγ controls Dectin-1 expression

required for host antifungal defense against Candida albicans. *PLoS Pathog, 6*(1), e1000714.

Gales, A., Conduche, A., Bernad, J., Lefevre, L., Olagnier, D., Beraud, M., . . . Pipy, B. (2010). PPARgamma controls Dectin-1 expression required for host antifungal defense against Candida albicans. *PLoS Pathog, 6*(1), e1000714. doi:10.1371/journal.ppat.1000714

Goodridge, H. S., Reyes, C. N., Becker, C. A., Katsumoto, T. R., Ma, J., Wolf, A. J., . . . Danielson, M. E. (2011). Activation of the innate immune receptor Dectin-1 upon formation of a/phagocytic synapse/'. *Nature, 472*(7344), 471-475.

Gottardi, W., Debabov, D., & Nagl, M. (2013). N-chloramines, a promising class of well-tolerated topical anti-infectives. *Antimicrob Agents Chemother, 57*(3), 1107-1114. doi:10.1128/aac.02132-12

Gottardi, W., & Nagl, M. (2002). Chemical Properties of N-Chlorotaurine Sodium, a Key Compound in the Human Defence System. *Archiv der Pharmazie, 335*(9), 411-421.

Gottardi, W., & Nagl, M. (2005). Chlorine covers on living bacteria: the initial step in antimicrobial action of active chlorine compounds. *Journal of Antimicrobial Chemotherapy, 55*(4), 475-482.

Greenblatt, M. B., Aliprantis, A., Hu, B., & Glimcher, L. H. (2010). Calcineurin regulates innate antifungal immunity in neutrophils. *J Exp Med, 207*(5), 923-931. doi:10.1084/jem.20092531

Hoetzel, A., Dolinay, T., Vallbracht, S., Zhang, Y., Kim, H. P., Ifedigbo, E., . . . Ryter, S. W. (2008). Carbon monoxide protects against ventilator-induced lung injury via PPAR-γ and inhibition of Egr-1. *American journal of respiratory and critical care medicine, 177*(11), 1223-1232.

Kawai, T., & Akira, S. (2011). Toll-like receptors and their crosstalk with

other innate receptors in infection and immunity. *Immunity, 34*(5), 637-650. doi:10.1016/j.immuni.2011.05.006

Kim, C., & Cha, Y.-N. (2014). Taurine chloramine produced from taurine under inflammation provides anti-inflammatory and cytoprotective effects. *Amino acids, 46*(1), 89-100.

Kim, C., Jang, J. S., Cho, M. R., Agarawal, S. R., & Cha, Y. N. (2010). Taurine chloramine induces heme oxygenase-1 expression via Nrf2 activation in murine macrophages. *Int Immunopharmacol, 10*(4), 440-446. doi:10.1016/j.intimp.2009.12.018

Kim, H. J., Joe, Y., Kim, S. K., Park, S. U., Park, J., Chen, Y., . . . Chung, H. T. (2017). Carbon monoxide protects against hepatic steatosis in mice by inducing sestrin-2 via the PERK-eIF2alpha-ATF4 pathway. *Free Radic Biol Med, 110*, 81-91. doi:10.1016/j.freeradbiomed.2017.05.026

Kim, W., Kim, H.-U., Lee, H.-N., Kim, S. H., Kim, C., Cha, Y.-N., . . . Kim, K. (2015). Taurine Chloramine Stimulates Efferocytosis Through Upregulation of Nrf2-Mediated Heme Oxygenase-1 Expression in Murine Macrophages: Possible Involvement of Carbon Monoxide. *Antioxidants & redox signaling, 23*(2), 163-177.

Kumar, H., Kumagai, Y., Tsuchida, T., Koenig, P. A., Satoh, T., Guo, Z., . . . Kawai, T. (2009). Involvement of the NLRP3 inflammasome in innate and humoral adaptive immune responses to fungal beta-glucan. *J Immunol, 183*(12), 8061-8067. doi:10.4049/jimmunol.0902477

Lackner, M., Binder, U., Reindl, M., Gonul, B., Fankhauser, H., Mair, C., & Nagl, M. (2015). N-Chlorotaurine Exhibits Fungicidal Activity against Therapy-Refractory Scedosporium Species and Lomentospora prolificans. *Antimicrob Agents Chemother, 59*(10),

6454-6462. doi:10.1128/aac.00957-15

Lee, S., Lee, S. J., Coronata, A. A., Fredenburgh, L. E., Chung, S. W., Perrella, M. A., . . . Choi, A. M. (2014). Carbon monoxide confers protection in sepsis by enhancing beclin 1-dependent autophagy and phagocytosis. *Antioxid Redox Signal, 20*(3), 432-442. doi:10.1089/ars.2013.5368

Lefèvre, L., Authier, H., Stein, S., Majorel, C., Couderc, B., Dardenne, C., . . . Valentin, A. (2015). LRH-1 mediates anti-inflammatory and antifungal phenotype of IL-13-activated macrophages through the PPAR [gamma] ligand synthesis. *Nature communications, 6*.

Lefevre, L., Gales, A., Olagnier, D., Bernad, J., Perez, L., Burcelin, R., . . . Coste, A. (2010). PPARgamma ligands switched high fat diet-induced macrophage M2b polarization toward M2a thereby improving intestinal Candida elimination. *PLoS One, 5*(9), e12828. doi:10.1371/journal.pone.0012828

LeibundGut-Landmann, S., Gross, O., Robinson, M. J., Osorio, F., Slack, E. C., Tsoni, S. V., . . . Reis e Sousa, C. (2007). Syk- and CARD9-dependent coupling of innate immunity to the induction of T helper cells that produce interleukin 17. *Nat Immunol, 8*(6), 630-638. doi:10.1038/ni1460

Liu, M., Luo, F., Ding, C., Albeituni, S., Hu, X., Ma, Y., . . . Yan, J. (2015). Dectin-1 Activation by a Natural Product beta-Glucan Converts Immunosuppressive Macrophages into an M1-like Phenotype. *J Immunol, 195*(10), 5055-5065. doi:10.4049/jimmunol.1501158

Marcinkiewicz, J., Grabowska, A., Bereta, J., & Stelmaszynska, T. (1995). Taurine chloramine, a product of activated neutrophils, inhibits in vitro the generation of nitric oxide and other macrophage inflammatory mediators. *J Leukoc Biol, 58*(6), 667-674.

Marcinkiewicz, J., & Kontny, E. (2014). Taurine and inflammatory diseases. *Amino Acids, 46*(1), 7-20.

Maruyama, N., Sekimoto, Y., Ishibashi, H., Inouye, S., Oshima, H., Yamaguchi, H., & Abe, S. (2005). Suppression of neutrophil accumulation in mice by cutaneous application of geranium essential oil. *J Inflamm (Lond), 2*(1), 1. doi:10.1186/1476-9255-2-1

Murray, P. J., Allen, J. E., Biswas, S. K., Fisher, E. A., Gilroy, D. W., Goerdt, S., . . . Lawrence, T. (2014). Macrophage activation and polarization: nomenclature and experimental guidelines. *Immunity, 41*(1), 14-20.

Nembrini, C., Marsland, B. J., & Kopf, M. (2009). IL-17-producing T cells in lung immunity and inflammation. *J Allergy Clin Immunol, 123*(5), 986-994; quiz 995-986. doi:10.1016/j.jaci.2009.03.033

Odegaard, J. I., Ricardo-Gonzalez, R. R., Goforth, M. H., Morel, C. R., Subramanian, V., Mukundan, L., . . . Ferrante, A. W. (2007). Macrophage-specific PPAR&ggr; controls alternative activation and improves insulin resistance. *Nature, 447*(7148), 1116-1120.

Onyiah, J. C., Sheikh, S. Z., Maharshak, N., Steinbach, E. C., Russo, S. M., Kobayashi, T., . . . Rawls, J. F. (2013). Carbon monoxide and heme oxygenase-1 prevent intestinal inflammation in mice by promoting bacterial clearance. *Gastroenterology, 144*(4), 789-798.

Pamplona, A., Ferreira, A., Balla, J., Jeney, V., Balla, G., Epiphanio, S., . . . Cunha-Rodrigues, M. (2007). Heme oxygenase-1 and carbon monoxide suppress the pathogenesis of experimental cerebral malaria. *Nature medicine, 13*(6), 703-710.

Ryter, S. W., & Choi, A. M. (2016). Targeting heme oxygenase-1 and carbon monoxide for therapeutic modulation of inflammation. *Translational Research, 167*(1), 7-34.

Serhan, C. N. (2017). Treating inflammation and infection in the 21st

century: new hints from decoding resolution mediators and mechanisms. *Faseb j*. doi:10.1096/fj.201601222R

Serhan, C. N., Chiang, N., Dalli, J., & Levy, B. D. (2015). Lipid mediators in the resolution of inflammation. *Cold Spring Harbor perspectives in biology, 7*(2), a016311.

Smith, J. A. (1994). Neutrophils, host defense, and inflammation: a double-edged sword. *Journal of leukocyte biology, 56*(6), 672-686.

Sturman, J. A. (1993). Taurine in development. *Physiol Rev, 73*(1), 119-147.

Tam, J. M., Mansour, M. K., Acharya, M., Sokolovska, A., Timmons, A. K., Lacy-Hulbert, A., & Vyas, J. M. (2016). The Role of Autophagy-Related Proteins in Candida albicans Infections. *Pathogens, 5*(2). doi:10.3390/pathogens5020034

Trinath, J., Holla, S., Mahadik, K., Prakhar, P., Singh, V., & Balaji, K. N. (2014). The WNT signaling pathway contributes to dectin-1-dependent inhibition of Toll-like receptor-induced inflammatory signature. *Mol Cell Biol, 34*(23), 4301-4314. doi:10.1128/mcb.00641-14

Tsoyi, K., Hall, S. R., Dalli, J., Colas, R. A., Ghanta, S., Ith, B., . . . Choi, A. M. (2016). Carbon Monoxide Improves Efficacy of Mesenchymal Stromal Cells During Sepsis by Production of Specialized Proresolving Lipid Mediators. *Critical care medicine*.

Underhill, D. M., & Goodridge, H. S. (2012). Information processing during phagocytosis. *Nat Rev Immunol, 12*(7), 492-502. doi:10.1038/nri3244

Underhill, D. M., & Goodridge, H. S. (2012). Information processing during phagocytosis. *Nature Reviews Immunology, 12*(7), 492-502.

Vernon, P. J., & Tang, D. (2013). Eat-me: autophagy, phagocytosis, and reactive oxygen species signaling. *Antioxid Redox Signal, 18*(6),

677-691. doi:10.1089/ars.2012.4810

Wegiel, B., Larsen, R., Gallo, D., Chin, B. Y., Harris, C., Mannam, P., . . . Otterbein, L. E. (2014). Macrophages sense and kill bacteria through carbon monoxide-dependent inflammasome activation. *J Clin Invest, 124*(11), 4926-4940. doi:10.1172/jci72853

Weiss, S. J. (1989). Tissue destruction by neutrophils. *New England Journal of Medicine, 320*(6), 365-376.

Weiss, S. J., Klein, R., Slivka, A., & Wei, M. (1982). Chlorination of taurine by human neutrophils: evidence for hypochlorous acid generation. *Journal of Clinical Investigation, 70*(3), 598.

Winkler, J. W., Orr, S. K., Dalli, J., Cheng, C.-Y. C., Sanger, J. M., Chiang, N., . . . Serhan, C. N. (2016). Resolvin D4 stereoassignment and its novel actions in host protection and bacterial clearance. *Scientific reports, 6*.

Yun, N., Cho, H. I., & Lee, S. M. (2014). Impaired autophagy contributes to hepatocellular damage during ischemia/reperfusion: heme oxygenase-1 as a possible regulator. *Free Radic Biol Med, 68*, 168-177. doi:10.1016/j.freeradbiomed.2013.12.014

국 문 초 록

유방암 치료를 위하여 많이 쓰이는 치료방법 중 하나는 화학요법이다. 그러나 화학 요법 치료 후 면역 시스템의 문제로 암의 재발이나 악성화가 진행 되기도 한다. 특히, 암 진행을 억제하는 중요한 역할을 가지고 있는 $CD8^+$ T세포가 화학 요법 후 활성이 떨어지기도 한다. 종양 미세환경에서 많은 부분을 차지하고 있는 종양 관련 대식세포는 화학 요법 치료에서 항암 면역 반응을 조절하는 역할을 가지고 있다. 화학 요법으로 인하여 생성된 사멸된 암세포는 종양 관련 대식세포를 조절 하여 암을 재발시키기도 한다. 그러므로 종양 관련 대식세포를 재프로그래밍 하여서 화학요법의 효과를 극대화시키는 방법이 항암 치료 전략 중 주목받고 있다. 이번 연구에서는 화학 요법 후 사멸된 암세포가 대식세포의 활성을 조절하여 항암 치료의 효과를 줄이는지 알아보았다. 4T1 유방암 모델에서 파클리탁셀을 처리한 군에서는 $CD86^+$M1 대식 세포와 $CD8^+$ T세포의 비율이 줄어들었다. 흥미롭게도 파클리탁셀을 투여한 군에서 사멸된 암세포를 잡아먹은 대식세포의 헴산화 효소 발현이 증가 되어있었다. 또한, 사멸된 암세포를 잡아먹은 골수 유래 대식 세포의 헴 산화 효소 발현도 확인 할 수

있었다. 사멸된 암세포를 잡아먹은 골수 유래 대식세포의 헴 산화 효소의 발현은 M1 극성화를 줄이고 M2 극성화를 증가 시켰다. 반대로 헴 산화 효소를 비활성화 시키면 사멸된 암세포를 잡아 먹은 골수 유래 대식 세포의 M1 활성이 유지됨을 관찰할 수 있었다. 헴 산화 효소 녹아웃 마우스를 사용한 4T1 유방암 모델에서는 파클리탁셀의 치료 효과가 증진되었다. 마찬가지로, 4T1 유방암 모델에서 zinc protoporphyin IX를 사용하여 HO-1 활성을 억제하니 $CD86^+$ M1 대식 세포 비율이 증진되어 파클리탁셀의 치료 효과를 증가시켰다. 또한 유방암 모델에서 헴 산화 효소의 억제는 $CD8^+$ T세포의 유입을 증진시켰다. 이를 통해, 화학요법으로 생성된 사멸된 암세포를 통하여 대식 세포의 증가된 헴 산화 효소는 항암 면역을 억제하여 항암치료 효과를 감소 시킨다는 것을 알았다. 이러한 결과는 유방암 종양 미세 환경에서 화학요법으로 증가된 헴 산화 효소를 표적으로 치료 하면 면역 시스템을 조절하여 화학 요법을 증진시킬 수 있음을 시사한다.

주요어: 유방암, 화학 요법, 종양 관련 대식세포, 사멸된 암세포, 헴 산화 효소

학번: 2014-30674